DOE/NV/0000939-31

Application of Monte Carlo Methods to Perform Uncertainty and Sensitivity Analysis on Inverse Water-Rock Reactions with NETPATH

Prepared by

David McGraw and Ronald L. Hershey

Submitted to

Nevada Field Office
National Nuclear Security Administration
U.S. Department of Energy
Las Vegas, Nevada

June 2016

Publication No. 45267

Nevada System of Higher Education

DOE/NV/0000939-31

Application of Monte Carlo Methods to Perform Uncertainty and Sensitivity Analysis on Inverse Water-Rock Reactions with NETPATH

Prepared by

David McGraw and Ronald L. Hershey

Division of Hydrologic Sciences
Desert Research Institute
Nevada System of Higher Education

Publication No. 45267

Submitted to

Nevada Field Office
National Nuclear Security Administration
U.S. Department of Energy
Las Vegas, Nevada

June 2016

The work upon which this report is based was supported by the U.S. Department of Energy under Contract #DE-NA0000939. Approved for public release; further dissemination unlimited.

THIS PAGE INTENTIONALLY LEFT BLANK

ACKNOWLEDGEMENTS

The authors thank the U.S. Department of Energy and the Underground Test Area Activity Lead, Bill Wilborn, for providing funding to accomplish the work described herein. We also thank the reviewers of this report, Irene Farnham, Andy Tompson, Rishi Parashar, Chuck Russell, and Karl Pohlmann for providing comments, suggestions, and recommendations that helped to improve this report substantially. We also thank Nicole Damon for support with report processing and publishing.

THIS PAGE INTENTIONALLY LEFT BLANK

ABSTRACT

Methods were developed to quantify uncertainty and sensitivity for NETPATH inverse water-rock reaction models and to calculate dissolved inorganic carbon, carbon-14 groundwater travel times. The NETPATH models calculate upgradient groundwater mixing fractions that produce the downgradient target water chemistry along with amounts of mineral phases that are either precipitated or dissolved. Carbon-14 groundwater travel times are calculated based on the upgradient source-water fractions, carbonate mineral phase changes, and isotopic fractionation.

Custom scripts and statistical code were developed for this study to facilitate modifying input parameters, running the NETPATH simulations, extracting relevant output, postprocessing the results, and producing graphs and summaries. The scripts read user-specified values for each constituent's coefficient of variation, distribution, sensitivity parameter, maximum dissolution or precipitation amounts, and number of Monte Carlo simulations.

Monte Carlo methods for analysis of parametric uncertainty assign a distribution to each uncertain variable, sample from those distributions, and evaluate the ensemble output. The uncertainty in input affected the variability of outputs, namely source-water mixing, phase dissolution and precipitation amounts, and carbon-14 travel time. Although NETPATH may provide models that satisfy the constraints, it is up to the geochemist to determine whether the results are geochemically reasonable.

Two example water-rock reaction models from previous geochemical reports were considered in this study. Sensitivity analysis was also conducted to evaluate the change in output caused by a small change in input, one constituent at a time. Results were standardized to allow for sensitivity comparisons across all inputs, which results in a representative value for each scenario.

The approach yielded insight into the uncertainty in water-rock reactions and travel times. For example, there was little variation in source-water fraction between the deterministic and Monte Carlo approaches, and therefore, little variation in travel times between approaches. Sensitivity analysis proved very useful for identifying the most important input constraints (dissolved-ion concentrations), which can reveal the variables that have the most influence on source-water fractions and carbon-14 travel times. Once these variables are determined, more focused effort can be applied to determining the proper distribution for each constraint.

Second, Monte Carlo results for water-rock reaction modeling showed discrete and nonunique results. The NETPATH models provide the solutions that satisfy the constraints of upgradient and downgradient water chemistry. There can exist multiple, discrete solutions for any scenario and these discrete solutions cause grouping of results. As a result, the variability in output may not easily be represented by a single distribution or a mean and variance and care should be taken in the interpretation and reporting of results.

THIS PAGE INTENTIONALLY LEFT BLANK

CONTENTS

LIST OF FIGURES

LIST OF TABLES

LIST OF ACROYNMS

C	carbon
^{14}C	carbon-14
Ca	calcium
CAU	corrective action unit
CDF	cumulative distribution function
Cl	chloride
CV	coefficient of variation
$\delta^{13}C$	carbon-13/carbon-12 isotopic ratio
DIC	dissolved inorganic carbon
EPA	Environmental Protection Agency
GLUE	Generalized Likelihood Uncertainty Estimation
GSA	Generalized Sensitivity Analysis
HSU	hydrostratigraphic unit
K	potassium
Kg	kilogram
LCA	Lower Carbonate Aquifer
MCMC	Markov Chain Monte Carlo
Max	maximum
Mg	magnesium
Min	minimum
mmols	millimoles
Na	sodium
NNSS	Nevada National Security Site
pmc	percent modern carbon
Q1	First quartile
Q3	Third quartile
RM/SM	Rainier Mesa/Shoshone Mountain
S	sulfur
SD	Standard Deviation
Si	silica
U.S.	United States

INTRODUCTION

The preemptive review committee from the Rainier Mesa/Shoshone Mountain (RM/SM) Geochemical Flow-path Evaluation task identified the need to quantify uncertainty in geochemical evaluations, water-rock reaction modeling, and calculation of groundwater travel times. In preparation for the Pahute Mesa Phase II geochemical evaluation, this report describes the development of methods to quantify uncertainty and sensitivity for NETPATH inverse water-rock reaction models and to calculate dissolved inorganic carbon (DIC) carbon-14 (^{14}C) groundwater travel times. These methods were tested on two previously developed Nevada National Security Site (NNSS) flow paths with water-rock reaction models.

The primary focus of this report was to apply methods to evaluate the uncertainty in water-rock reaction models, specifically, upgradient groundwater mixing ratios that produce the downgradient target water chemistry, amount of mineral phases that are either precipitated or dissolved, and calculated groundwater travel times. The methods applied in this study supported uncertainty and sensitivity analysis to provide a better understanding of water-rock reaction model uncertainty and the relative importance of each parameter. Understanding the solution space for these models can help quantify uncertainty in geochemical flow paths, groundwater ages, and groundwater travel times.

PREVIOUS STUDIES

Uncertainty analysis using Monte Carlo methods is a common activity in environmental applications, a small sample of which includes: climate change simulations (Murphy *et al.*, 2004), water quality in soils (Ma, 2000), pesticides and solid waste (EPA, 1997), radioactive waste disposal (Helton *et al*., 2006; Makino *et al.*, 2001), groundwater modeling (Kunstmann *et al*., 2002), watershed modeling (Blasone *et al.*, 2008; Al-Issa, 1996), pesticide transport (Zhang, 2006), and geochemical modeling (Ekberg, 1999; Srinivasan, 2007; Dethlefsen *et al.*, 2011). The methods employed in this study share many of the same techniques. Before evaluating uncertainty, it is important to identify what kind of uncertainty will be analyzed. In this study, parametric uncertainty was addressed; parameter, or epistemic, uncertainty is associated with model inputs. Model, or aleatory, uncertainty relates to the model structure and assumed algorithms of the system (Srinivasan *et al.*, 2007; Helton *et al.*, 2006). Model uncertainty was not addressed in this study.

Monte Carlo analysis of parametric uncertainty includes assigning a distribution to each uncertain variable, sampling from those distributions, and evaluating the ensemble output. Sampling includes brute-force methods and Bayesian methods. In the brute-force method, samples are generated from a fixed prior distribution. These distributions can be based on field data or expert judgment, but remain fixed throughout the analysis (Helton *et al*., 2006). Bayesian, or quasi-Bayesian, methods involve updating the prior distribution based on the results of the previous simulation. Several updating methods include Generalized Likelihood Uncertainty Estimation (GLUE) (e.g., Zhang [2006] and Beven and Binley [1992]), Markov Chain Monte Carlo (MCMC) (e.g., Blasone *et al.* [2008]), Generalized Sensitivity Analysis (GSA) (e.g., Makino *et al.* [2001]), and Shuffled-Complex Evolution (e.g., Duan *et al.* [1992]). These methods are similar in that

they use a likelihood measure to assign weights to input data based on some measure of goodness of fit. The prior distributions are then updated using this information and the next sample is taken from this updated distribution. This differs from the brute-force approach in which samples are taken from a fixed distribution that doesn't change, regardless of results.

For this unique application, however, Bayesian methods do not apply. The purpose of a Bayesian approach would be in updating the prior distributions, which in this study are the distributions of the constraints. The method of updating requires a likelihood function, which in turn requires some knowledge of model outputs. Without measured travel times or extensive sampling of mineral phases, neither of which applies in this study, there can be no likelihood function to inform the distribution modification.

The choice of prior distributions for input variables can be an important consideration in the brute-force approach and the characterization of uncertainty in inputs is essential to the performance of uncertainty and sensitivity analyses (Helton *et al.*, 2006). The uniform distribution is one of the simplest ways to represent uncertainty in model input. It is defined only by its range and in the absence of enough data to identify a more likely distribution, it is commonly used as a first estimate (VanBriesen *et al.*, 2010; Makino *et al.*, 2001; Helton *et al.*, 2006; Blason *et al.*, 2008; Jackman, 2000). The uniform distribution can also be used to run a preliminary analysis to identify the most influential variables to the output. Then, resources can be applied to those variables to better define the distribution (Helton *et al*., 2006).

If enough data exist, an empirical distribution can be used. This distribution can be defined by the quantiles of observed data. This will ensure that the distribution matches observed data (Helton *et al.*, 2006). Although many believe the initial choice of distribution is important, conflicting results exist in evaluating the importance of the form of the input distributions. In a study of model output uncertainty using a soil and water-quality model, it was found that changing the type of distribution of input parameters has little to no effect on output uncertainty; rather, it is the coefficient of variation that has the most influence (Al-Issa and Haan, 1996). Other studies (e.g., Haan and Zhang [1996], Ma *et al*. [2000], and Hammonds *et al*. [1994]) came to similar conclusions. The authors of the United States Environmental Protection Agency's (U.S. EPA) guiding principles for Monte Carlo analysis (EPA, 1997) concluded that "the range of model output is more dependent on the ranges of the input variables than it is on the actual shapes of the input distributions." On the other hand, the *shape* of the input distribution can have a large influence on the shape of the output distribution.

Using data also relevant to this study, Hershey *et al.* (2008) evaluated water chemistry data from the Rainier Mesa/Shoshone Mountain Corrective Action Unit (CAU). Data were compiled from 62 boreholes and springs to develop distributions for flow-path evaluation. Constituents at all locations had between 2 and 37 samples, although 82 percent of the datasets have fewer than 10 samples. Of the datasets with a sufficient number of samples, four were found to be associated with a single distribution, three were associated with both normal and log-normal distributions, and seven did not follow either distribution. The analysis was performed to find the best estimator of a representative (single) value, but the conclusion of Hershey *et al.* (2008) that it is difficult to assign a distribution to water chemistry data with confidence, even with an adequate number of samples, is also relevant to this study.

In a study by Parkhurst (1997), equations were added to the geochemical computer code PHREEQC (Parkhurst, 1995), so that the code could also consider uncertainty in isotopic mole-balance in geochemical mole-balance models. Geochemical mole-balance models are sets of chemical reactions that account for changes in the chemical composition of water along a flow path (Parkhurst, 1997). The code was modified to include uncertainty in aqueous chemical concentrations, which corresponds to uncertainty in phase mole balance. In a test case, many of the phases required to achieve mole balance in the deterministic models could be eliminated when allowing up to 5 percent uncertainty in aqueous concentrations. This resulted in a simplified system and a reduction of uncertainty in mineral phase composition.

DEMONSTRATION SIMULATIONS

In this study, the computer code NETPATH (Plummer *et al.*, 1994) was used to simulate water-rock reactions along groundwater flow paths and to estimate groundwater travel times. NETPATH inverse water-rock reaction models have been used routinely in southern Nevada (e.g., Morse [2002], Hershey and Acheampong [1997], Thomas *et al.*, [1996], and Chapman *et al.* [1995]) and the UGTA Activity (e.g., Hershey *et al.* [2008], Farnham *et al.* [2006], Rose *et al.* [2006], Hershey *et al.* [2005], and Thomas *et al.* [2002]) to corroborate potential flow paths identified by other methods such as groundwater contours, groundwater modeling, and conservative tracers and to estimate groundwater travel times. Typically, NETPATH models attempt to explain the geochemical evolution of groundwater along a flow path by identifying the net changes in reactive species occurring in the aquifer between the upgradient and downgradient waters. The reactive components considered by the NETPATH models usually limit the number of possible mixing models to a subset of models where plausible water-rock reactions can also be found.

Figure 1 shows a simplification of a NETPATH simulation. The upgradient wells are represented by wells 1, 2, and 3 on the left and the downgradient well is represented by well 4. The possible mineral phases in the system, as specified by the modeler, are represented here by phases A, B, C, D, E, and F. In a simulation such as this, there can exist multiple models (here, a *model* is a unique set of mineral phases; all models in a simulation are mutually exclusive) that satisfy the constraints. In NETPATH, a constraint is equal to a dissolved chemical constituent, such as calcium (Ca) or sulfate. To minimize confusion in this report, the term constraint will be used when both talking about NETPATH models and chemical constituent input data. NETPATH will produce output for each feasible model without regard to the appropriateness of the dissolution or precipitation amounts. In effect, NETPATH is providing all possible combinations of phases and it is up to the geochemist to determine the models that are geochemically feasible.

The models inside the brackets in Figure 1 are determined to be possible by NETPATH. Each phase within each model will result in a precipitation or dissolution amount, a source-water fraction (designated as Init 1, Init 2, and Init 3 in NETPATH output), and if desired, a ^{14}C travel time. The outputs of these simulations include model selection, phase precipitation or dissolution amount, source-water fraction, carbon-13/carbon-12 isotopic ratio ($\delta^{13}C$), and ^{14}C travel time.

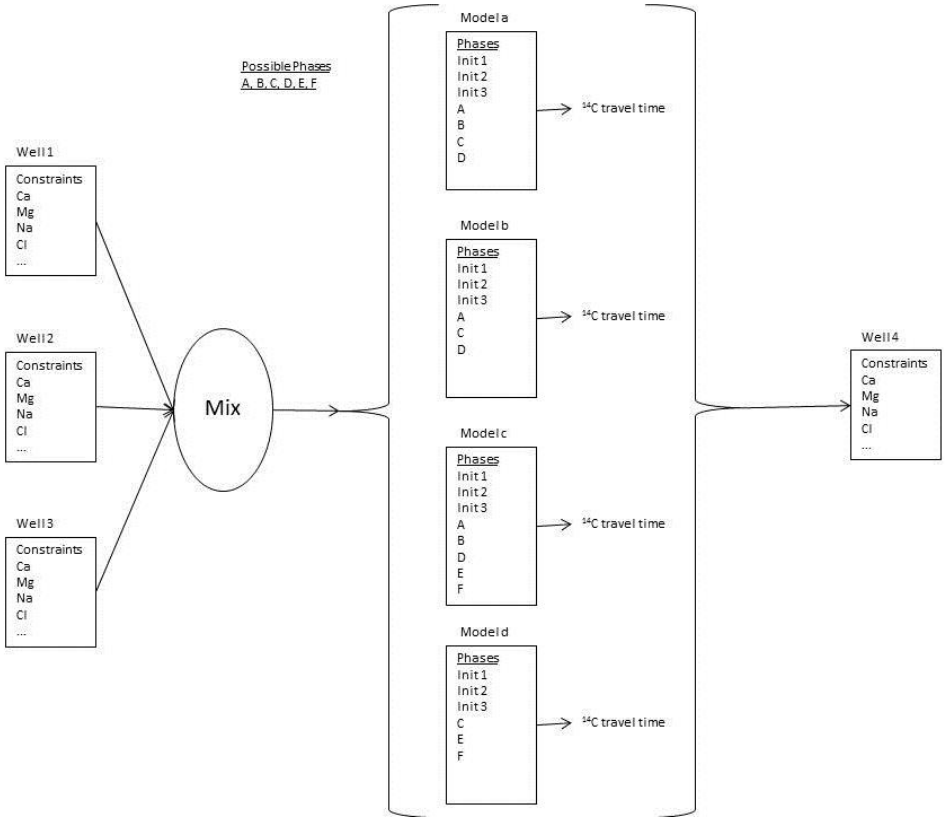

Figure 1. Conceptual model of a NETPATH simulation.

Testing of the methods to quantify uncertainty in water-rock reaction models using NETPATH was conducted on two previously modeled NNSS flow paths, one in the Frenchman Flat CAU and one in the Rainier Mesa/Shoshone Mountain CAU. Throughout this study, the nomenclature of the source wells used by NETPATH was maintained. NETPATH numbers the upgradient wells according to their order in the input file. The order is arbitrary, but for the purpose of this study, the following applies: In the Frenchman Flat example (Hershey *et al.*, 2005), wells 1, 2, and 3 are represented by Cane Spring, well ER-5-3 #2, and Indian Springs. The downgradient well is Army #1 Water Well (Figure 2). For the Rainier Mesa example (Hershey *et al.*, 2008), wells 1, 2, and 3 are U12e Tunnel, well USGS HTH #1, and well UE-1c. The downgradient well is ER-12-3 (Figure 2). Also, in NETPATH, a *model* is simply a unique set of mineral phases in a given simulation and should not be confused with a computer model. To avoid confusion, the computer models in this study will be specified by name and a *simulation* will refer to a single execution of the NETPATH computer code.

It is important to note that the construction and justification of the example flow paths and water-rock reaction models used in this study are from previous geochemical reports. The uncertainty and sensitivity methods developed in this study for NETPATH are applied to the two examples (from previous reports) to examine how the methods work. It is not the purpose of this report to reexamine the flow path and the water-rock reaction models or to evaluate whether they are still valid based upon new information about the CAUs since the original geochemical reports (Hershey *et al.*, 2005 and Hershey *et al.*, 2008) were written.

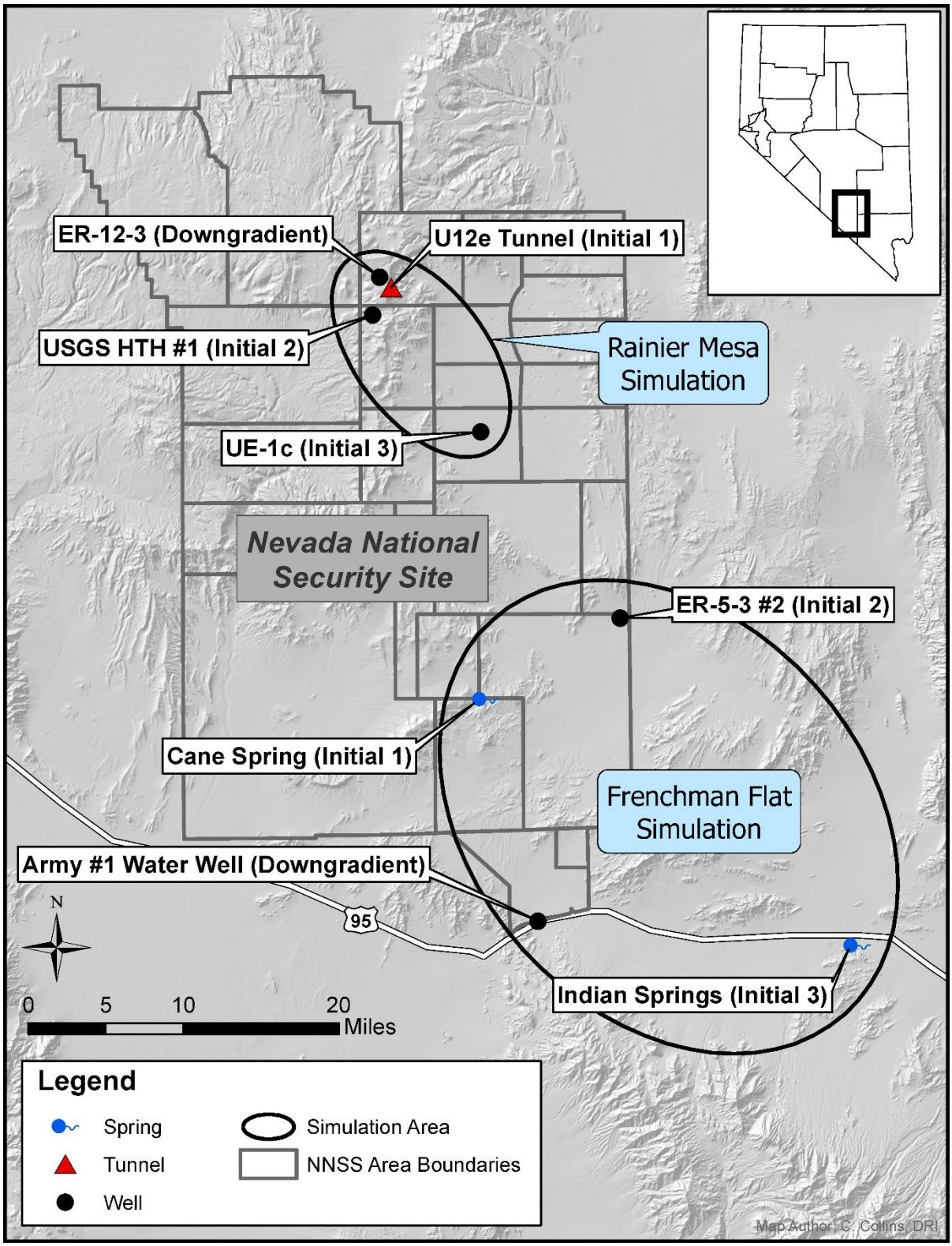

Figure 2. Location map of NNSS and example simulations.

The same computer code was used to run the Monte Carlo simulations that was used for the single, deterministic simulation. To compare models across simulations in the Monte Carlo analysis, it was necessary to rename models. Instead of Model 1, Model 2, etc., models were renamed with a two-letter code, resulting in model names such as Model aG or Model be. Finally, NETPATH does not consistently maintain the names of wells throughout the simulations. Upgradient wells are numbered and source-water fractions—represented by each upgradient well—are called "Init 1", "Init 2", etc., to correspond to well numbers assigned by NETPATH.

Figure 3 shows some of the results for the Frenchman Flat example simulation, described below. Five geochemically feasible models were found, each with a different set of phases. Each phase is precipitated or dissolved as shown and each model has an associated source-water fraction and ^{14}C travel time. A positive value for the amount of a phase change means the phase dissolved; a negative value means the phase precipitated. The reason for including these sample results here is to note that for one set of input constraint concentrations, there will exist multiple models, each with its own phase dissolution or precipitation amounts. In other words, one input can produce many outputs. It is this phenomenon that complicates the uncertainty and sensitivity analyses in this study.

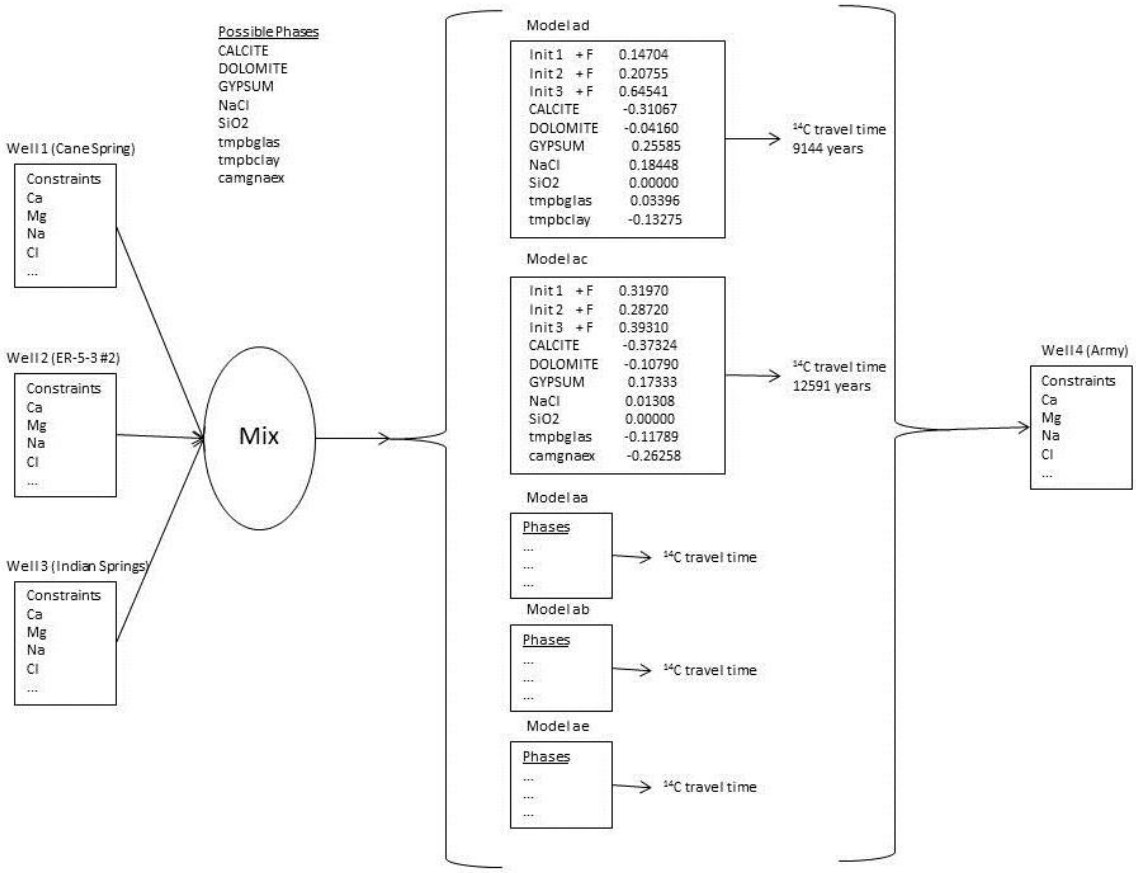

Figure 3. Example results from the Frenchman Flat example simulation. See Table 1 for model aa, ab, and ae results.

Although NETPATH may provide models that satisfy the constraints, it is up to the geochemist to determine if the results are geochemically reasonable. In this study, a water-rock reaction model was considered valid based upon criteria from previous studies at the NNSS (Hershey *et al.*, 2008; Farnham *et al.*, 2006; Rose *et al.*, 2006; Hershey *et al.*, 2005; Thomas *et al.*, 2002). In these previous studies the relatively dilute chemical makeup of most groundwater at the NNSS was taken into account when determining the criteria for valid water-rock reactions models. For a model to be considered valid, mass transfers had to be less than 1.0 millimole (mmol) of a given phase per kilogram (Kg) of water. Mass transfers greater than 1.0 mmol/Kg water indicated unrealistically large amounts of material (constraints and phases) moving into or out of solution. If this criterion was not met, then the model was considered to be invalid and was excluded from the analysis.

Also, to estimate ^{14}C groundwater travel times, the modeled $\delta^{13}C$ of the mixture should be close to the $\delta^{13}C$ signature of the final downgradient water. The analytical error in $\delta^{13}C$ by isotope ratio mass spectrometry ranges between 0.1 and 0.2 ‰. In previous studies (Hershey *et al.*, 2008; Farnham *et al.*, 2006; Hershey *et al.*, 2005; Rose *et al.*, 2006; Thomas *et al.*, 2002), modeled $\delta^{13}C$ signatures that were more than 1 ‰ different from the final downgradient water indicating a poor representation of the reactions for the carbon-containing phases along the flow path. These models were not used to estimate groundwater travel times. The $\delta^{13}C$ signatures that varied by more than 1 ‰ of the measured downgradient signature indicate that (1) the C-containing phases in the model are not all accounted for, (2) the $\delta^{13}C$ signatures used for calcite and dolomite in the models are not representative of the rock units or they have greater variability than measured, (3) the groundwaters chosen for the model are not representative of the actual mixture, or (4) some combination of these factors. To demonstrate these methods and provide realistic results, two demonstration simulations were analyzed for this study.

Frenchman Flat Example

One example of a NETPATH water-rock reaction model examined groundwater flowing southward out of Frenchman Flat (Figure 2) along a hypothetical flow path in the Lower Carbonate Aquifer (LCA) that included deep groundwater in Frenchman Flat represented by well ER-5-3 #2, groundwater from the Spring Mountains represented by Indian Springs, and local recharge represented by Cane Spring on the western edge of Frenchman Flat, mixing together to make downgradient groundwater south of Frenchman Flat represented by Army #1 Water Well (Hershey *et al.*, 2005). The constraints used in the water-rock reaction model from Hershey *et al.* (2005) included Ca, magnesium (Mg), sodium (Na), potassium (K), C, chloride (Cl), sulfur (S), and silica (Si). The phases used in the water-rock reaction model included calcite, dolomite, gypsum, NaCl, SiO_2, composite volcanic glass, composite clay, and Ca+Mg/Na exchange. The chemical compositions of the composite volcanic glass and composite clay represent average compositions for these phases as measured for the Timber Mountain hydrostratigraphic unit (HSU) in the Pahute Mesa CAU (Thomas *et al.*, 2002, Tables 1-3).

The NETPATH simulation of this system in Hershey *et al.* (2005) resulted in three valid models, each with a unique set of phases, source-water fractions, and travel times. In the Hershey *et al.* (2005) simulation, the composite volcanic glass was only allowed (forced) to dissolve, the composite clay was only allowed to precipitate, and Ca+Mg/Na ion exchange

was only allowed to dissolve (Ca and Mg in groundwater could only be removed, whereas Na could only be added). In the NETPATH simulation for the same system in this study, the forcing of these phases was not included to allow more variation in model results. In this example in this study, NETPATH produced six valid models. NETPATH models using these three sources of water produced mixtures between 14 and 29 percent ER-5-3 #2, 37 to 86 percent Indian Springs, and zero to 33 percent Cane Spring to make the water chemistry observed at Army #1 Water Well (Table 1). Small amounts of NaCl and gypsum dissolved while a small amount of calcite precipitated. Small amounts of dolomite, composite glass, and composite clay either precipitated or dissolved. Small amounts of Ca and Mg exchanged with Na in both directions, whereas SiO_2 was not involved in any of the reactions (Table 1).

Modeled $\delta^{13}C$ signatures for these mixtures ranged from -6.8 to -6.5 ‰, all within 1 ‰ of the measured $\delta^{13}C$ signature of Army #1 Water Well. For the mixtures of Cane Spring, ER-5-3 #2, and Indian Springs, groundwater travel times ranged from 3,900 to 5,700 years when the local recharge component from Cane Spring was very small (zero to four percent) and the Indian Springs component was large (80 to 86 percent). The mixtures with much more Cane Spring (15 to 33 percent) and less Indian Springs (37 to 86 percent) produced much longer travel times (9,100 to 12,800 years). The substantially longer travel times result from the larger proportion of local recharge from Cane Spring, which has a high ^{14}C activity (93 percent modern carbon [pmc]) relative to the downgradient well, Army #1 Water Well, which has a very low ^{14}C activity (4.1 pmc). Large differences in ^{14}C activity between upgradient and downgradient groundwater require more time for radioactive decay of ^{14}C to occur. A summary of precipitation/dissolution amounts, source-water fractions, and travel times for each model of the deterministic model is shown in Table 1. The NETPATH output is in Appendix A.

Table 1. Summary of deterministic model results for the Frenchman Flat example. For mineral phases, positive values denote dissolution and negative values denote precipitation.

	Model aa	**Model ab**	**Model ac**	**Model ad**	**Model ae**	**Model af**
Calcite (mmol/Kg water)	-0.38	-0.32	-0.37	-0.31	-0.26	-0.27
Dolomite (mmol/Kg water)	-0.11	-0.06	-0.11	-0.04	0.01	
Gypsum (mmol/Kg water)	0.17	0.24	0.17	0.26	0.33	0.31
NaCl (mmol/Kg water)		0.15	0.01	0.18	0.33	0.29
SiO_2 (mmol/Kg water)	0	0	0	0		0
Ca+Mg/Na Exchange (mmol/Kg water)	-0.28	-0.06	-0.26		0.22	0.16
Composite Clay (mmol/Kg water)	0.01	-0.10		-0.13	-0.25	-0.22
Composite Glass (mmol/Kg water)	-0.13		-0.12	0.03	0.16	0.13
$\delta^{13}C$ (‰)	-6.50	-6.63	-6.51	-6.66	-6.78	-6.76
Cane Spring (%)	0.33	0.19	0.32	0.15	0.00	0.04
ER-5-3 #2 (%)	0.29	0.22	0.29	0.21	0.14	0.16
Indian Springs (%)	0.37	0.59	0.39	0.64	0.86	0.80
^{14}C Travel Time (years)	12,800	10,100	12,600	9,100	3,900	5,700

Rainier Mesa Example

A second example of a water-rock reaction model examined hypothetical groundwater flow downward from the unsaturated volcanic units in Rainier Mesa to the LCA beneath Rainier Mesa. This flow path included U12e Tunnel representing the water in the unsaturated volcanic units mixing with volcanic groundwater (USGS HTH #1) and upgradient LCA carbonate groundwater (UE-1c used as a surrogate to represent this groundwater) to make the observed water chemistry in the LCA beneath Rainier Mesa represented by well ER-12-3 (Hershey *et al.*, 2008). The constraints used in the water-rock reaction model from Hershey *et al.* (2008) included Ca, Mg, Na, K, C, Cl, S, and Si. The phases used in the water-rock reaction model included calcite, dolomite, CO_2 gas, gypsum, NaCl, SiO_2, composite volcanic glass, composite feldspar, composite clay, composite zeolite, strontianite, and Ca+Mg/Na exchange. The chemical compositions of the composite volcanic glass and feldspar and composite clay and zeolite represent average compositions for these phases as described in (Hershey *et al.*, 2008; Tables 14 and 15). The criteria for a valid water-rock reaction model and the estimation of ^{14}C travel times are the same as described above for the Frenchman Flat example.

Mixtures included U12e Tunnel (23 to 25 percent) with volcanic groundwater from USGS HTH #1 (31 to 33 percent) and surrogate upgradient LCA groundwater from UE-1c (42 to 46 percent). Small amounts of a few phases dissolved (gypsum and SiO_2) while small amounts of multiple other phases precipitated (calcite, CO_2 gas, composite clay, and composite zeolite). Small amounts of Ca and Mg in solution exchanged with Na from mineral surfaces. Insignificant amounts of composite feldspar and composite glass were involved in the reactions.

Modeled $\delta^{13}C$ signatures for the valid mixtures ranged from -6.0 to -5.6 ‰. For the mixtures of tunnel water, volcanic groundwater, and surrogate upgradient LCA water, groundwater travel times ranged from 14,800 to 15,700 years. Because this simulation had many more phases than constraints, there were 495 possible combinations of phases. The NETPATH simulation found 43 models that satisfied the constraints. Further evaluation of the models, subject to the constraints described above, showed many models to be geochemically unreasonable and were discarded. There were five models that satisfied all criteria. These models are summarized in Table 2. Extremely small values are represented by 0.00 in the table to identify the phases that were considered for each model, even if their precipitation amounts were trivial. The NETPATH output is in Appendix B.

Table 2. Summary of deterministic model results for the Rainier Mesa example. For mineral phases, positive values denote dissolution and negative values denote precipitation.

	Model aB	Model aJ	Model af	Model aj	Model as
Calcite (mmol/Kg water)	-0.15	-0.22	-0.22	-0.22	-0.22
CO_2 Gas (mmol/Kg water)	-0.53	-0.58	-0.58	-0.58	-0.58
Dolomite (mmol/Kg water)					
Exchange (mmol/Kg water)	-0.21	-0.23	-0.23	-0.23	-0.23
Gypsum (mmol/Kg water)	0.06	0.05	0.05	0.05	0.05
NaCl (mmol/Kg water)					
Composite Clay (mmol/Kg water)		-0.17	-0.17	-0.17	-0.17
Composite Feldspar (mmol/Kg water)			0.00	0.00	
Composite Glass (mmol/Kg water)	0.00	0.00			
Composite Zeolite (mmol/Kg water)	-0.34	-0.01		-0.01	-0.01
Strontianite (mmol/Kg water)	0.00	0.00	0.00	0.00	0.00
SiO_2 (mmol/Kg water)	0.90		-0.01		0.00
$\delta^{13}C$ (‰)	-6.0	-5.6	-5.6	-5.6	-5.6
U12e Tunnel (fraction)	0.25	0.23	0.23	0.23	0.23
USGS HTH #1 (fraction)	0.33	0.31	0.31	0.31	0.31
UE-1c (fraction)	0.42	0.46	0.46	0.46	0.46
^{14}C Travel Time (years)	15,700	14,800	14,800	14,800	14,800

APPROACH

Uncertainty Analysis Using Monte Carlo Sampling

Overview

For this analysis, a Monte Carlo approach was chosen to evaluate uncertainty. In this approach, because uncertainty exists in constraints, phases, and flow paths, uncertainty exists in outputs such as phase dissolution/precipitation and travel time. Uncertain variables are represented by a probability distribution rather than a discrete value. Samples were selected randomly from these distributions, the simulation was performed with these random samples, and the output was recorded. After many simulations, the output was aggregated and evaluated.

A Monte Carlo approach explores the parameter space of uncertain variables and examines the effect this uncertainty has on outputs. With this method, one can answer the question: Given a reasonable uncertainty in inputs, what variability can be expected in the output?

More specifically, the approach for this study included:

- identifying the uncertain variables and parameters
- determining or assuming a distribution of each random variable
- selecting a random sample from each distribution
- running the simulation and recording the output
- repeating the previous two steps until each distribution is adequately represented
- summarizing the output and evaluating the uncertainty using all simulation results.

Using the Frenchman Flat and Rainier Mesa example problems, it was assumed that all constraints contain uncertainty. Ideally, there would be enough sample data for each constraint at each well to determine a representative distribution, but unfortunately this is not the case (for an in-depth discussion of constraint distributions in groundwater for the Rainier Mesa CAU, see Hershey *et al.* [2006]). Therefore, a simple uniform distribution was assumed appropriate and a coefficient of variation (defined as the standard deviation divided by the mean) was estimated. The measured value of each constraint was assumed to be the mean.

Evaluation

For this study, it was necessary to evaluate the results slightly differently from a typical Monte Carlo analysis. A typical Monte Carlo analysis will have uncertain variable inputs, fixed model parameters, and the resulting variable output. Flow-path, inverse, water-rock reaction modeling using NETPATH usually results in nonunique solutions. The nonuniqueness is represented by one or more models, each of which satisfies the constraints of the simulation. Also, these models differ from simulation to simulation. For example, one simulation may result in models A, B, and C, whereas another simulation results in models B and D. The complication arises in interpreting the variability in model selection as a result of variability in constraints. Because a model in this context is a unique set of phases and not a continuous random variable, it is conceptually difficult to interpret the relationship between uncertainty in constraints and variability in model selection. Instead, model selection was simply tabulated from all simulations and ranked according to frequency of occurrence.

Another result from Monte Carlo analysis is the dissolution/precipitation amounts of each phase, the fraction of each upgradient well, and distribution of travel times. Evaluation of these data is complicated by the fact that each simulation can result in many values of source-water fraction and travel time, one result for each model. In other words, one input can produce many outputs. However, even allowing for these idiosyncrasies, interpretation of the results is straight forward and includes summary statistics and histograms or boxplots to assist the geochemist.

Sensitivity Analysis

Overview

In contrast to Monte Carlo simulations, where the uncertainty in output is evaluated because of uncertainty in the entire system, sensitivity analysis is the evaluation of the change in output caused by a small change in the input of one constituent at a time. Sensitivity is calculated as the slope of the output-input relationship centered around the input's mean value:

$$S = {}^{\partial Y}/_{\partial X} \quad (1)$$

where S is sensitivity, ∂Y is the partial derivative of the output, and ∂X is the partial derivative of the input. This value depends on the units of Y and X, which makes it difficult to compare sensitivity across variables. This problem is solved by standardizing the changes in output and input. Standardizing consists of dividing each change by its original value, making S dimensionless:

$$S = \frac{{}^{\partial Y}/_{Y}}{{}^{\partial X}/_{X}} \quad (2)$$

In discrete form:

$$S = \frac{\Delta Y}{\Delta X}\frac{X}{Y} \quad (3)$$

Both the change in output and input can now be expressed as fractions of their original values and the dimensionless S can be compared across constituents. Sensitivity can be expressed as the percent change in output because of a small change in input, holding all other input variables fixed at their original (mean) values. The change in X is assigned by the user and must be a small enough change such that the equilibrium of the simulation is not affected. For this study, a one percent change in input was used.

Computation

Custom scripts

For this study, the simulations were facilitated by custom scripting and statistical code. Codes written in Python and R modify input parameters, run the NETPATH simulations, extract relevant output from text files, postprocess the results, and produce graphs and summaries. The code reads user-specified values for each constituent's coefficient of variation, distribution, sensitivity parameter, maximum dissolution or precipitation amounts, and number of Monte Carlo simulations. Currently the available distributions are: uniform, normal, and log-normal and are implemented in the Python code using the numpy random module. Also, each constituent can be described by a unique coefficient of variation and distribution. The specifications are included in an editable, well-commented configuration file listed in Appendix C.

These custom scripts are designed to read the output from DB and NETPATH version 2.13. For these codes to be applicable to other versions of DB and NETPATH, the output must have the identical form as version 2.13. The scripts look for specific words, phrases, or other identifiers in the output to find the relevant information for postprocessing.

The scripts can be applied by running the files through a Python or R interpreter. Python version 2.7 and R version 2.11 were used during development. It is expected that the Python code will run successfully under any Python 2.7 version and the R code will run under any R v2.x branch; the code was not tested on the Python v3 branch or the R v3 branch. The scripts should be run interactively by someone with a good knowledge of Python and R. There are parts of each code dedicated to making plots for quality assurance and running these codes non-interactively may results in hundreds of unwanted files. Also, the code is documented in-line to guide the user, as there is no user's manual.

NETPATH and DB

When geochemical modelers refer to the program NETPATH, they typically mean the combination of two codes: DB and NETPATH. Originally, modelers were required to use DB first, then NETPATH. The database program DB allows entering and editing of chemical and isotopic data for a set of water analyses (Plummer *et al.*, 1994). The DB output files are then used directly as input to NETPATH. NETPATHXL is an upgrade to the DB/NETPATH models and allows the constraints to be read from a formatted Excel spreadsheet. NETPATHXL runs DB automatically and transparently without any user interaction.

To run Monte Carlo or sensitivity analysis, constraint concentrations have to be modified and then DB run to calculate the concentrations of different ionic species of the dissolved constraints. For example, for the Ca constraint, some of the ionic species include Ca^{2+}, $CaOH^{+}$, and $CaHCO_3^{+}$, etc. Once this step is complete the NETPATH simulation can begin. To run hundreds or thousands of simulations, it is necessary to use scripts to change text files, run software, and read the output programmatically. Ideally, the Excel spreadsheet in NETPATHXL would be modified programmatically. However, this proved to be a fragile and unreliable task. Therefore, using the custom code developed for this study, an original Excel data file is read to get initial constraint concentrations and generate the input files required to run DB. The output of DB is then used as input to NETPATH. To run thousands of simulations, it was necessary to run DB and NETPATH separately rather than using NETPATHXL.

To run DB and NETPATH, it was also necessary to recompile the FORTRAN code for modern, 64-bit operating systems. The source codes for NETPATH and DB, both versions 2.13, were compiled for this study. The codes have no external dependencies and compiled without errors using the GFortran (v.4.5.2) compiler. Simulations were performed on the Rainier Mesa problem using (1) the newly-compiled DB and NETPATH, and (2) NETPATHXL. Results were compared and confirmed that each code produces identical results. This was expected because according to the NETPATHXL documentation (Parkhurst and Charlton, 2008), the NETPATHXL calculation engine is identical to the original NETPATH. Only very minor modifications to the DB and NETPATH codes were needed. Several lines in the original FORTRAN code were changed to allow the simulations to run without user intervention. The output from each version's simulation is included on the CD Appendix. For the purposes of this study, NETPATH refers to a DB/NETPATH simulation and the original simulation is called the deterministic simulation.

All source code and documentation used in this study, including the modified NETPATH and DB codes and custom scripts, are included in Appendix D. For the digital version of this report Appendix D will be delivered as an attached zip file. For the hardcopy version Appendix D will be included as an attached compact disk. A detailed description of the contents is included in a file named README.txt.

UNCERTAINTY ANALYSIS RESULTS

To evaluate uncertainty, 15,000 simulations were run, but any number of simulations can be run depending on the modeler's requirements. Each simulation used a different input data set with concentrations drawn from a uniform distribution with a coefficient of variation (CV) of 0.1. The value for CV was arbitrarily chosen for this study simply to demonstrate the approach. Upon inspection of the corresponding range of values for constraints, it was concluded the assumption is reasonable. However, for future studies, there may be a benefit in testing how the CV affects the results. For example, measured Ca in the U12e Tunnel well was 5.53 mmols/Kg water. With a CV equal to 0.1, the standard deviation was 0.553 and the resulting range of its uniform distribution was 4.57 to 6.49 mmols/Kg water. For a uniform distribution, the distribution is defined by its range. The range is calculated as: $range = \sqrt{\sigma^2 * 12}$ where σ is the standard deviation. The models, phase dissolution/precipitation, source-water fraction, and ^{14}C travel time were saved from each simulation for postprocessing. Postprocessing included removing the results that didn't satisfy the user-specified restrictions for valid models, computing summary statistics, and producing plots.

To ensure that inputs were selected properly, it was important to compute summary statistics and evaluate the distribution of the inputs. Recall that input constraints were selected randomly from their prescribed distributions. It is important to ensure that the computed mean and coefficient of variation of the random samples equals those prescribed by the user. This is simply a quality assurance step before continuing with the analysis. The mean and CV for each constraint were compared to their prescribed values and all results were within 0.05 percent. The Chi-squared hypothesis test was used to compare the sample distribution to a synthetic, prescribed distribution with the same mean and variance under the null hypothesis that the two samples come from the same distribution. This test was performed for each well-constraint combination and all tests passed at the 0.05 confidence level. For a visual comparison, the empirical cumulative distribution functions (CDFs) of the prescribed and sample distributions were plotted as in Figure 4, where *sample* refers to the sample dataset and *reference* refers to the prescribed distribution.

Also, it is important to ensure that results from Monte Carlo simulations have stabilized. The law of large numbers states that the difference between the sample mean and the true mean decreases as the number of samples increases (Bean, 2001). In application to Monte Carlo simulations, when the cumulative mean stabilizes, additional samples will not significantly improve the estimate and the Monte Carlo simulation has enough samples to describe sufficiently the underlying distribution. To evaluate this graphically, the cumulative mean travel time was plotted against simulation number. If the results stabilized, then the cumulative mean stabilized. Figure 5 shows the stabilized mean ^{14}C travel time for the Rainier Mesa example problem. To be conservative and ensure the number of samples was sufficient, 15,000 samples were used in this study. A similar result was found for the Frenchman Flat example.

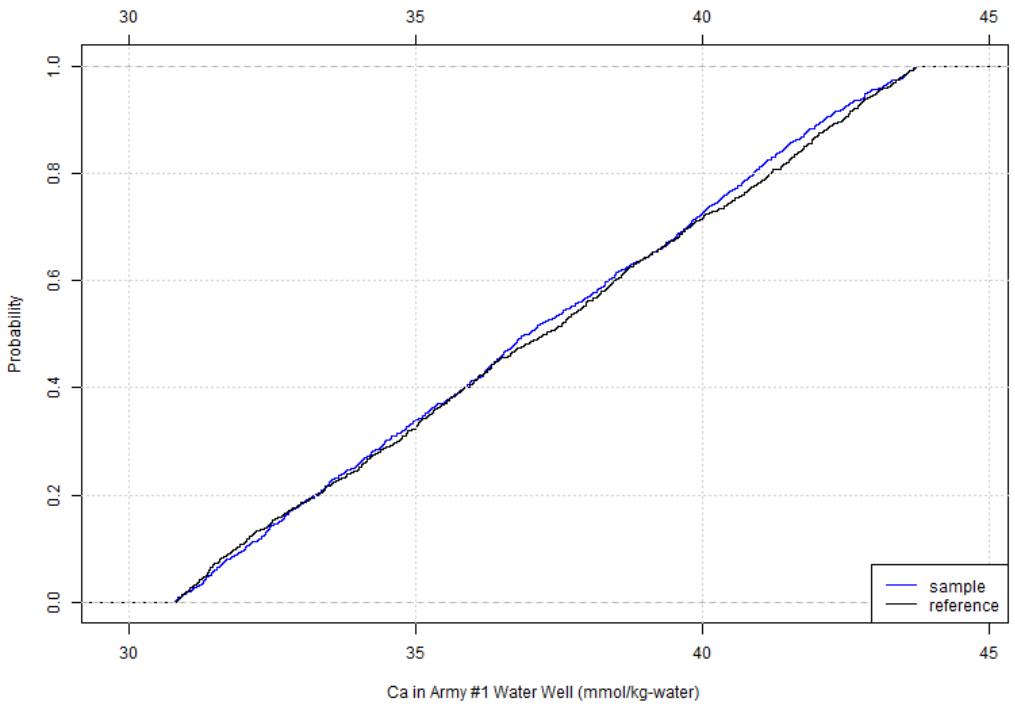

Figure 4. Empirical cumulative distribution function of the prescribed and sample distributions for calcium in the Army #1 Water Well.

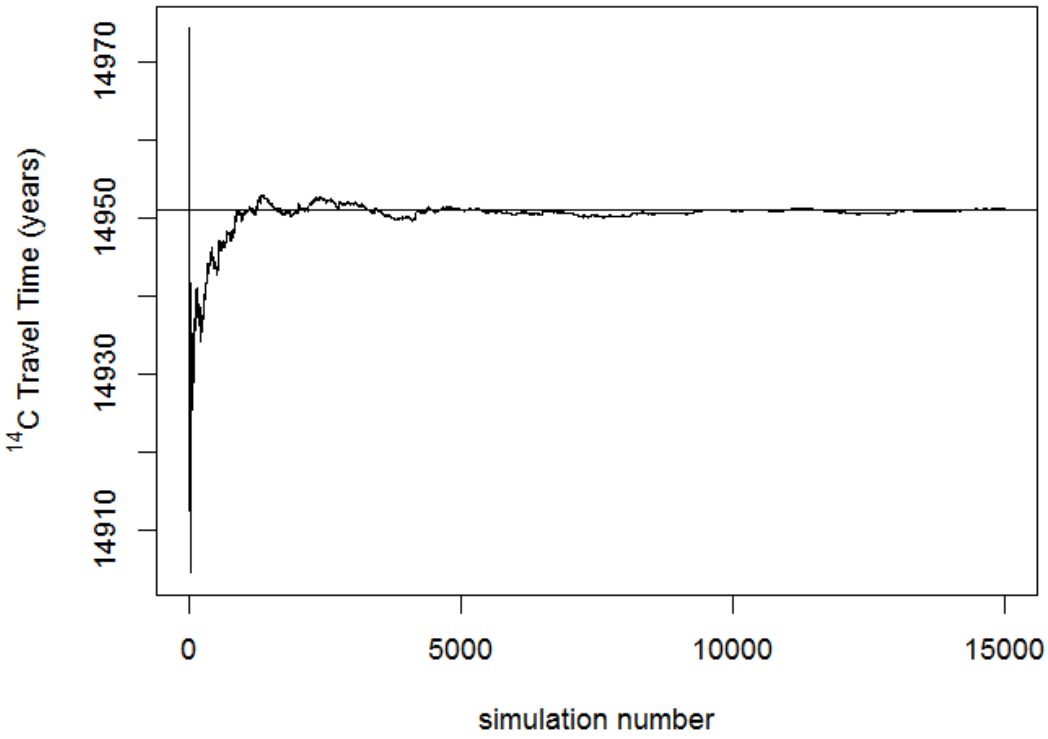

Figure 5. Cumulative mean ^{14}C travel time for the Rainier Mesa Monte Carlo simulations.

Models

The resulting models from a NETPATH simulation are not necessarily fixed from one simulation to the next if the constraint concentrations change. One simulation may result in eight models, whereas another may result in four. The four models from the second simulation are also not necessarily a subset of the eight models from the first. Combining the results from these two simulations results in between 8 and 12 feasible models.

The selection of models is a noncontinuous result and cannot be evaluated in the same manner as phases, source-water fraction, or travel time. Some models occurred more frequently than others. That is, some exist in most simulations, whereas some are feasible only as a result of rare combinations of constraint inputs. However, model frequency does not mean a model is more or less likely to be valid. All models produce valid flow paths where dissolution or precipitation of the mineral phases satisfies the up- and downgradient geochemical criteria.

Phases

How the uncertainty in constraints affects phase dissolution or precipitation is also of interest. This approach is more straightforward because both inputs and outputs are continuous, but it is complicated by the fact that each random sample of constraints results in multiple values of each phase. By itself, the amount of phase dissolution or precipitation is not very important, per se, to the geochemist other than meeting the previously specified criterion of less than 1 mmol/Kg water phase change. Rather, these amounts and the source-water fractions directly affect travel times. Therefore, the effect of uncertainty on changes in phase amounts is presented here only to highlight patterns or outliers. The restrictions described above—namely that precipitation or dissolution amounts must be less than 1 mmol/Kg water and the $\delta^{13}C$ balance must be within 1.0 ‰—serve to eliminate unrealistic models, so all remaining results should be valid.

Results from the deterministic simulations are presented in Tables 1 and 2. The results of the Monte Carlo simulations can be presented as summary statistics in tables (e.g., Tables 3 and 4) or figures (for example the calcite results in the Frenchman Flat example shown in Figure 6). For this study, each example problem was run 15,000 times.

Simulation results for each phase can be evaluated further. For example, in Figure 6, the deterministic simulation's histogram shows calcite values equally distributed between -0.32 and -0.22 mmol/Kg water, whereas the Monte Carlo results show a wider distribution and slightly higher frequencies around -0.38 and -0.28 mmol/Kg water. These modes are the result of several models, each with a narrower range of calcite dissolution amounts. Identifying the range by model may yield additional insight. The benefit of presenting Monte Carlo results separated by model is the ability to see which models are responsible for different parts of the histogram. Note that the maximum amount of calcite precipitation in the Monte Carlo simulations (-0.38 mmol/Kg water) equates to 15 mg/L of Ca being removed from solution, or approximately one third the amount of Ca in the groundwater system being modeled (Army #1 Water Well = 44 mg/L Ca, Indian Springs = 42 mg/L Ca, ER-5-3 #2 = 77 mg/L Ca, Cane Spring = 37 mg/L Ca). However, the maximum amount of dissolution of gypsum (0.32 mmol/Kg water, Table 3) adds 12.8 mg/L to solution, so net change in Ca in solution is only 2.2 mg/L, ignoring the other Ca containing phases (dolomite, Ca+Mg/Na exchange, tmpbclay, and tmpbglass).

Figure 7 shows the same results grouped by model. This style of plot is only feasible if the total number of models is small. With identical horizontal and vertical scales, one can compare the range and frequency of a phase across models, and also compare the Monte Carlo results (represented by the histogram) with the deterministic result (red line). This figure shows that Models aa and ac are responsible for most of the lower values, Models ab and ad are responsible for the middle values, and Models ae and af are primarily responsible for the higher values. Figure 8 shows an example for calcite in the Rainier Mesa simulation.

Table 3. Summary statistics of Monte Carlo simulations for the Frenchman Flat example. Values in mmol/Kg water except for $\delta^{13}C$ (‰) and ^{14}C (years); Q1 and Q3 refer to the first and third quartiles of the sample distribution; SD is the standard deviation of the distribution.

Phase	Min	Q1	Median	Mean	Q3	Max	SD
Calcite	-0.38	-0.31	-0.27	-0.28	-0.24	-0.18	0.05
$\delta^{13}C$	-9.77	-8.72	-8.13	-8.11	-7.46	-6.61	0.77
^{14}C travel time	3,800	4,400	9,600	9,200	12,400	15,600	3,600
Dolomite	-0.18	-0.11	-0.06	-0.07	-0.04	0.00	0.05
Gypsum	0.03	0.15	0.20	0.19	0.25	0.32	0.07
NaCl	-0.21	0.00	0.14	0.14	0.26	0.32	0.13
SiO_2	0.00	0.00	0.00	0.00	0.00	0.00	0.00
Ca+Mg/Na Exchange	-0.56	-0.25	-0.06	-0.09	0.16	0.21	0.21
tmpbclay	-0.22	-0.18	-0.10	-0.09	0.00	0.15	0.09
tmpbglas	-0.27	-0.10	0.02	-0.01	0.11	0.14	0.12

Table 4. Summary statistics of Monte Carlo simulations for the Rainier Mesa example. Values in mmol/Kg water except for $\delta^{13}C$ (‰) and ^{14}C (years); Q1 and Q3 refer to the first and third quartiles of the sample distribution; SD is the standard deviation of the distribution.

Phase	Min	Q1	Median	Mean	Q3	Max	SD
Calcite	-0.26	-0.23	-0.21	-0.21	-0.19	-0.13	0.03
CO_2 GAS	-0.68	-0.62	-0.57	-0.57	-0.52	-0.17	0.06
$\delta^{13}C$	-7.29	-6.33	-5.72	-5.70	-5.10	-4.34	0.75
^{14}C travel time	14,800	14,800	14,800	15,000	14,800	19,100	400
Dolomite	0.10	0.10	0.10	0.10	0.10	0.11	0.00
Ca+Mg/Na Exchange	-0.33	-0.25	-0.23	-0.23	-0.21	-0.17	0.03
GYPSUM	0.04	0.05	0.06	0.06	0.06	0.13	0.01
PBR.Clay	-0.20	-0.18	-0.17	-0.17	-0.15	-0.07	0.02
PBR.Feld	0.00	0.00	0.00	0.00	0.00	0.00	0.00
PBR.Glas	0.00	0.00	0.00	0.00	0.00	0.00	0.00
PBR.Zeol	-0.38	-0.01	-0.01	-0.08	-0.01	-0.00	0.13
Strontianite	-0.00	-0.00	-0.00	-0.00	-0.00	-0.00	0.00
SiO_2	-0.02	-0.01	0.00	0.25	0.78	1.00	0.40

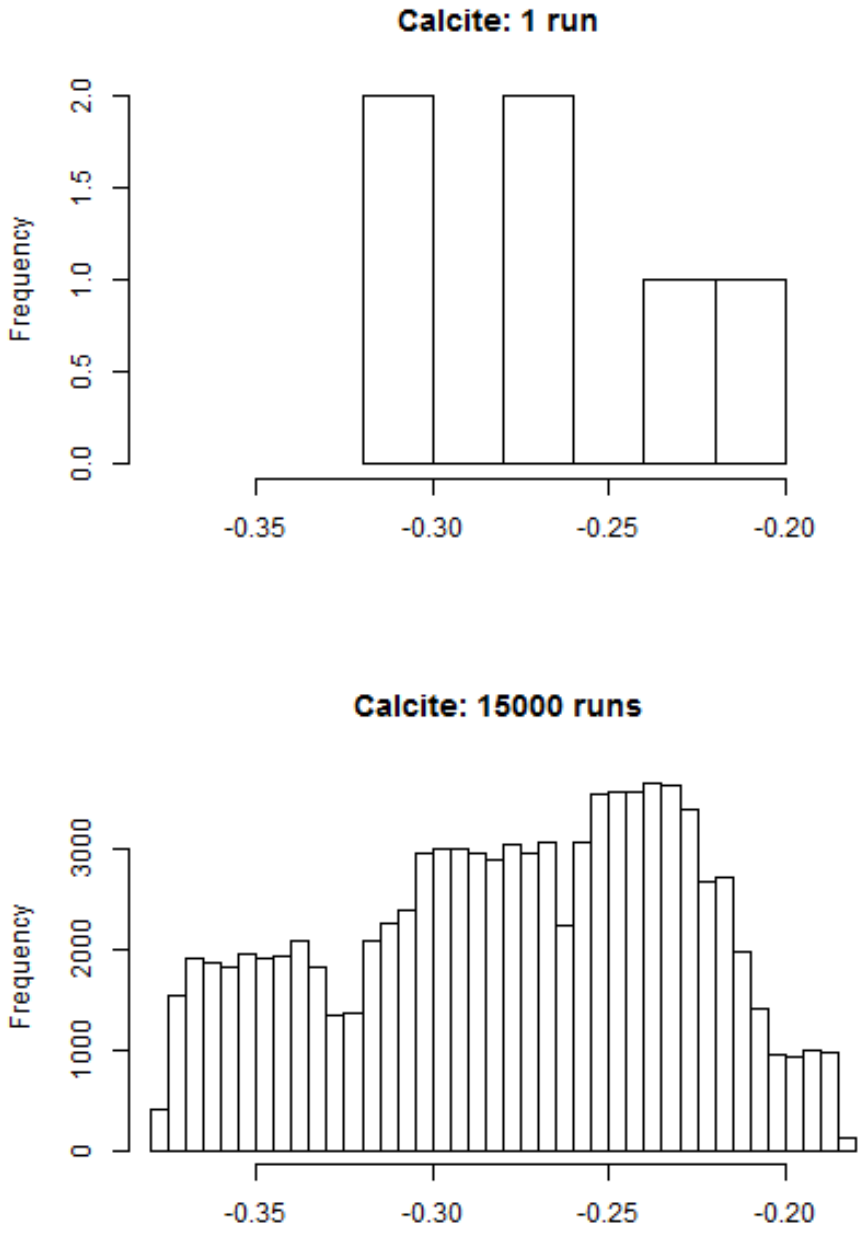

Figure 6. Comparison of results from the deterministic (top) and Monte Carlo (bottom) simulations for calcite in the Frenchman Flat example. Negative values along *x*-axis denote mmol/Kg of water of the mineral phase (calcite) precipitated.

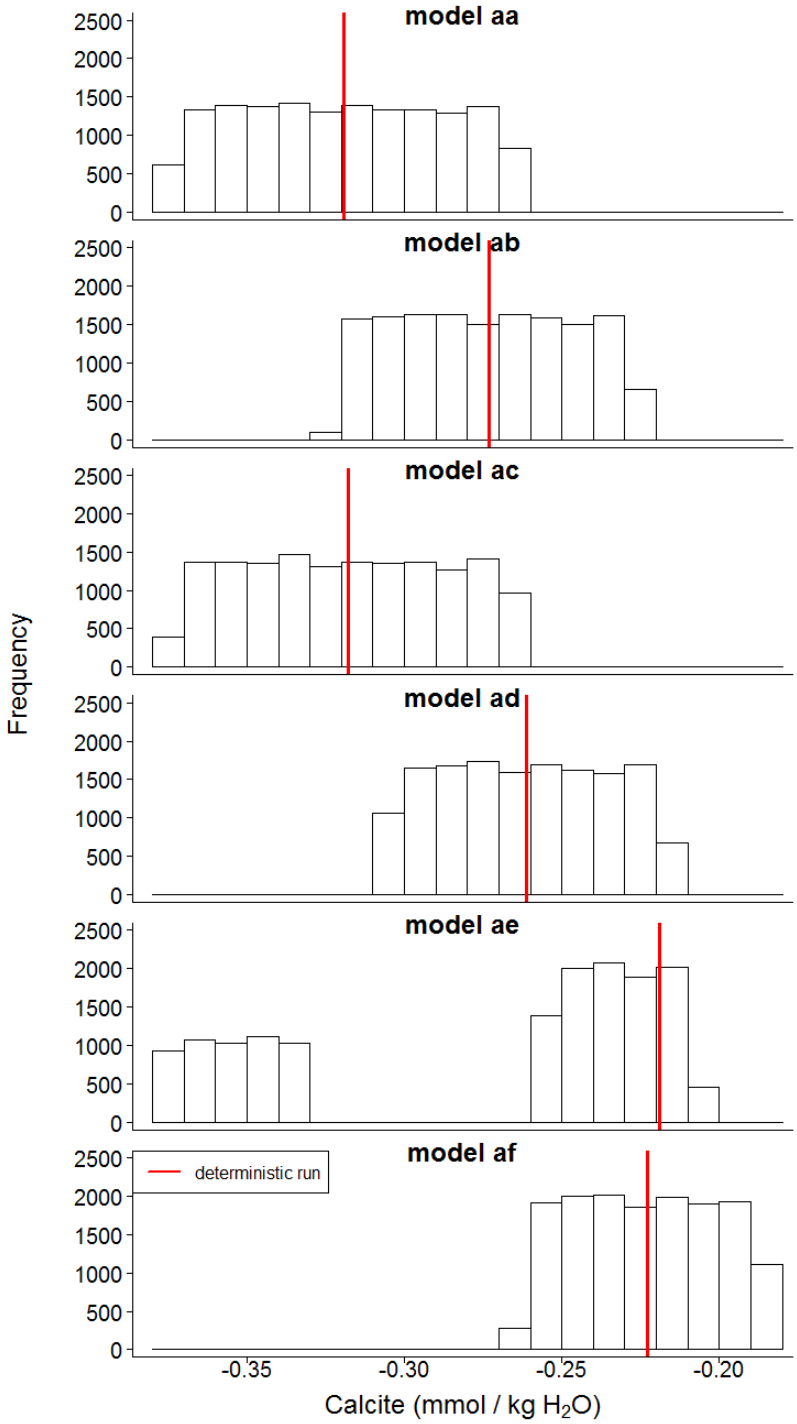

Figure 7. Monte Carlo simulation results for calcite in the Frenchman Flat example separated by model. The red line represents the results of the deterministic solution.

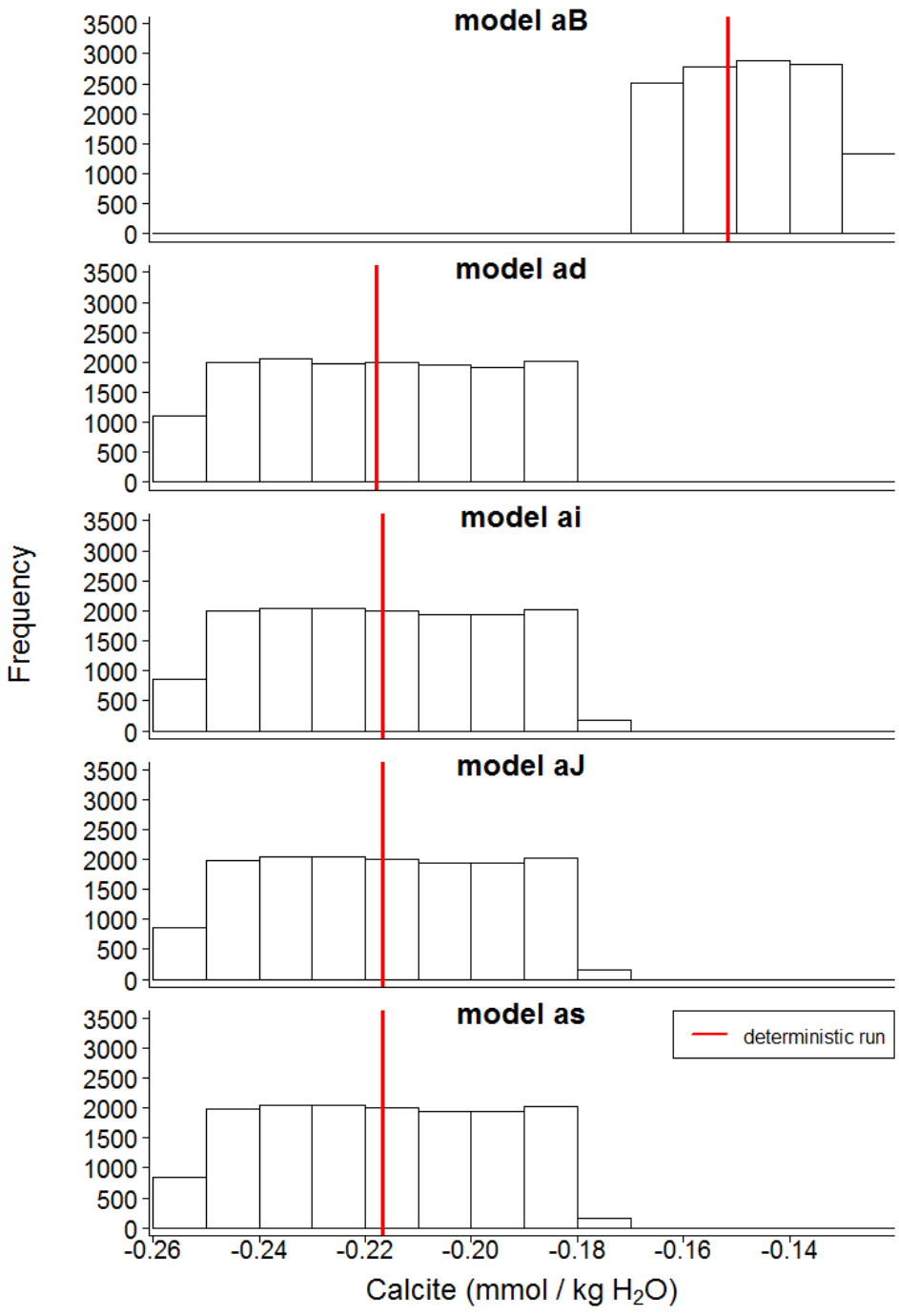

Figure 8. Monte Carlo simulation results for calcite in the Rainier Mesa example separated by model. The red lines represent the results of the deterministic simulations.

Source-water Fraction

A similar analysis can be performed for source-water fraction. These values are represented in NETPATH as Init 1, Init 2, and Init 3. Histograms (Figure 9 for the Frenchman Flat example; Figure 10 for the Rainier Mesa example) and summary statistics (Tables 5 and 6) again provide the most information. Referring to the histograms in Figures 9 and 10, there is almost no variation within or across models. Allowing variation in the constraints appears to affect only Model ae in the Frenchman Flat example and has no effect on source-water fractions in Rainier Mesa. By inspection, the values from the deterministic run for each well (the red lines in Figure 9; red lines not shown in Figure 10) appear to be representative of the system as a whole, with the exception of model ae for Frenchman Flat.

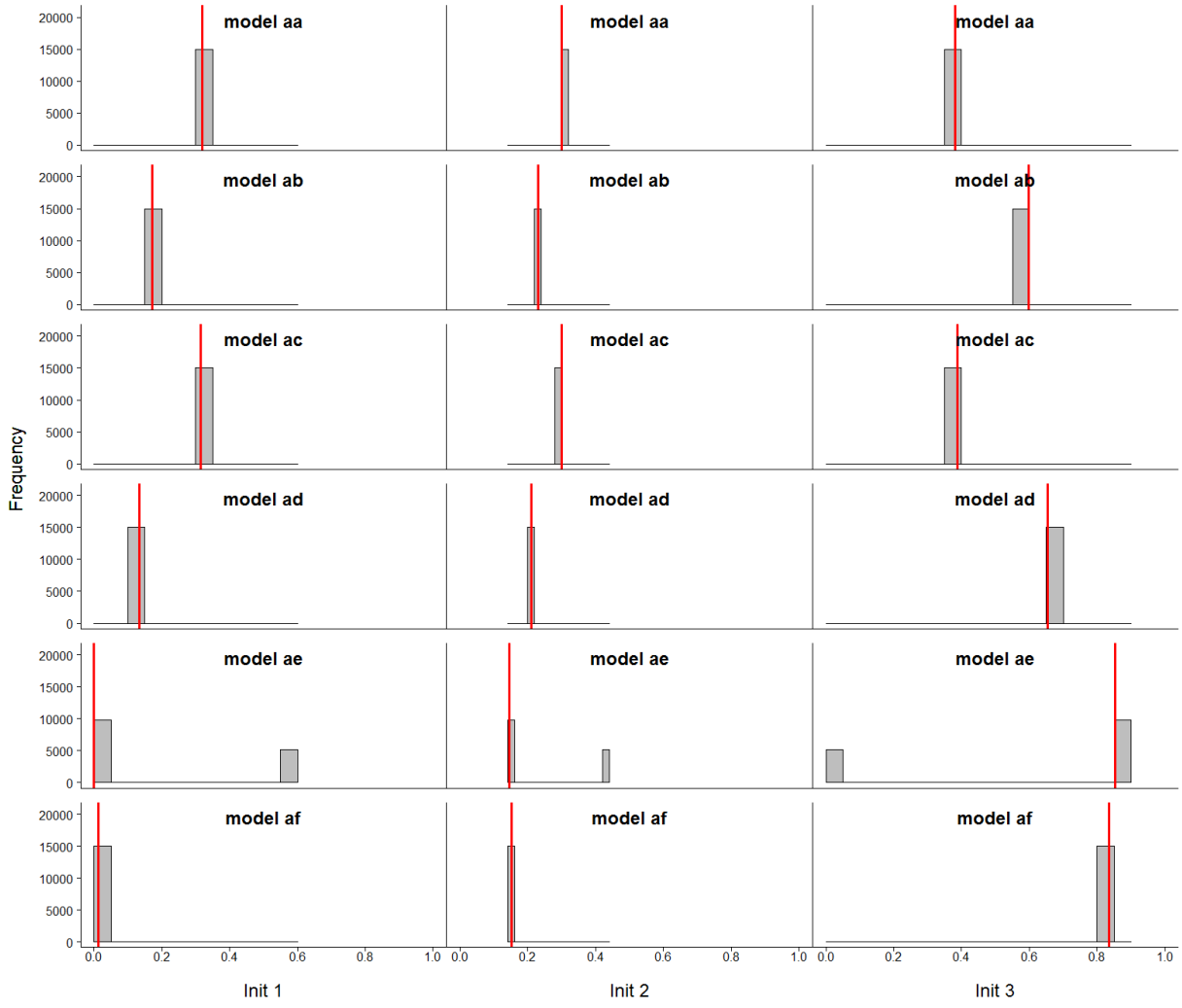

Figure 9. Histograms of source-water fractions for each well in the Frenchman Flat example separated by model. The red lines represent the results of the deterministic simulation.

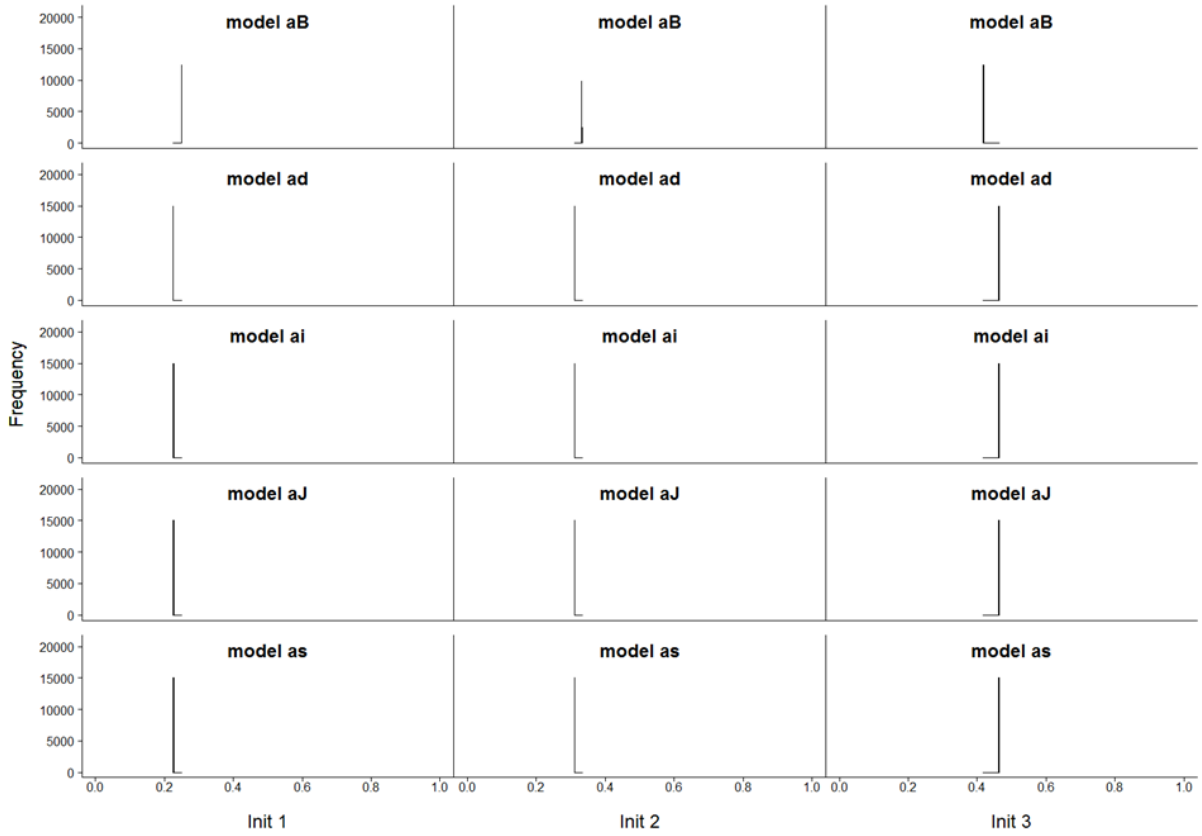

Figure 10. Histograms of source-water fractions for each well in the Rainier Mesa example separated by model. The red lines for the deterministic simulation are not shown for clarity because they plot on top of the Monte Carlo results.

Table 5. Summary statistics of source-water fractions from the Monte Carlo simulations for the Frenchman Flat Example; Q1 and Q3 refer to the first and third quartiles of the sample distribution; SD is the standard deviation of the distribution.

Source	Min	Q1	Median	Mean	Q3	Max	SD
Cane Spring	0.00	0.01	0.17	0.19	0.31	0.58	0.15
ER-5-3 #2	0.15	0.15	0.23	0.24	0.30	0.43	0.07
Indian Springs	0.00	0.39	0.60	0.57	0.84	0.85	0.23

Table 6. Summary statistics of source-water fractions from the Monte Carlo simulations for the Rainier Mesa example; Q1 and Q3 refer to the first and third quartiles of the sample distribution; SD is the standard deviation of the distribution.

Source	Min	Q1	Median	Mean	Q3	Max	SD
U12e Tunnel	0.23	0.23	0.23	0.23	0.23	0.25	0.01
USGS HTH #1	0.31	0.31	0.31	0.31	0.31	0.33	0.01
UE-1c	0.42	0.46	0.46	0.45	0.46	0.46	0.02

Travel Time

The ^{14}C travel time in the Frenchman Flat example for the deterministic simulation ranged from 5,700 to 12,800 years; the Monte Carlo simulations produced a slightly larger range in travel times from 3,800 to 15,600 years (Figures 11 and 12), but this is because of the variation in source-water fraction observed in one model, Model ae (see Figure 12). Approximately one-third of the Monte Carlo simulations produced a travel time in Model ae of 15,600 years. Aside from this variation, the Monte Carlo simulations did not provide any more insight into variation in travel time over the deterministic simulation. For the Rainier Mesa example, the ^{14}C travel times for the deterministic and Monte Carlo simulations ranged from 14,700 to 15,700 years (Figures 13 and 14) and were nearly identical. In this example, separating travel times by model in the Monte Carlo simulations did not provide any more insight than the deterministic results.

As stated above in the Frenchman Flat example, the histograms in Figure 12 show that Models aa and ac are responsible for the longer travel times, Models ae and af are generally responsible for the shorter travel times, and Models ab and ad are responsible for those in the middle. This information shows that an increase in source-water fraction from Cane Spring with a decrease in contribution from Indian Springs results in longer travel times. Similarly, a decrease in contribution from Cane Spring and an increase in contribution from Indian Springs results in shorter travel times. In general, source-water represented by well 3 (Indian Springs) contributes more than that represented by wells 1 or 2 and is inversely related to travel time. Well 1 (Cane Spring) is a local spring with a significant amount of ^{14}C (93 pmc), whereas the downgradient final well, Army #1 Water Well, has low ^{14}C (4.1 pmc). The greater amount of source-water fraction from Cane Spring produces a mixture with greater ^{14}C content, which then requires more time (years) for radioactive decay to reduce the ^{14}C in the mixture to that at Army #1 Water Well.

Monte Carlo results for the Rainier Mesa example show similar behavior to the Frenchman Flat example. The greater amount of source-water fraction from water with the highest ^{14}C content—in this example, U12e Tunnel (85 pmc)—produces the longest travel times. A secondary contributor to longer travel times is greater fractions of well USGS HTH #1 because it still has considerably more ^{14}C (30 pmc) relative to well UE-1c (3 pmc) and the final well, ER-12-3 (3 pmc), but USGS HTH #1 has much less effect than U12e Tunnel. The travel times for both the Frenchman Flat and Rainier Mesa examples are consistent with dissolved inorganic carbon ^{14}C ages previously estimated for these flow systems (e.g., Hershey *et al.* [2008], Hershey *et al.*, [2005], and Hershey and Acheampong [1997]).

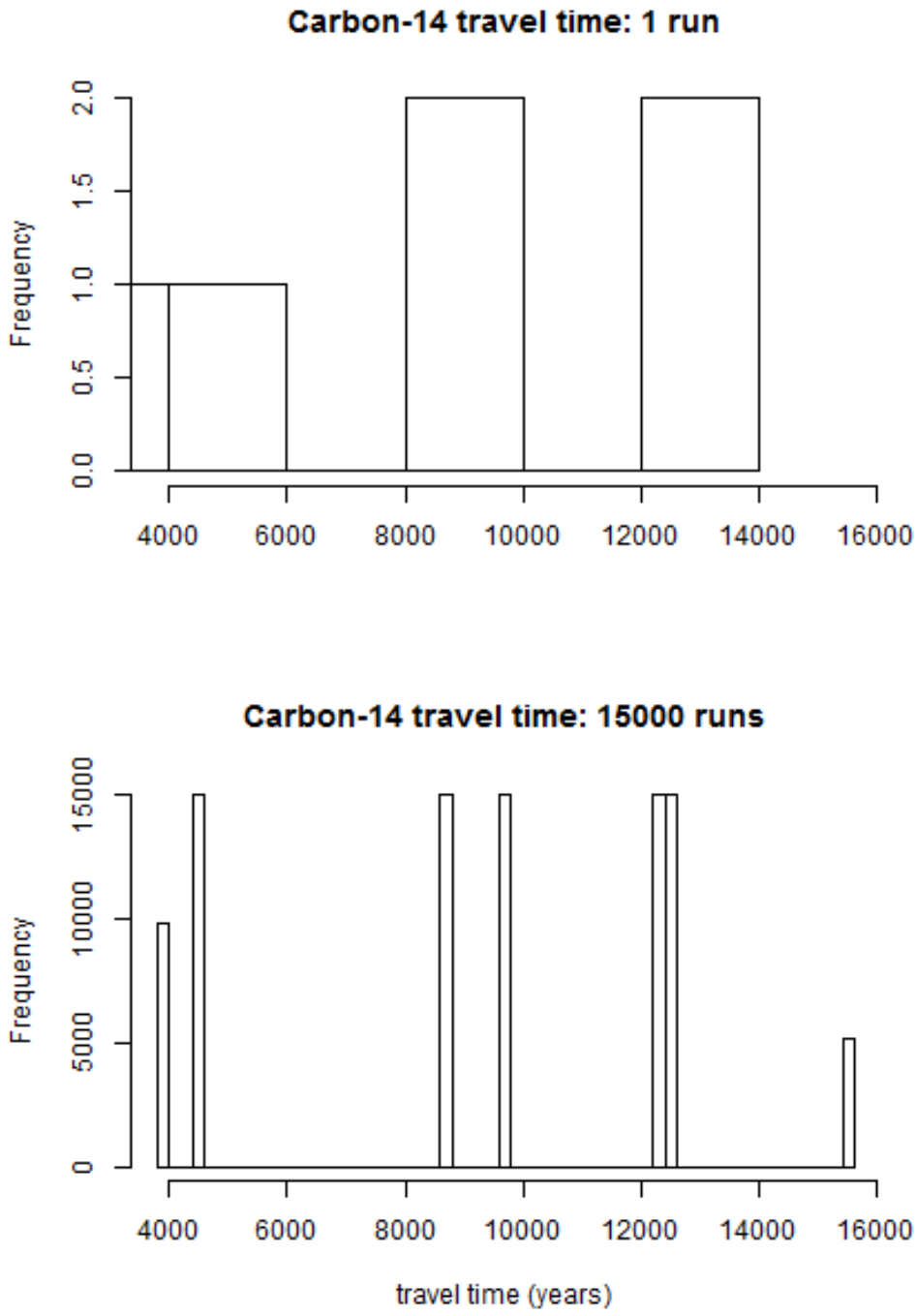

Figure 11. Comparison of results from the deterministic and Monte Carlo simulations for ^{14}C travel time in the Frenchman Flat example.

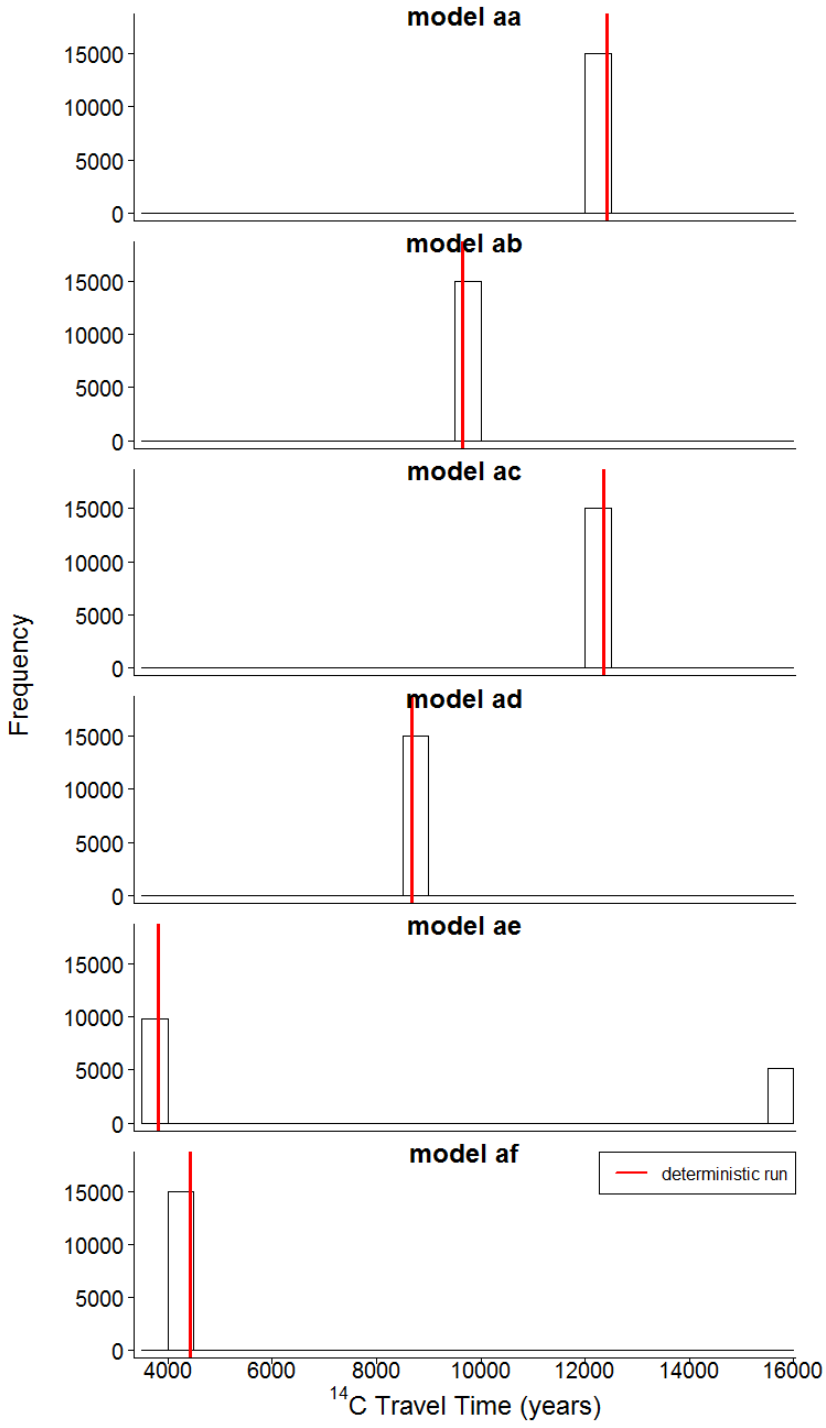

Figure 12. Monte Carlo simulation results for ^{14}C travel time in the Frenchman Flat example separated by model.

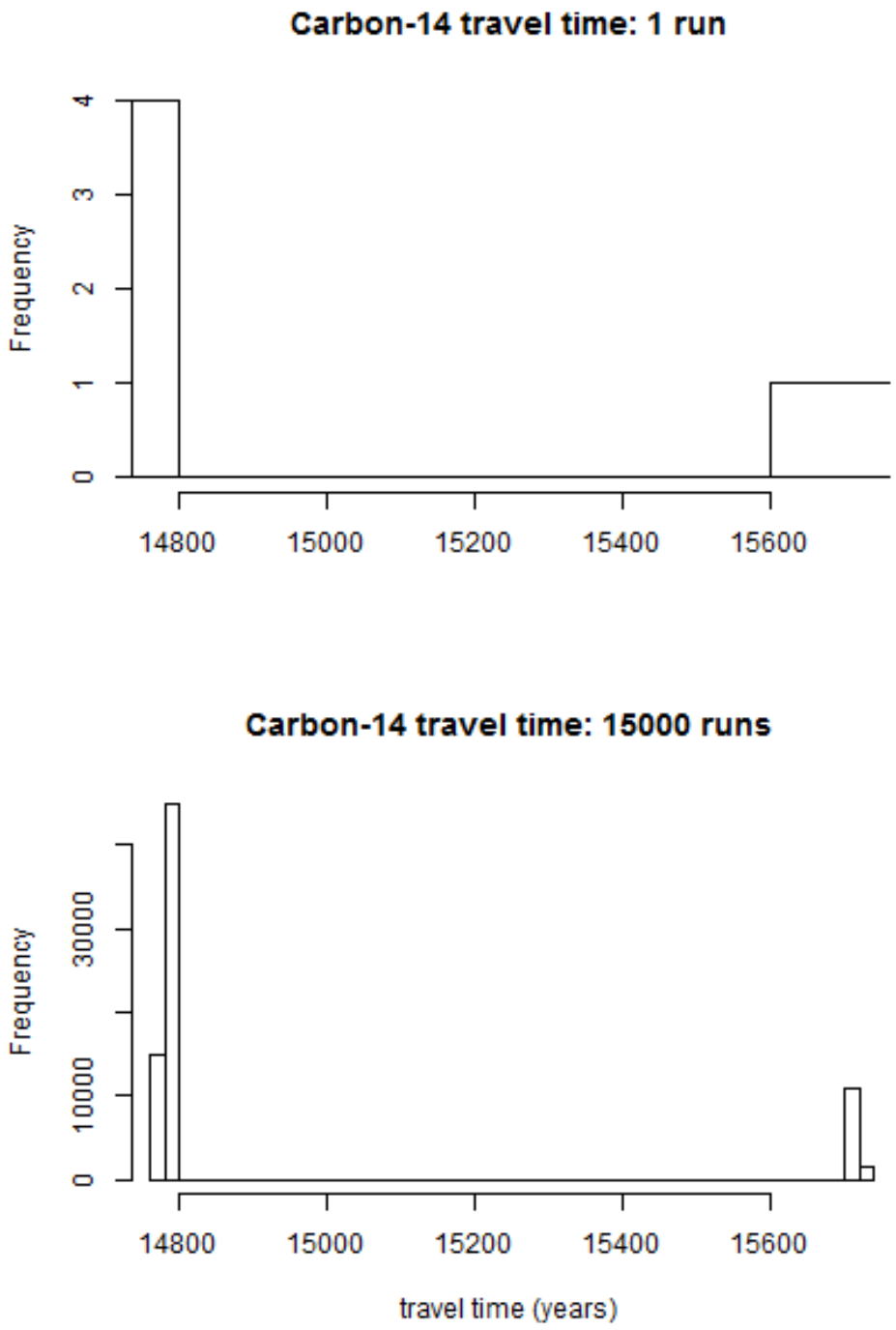

Figure 13. Comparison of results from the deterministic and Monte Carlo simulations for ^{14}C travel time in the Rainier Mesa example.

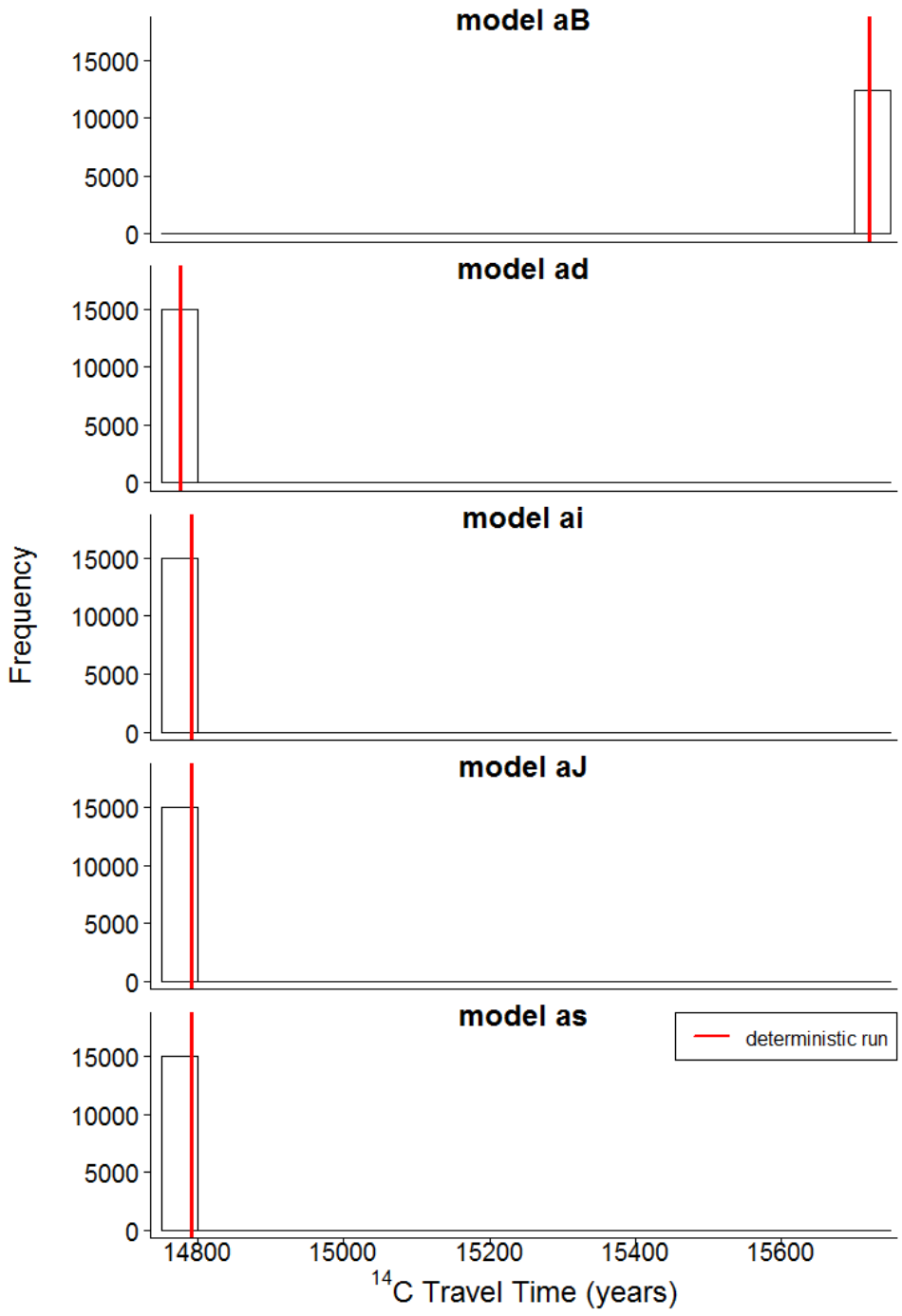

Figure 14. Monte Carlo simulation results for ^{14}C travel time in the Rainier Mesa example separated by model.

Figures 15 and 16 show another representation of the same results as plots of the relationship between the source-water fraction from each well grouped by model. For the Frenchman Flat example, higher contributions from Indian Springs and lower contributions from Cane Spring and ER-5-3#2 result in shorter travel times, although the main driver is the amount of Cane Spring water. In the Rainier Mesa example, the conclusion is less clear. Lower contributions from UE-1c result in both shorter and longer travel times, meaning travel time is less sensitive to source-water fraction in that well. It appears that shorter travel times in this system are a result of a higher fraction from USGS HTH #1 and a lower fraction from U12e Tunnel. Similarly, longer travel times are the result of low to medium contributions from USGS HTH #1 and higher contributions from U12e Tunnel.

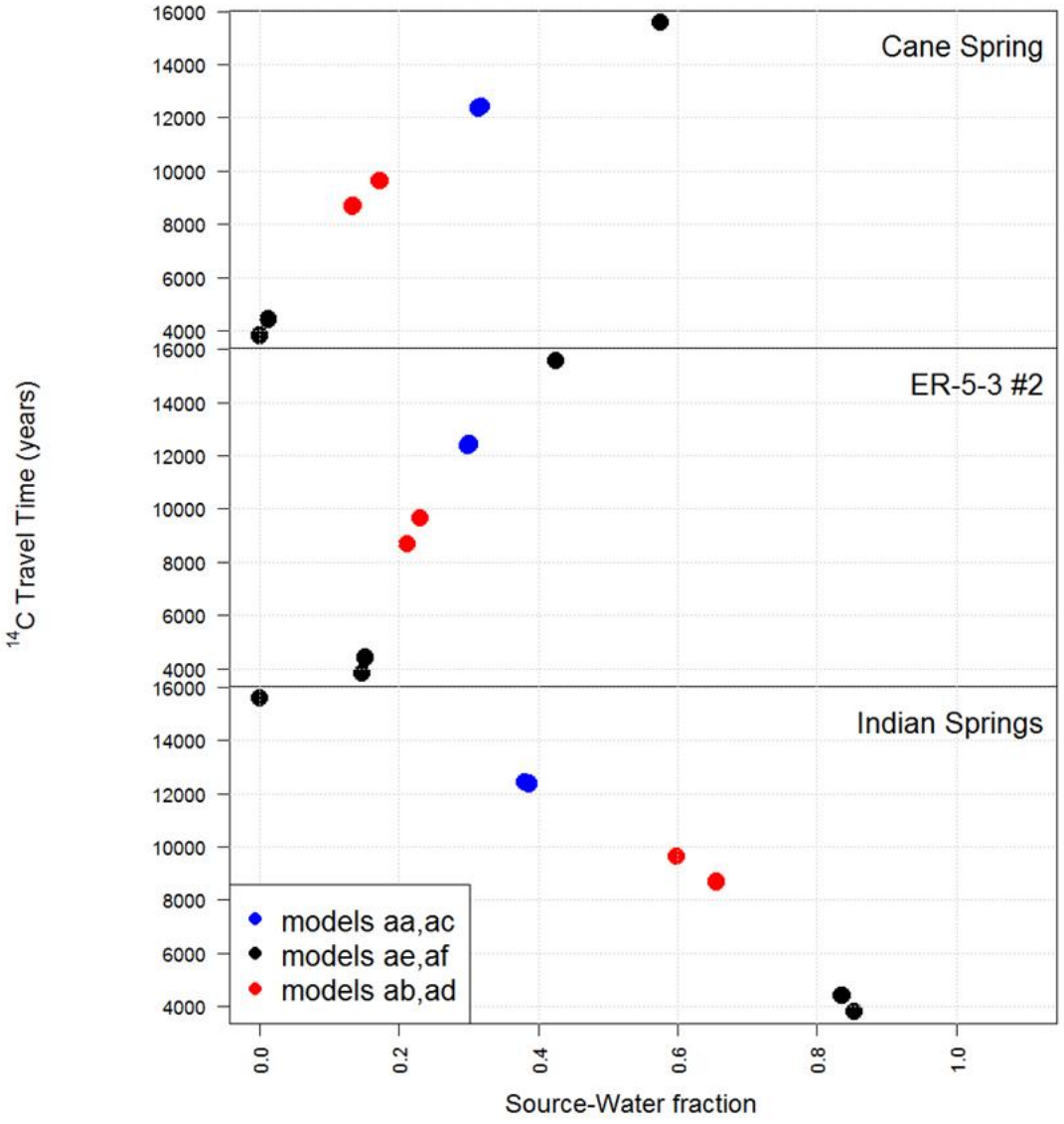

Figure 15. ^{14}C travel time versus source-water fraction for the Frenchman Flat example.

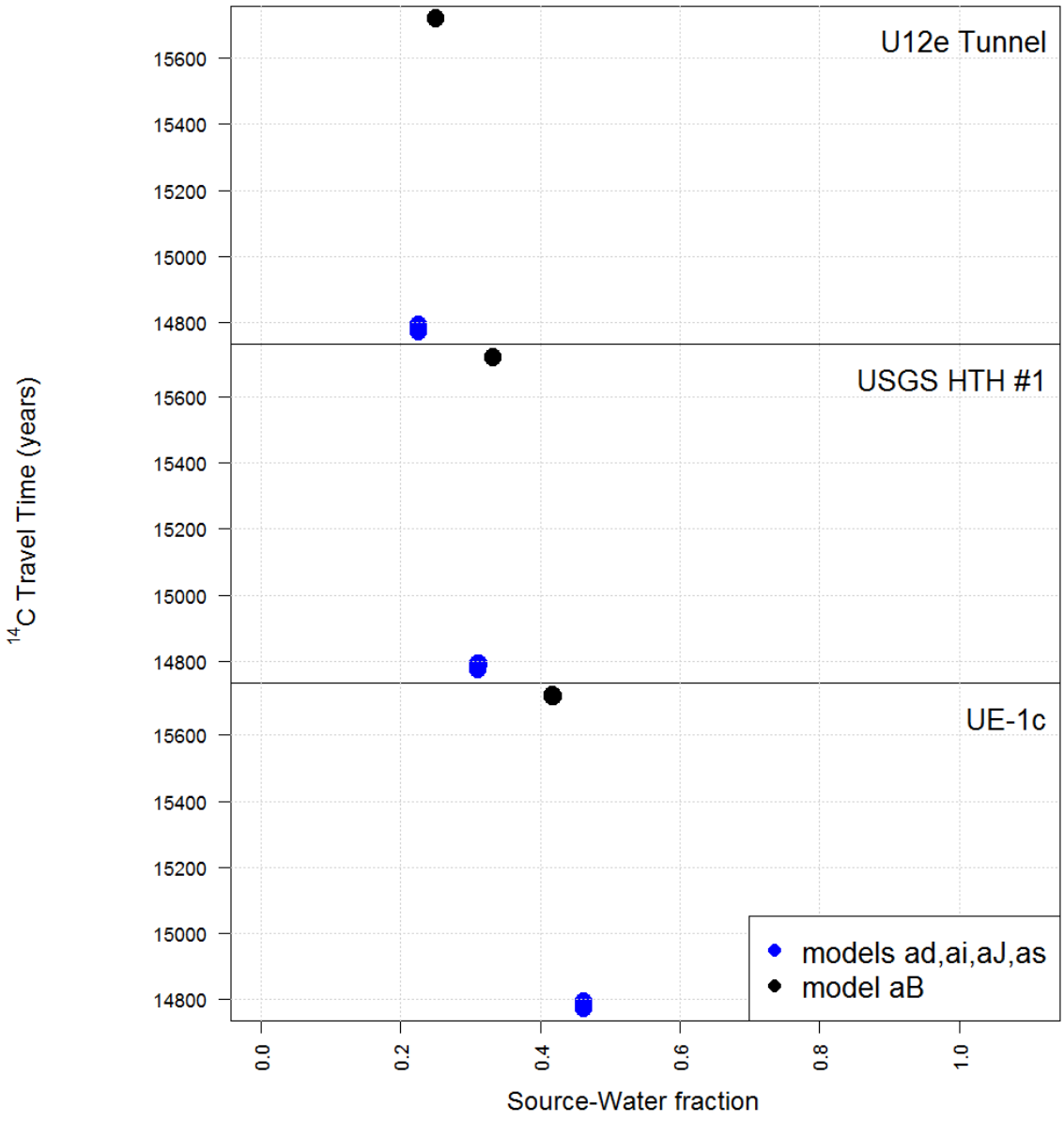

Figure 16. ^{14}C travel time versus source-water fraction for the Rainier Mesa example.

SENSITIVITY ANALYSIS RESULTS

Sensitivity is the slope of the output-input relationship. The sensitivity of each phase, source-water fraction, and travel time to changes in constituents in each well was computed using the approach described above. The concentration of each constraint was decreased or increased by one percent, the simulation run, and results collected. For this study, the changes in output and input were standardized to their mean value to allow comparison across all variables.

Phases

Applying this method to NETPATH results was complicated by the fact that for each simulation there is one input concentration for a constraint, but multiple amounts of phase change (either precipitation or dissolution) for each phase in the output. Figure 17 demonstrates this phenomenon in the Frenchman Flat example for the relationship between calcite precipitation and variations with *S* concentrations in Army #1 Water Well. For each concentration of *S*, there were six amounts of calcite that precipitated. For this study, the sensitivity is not simply the slope of the best-fit line through these points; rather, the sensitivity for each individual model was calculated and the median value was selected. For example, in the Frenchman Flat example, each simulation resulted in six models and each model had three amounts of calcite precipitated, one amount for each sensitivity simulation. Recall the sensitivity simulations were those using 0.99, 1.00, and 1.01 times the measured constraint concentration. The computed values of sensitivity are 1.36, 1.42, 1.45, 1.60, 1.66, and 2.33 for the six models. The sensitivity of calcite precipitation to variations in *S* concentration in Army #1 Water Well is the median value of 1.52. Figure 17 shows the results, with each red line corresponding to the nonstandardized sensitivity. The slope of the lines do not represent the standardized sensitivity; rather, they only give an indication of the magnitude and direction of sensitivity.

Sensitivity was computed considering whether or not a phase was precipitating or dissolving. However, care must be taken during interpretation. In NETPATH, a positive phase amount (in mmol/Kg water) means the phase dissolved (i.e., the more positive the value, the greater amount of the phase dissolved). A negative phase amount means the phase precipitated (i.e., the more negative the value, the greater amount of the phase precipitated). In the example above, although the slope of the sensitivity line is negative, an increase in *S* results in an *increase* in the amount of calcite that *precipitates*. In this case, an increase in output for an increase in input is a positive sensitivity. Alternatively, dissolving phases (positive values) are considered without modification. That is, an increase in the amount of phase dissolved for an increase in constraint results in a positive sensitivity. In this case, a positive slope of the sensitivity line corresponds to a positive sensitivity.

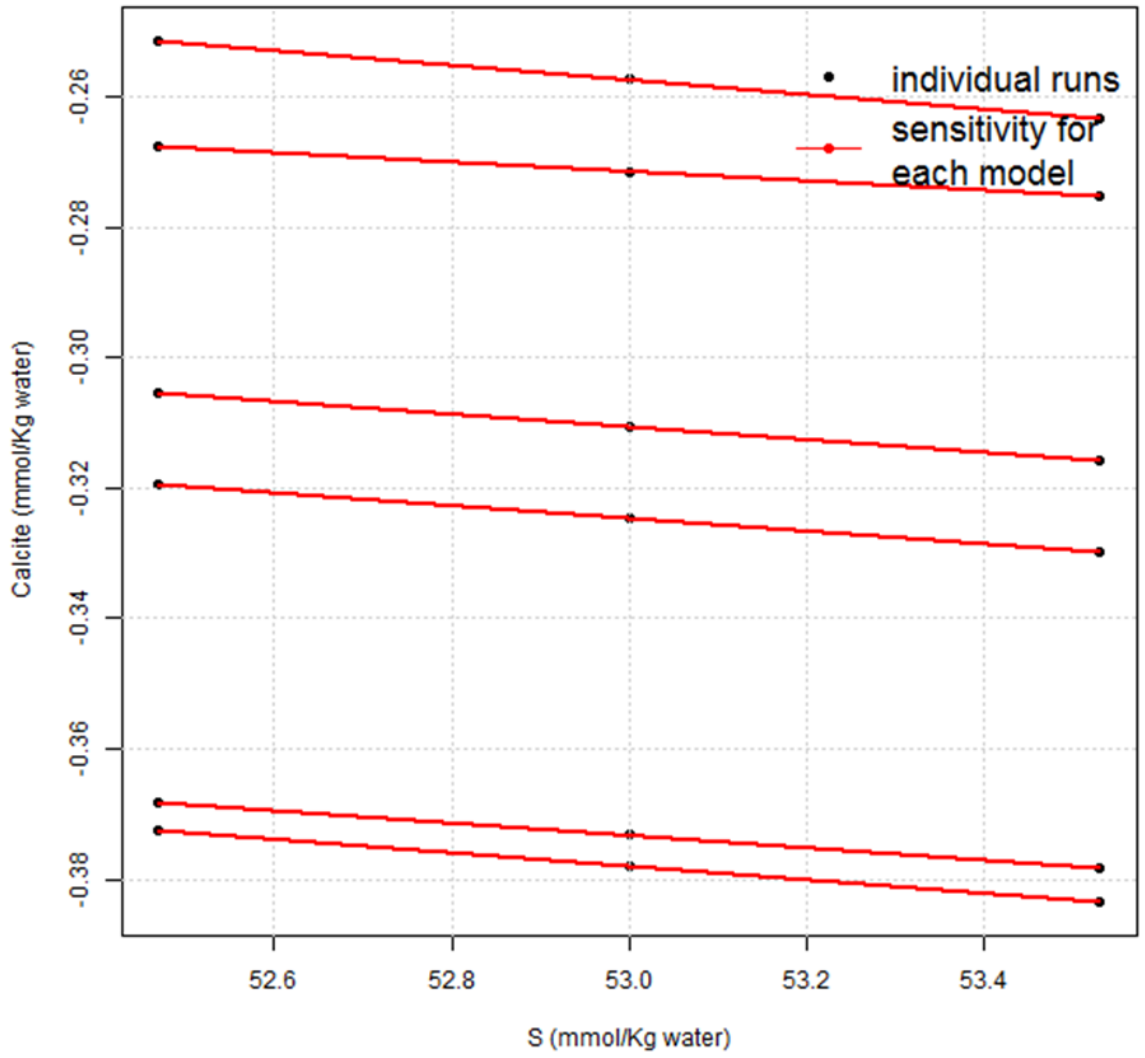

Figure 17. Sensitivity simulation results of calcite precipitation to variations in *S* concentrations in Army #1 Water Well for the Frenchman Flat example. The *S* concentrations (mmol/Kg water) are 99, 100, and 101 percent of the measured concentration. Red lines correspond to the nonstandardized sensitivity. Negative calcite concentrations (mmol/Kg water) mean precipitation of calcite. The more negative the concentration, the more mmols/Kg water of calcite precipitated.

The value of this sensitivity analysis is in the comparison of constraints and wells (for example, the sensitivity of calcite and gypsum is shown in Figures 18 and 19 for the Frenchman Flat example). This comparison is only possible with standardized values of sensitivity. With this information, it is possible to evaluate which constraints have the most influence on each phase. For the Frenchman Flat example (Figure 18), calcite is allowed to either precipitate or dissolve; precipitation of calcite is most sensitive to the Ca concentration in Army #1 Water Well. Calcite dissolution is next most sensitive to the Mg concentration in Army #1 Water Well. In general, in the Frenchman Flat example, dissolution or precipitation of the calcite phase is most sensitive to the constraints (in all source waters) that directly affect calcite solubility, which are Ca, Mg, C, and S. In this model (flow system), Ca concentrations can change because of precipitation of calcite (contains Ca and C), dissolution of dolomite (contains Ca, Mg, C), and/or dissolution of gypsum (contains Ca and S). In the Frenchman Flat example (Figure 19), dissolution of gypsum is most sensitive to the sulfate concentrations in all wells and alkalinity in Army #1 Water Well. Tables 7 and 8 show the sensitivity of every phase to the highest constraint/well combinations, respectively, for both the Frenchman Flat and Rainier Mesa examples. The greater the absolute value of sensitivity (for example, Dolomite, C, Army #1 Water Well, sensitivity =13.98), the more sensitive the amount of the phase (precipitated or dissolved) is to small changes in input concentrations of the specified constraint for the specified well. Knowing how sensitive a mineral phase is to changes in the initial input concentration of a constraint can help guide future water sampling and analysis. Targeted sampling and analysis can then help to minimize uncertainty in input concentrations and water-rock reaction models, and therefore, minimizing uncertainty in the likelihood that the flow path is possible/valid.

Note that the amount of precipitation or dissolution of any given phase is not particularly important as long as all the phases meet the specified model criteria (e.g., phase changes must be less than 1 mmol/Kg water). It is more important to know that a flow path is possible as specified by the model criteria. However, both the phase quantities and the source-water fraction directly influence the travel time, and therefore the sensitivity of phases may provide an indirect benefit to the modeler.

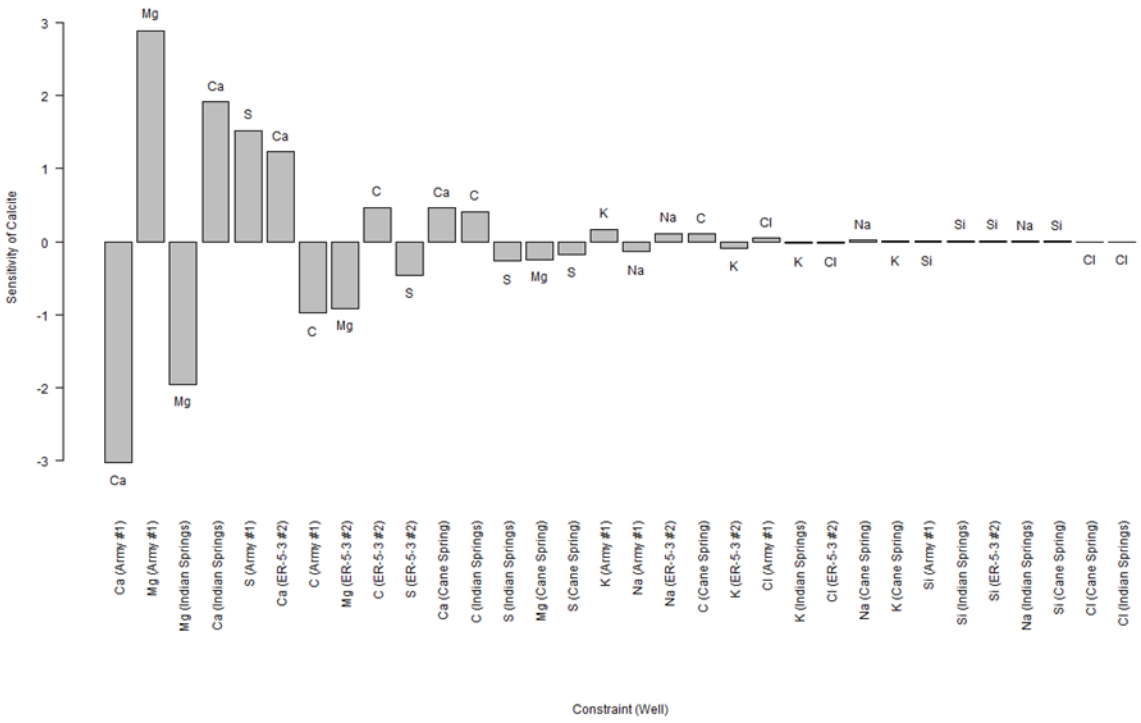

Figure 18. Sensitivity of calcite to constraint/well combinations in the Frenchman Flat example.

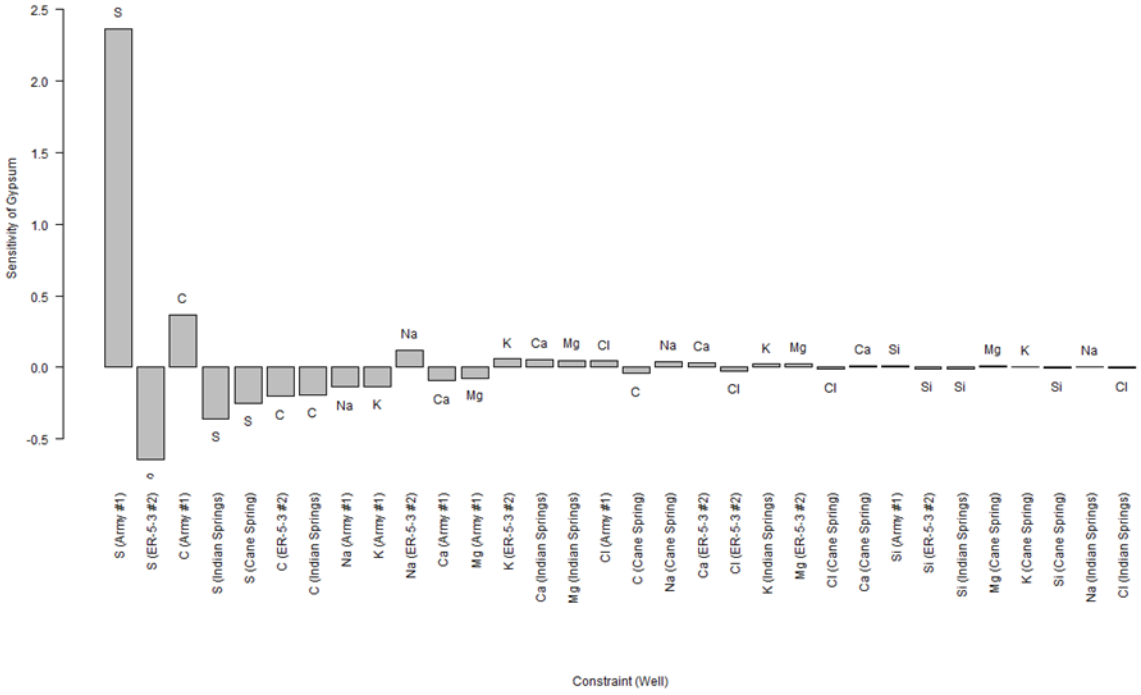

Figure 19. Sensitivity of gypsum to the constraint/well combinations in the Frenchman Flat example.

Table 7. Sensitivity of each phase to important constraint/well combinations in the Frenchman Flat example.

Phase	Constraint	Well	Sensitivity
Calcite	Ca	Army #1 Water Well	-3.03
	Mg	Army #1 Water Well	2.89
	Mg	Indian Springs	-1.95
	Ca	Indian Springs	1.92
	S	Army #1 Water Well	1.53
	Ca	ER-5-3 #2	1.23
	C	Army #1 Water Well	-0.98
	Mg	ER-5-3 #2	-0.91
Ca+Mg/Na exchange	Na	Army #1 Water Well	-3.59
	Na	ER-5-3 #2	3.43
	Cl	Army #1 Water Well	2.88
	C	ER-5-3 #2	-1.50
	Na	Cane Spring	1.09
	C	Army #1 Water Well	1.06
	Cl	ER-5-3 #2	-0.89
	Ca	Army #1 Water Well	-0.66
Dolomite	C	Army #1 Water Well	13.98
	Mg	Army #1 Water Well	-9.82
	C	ER-5-3 #2	-8.19
	Na	Army #1 Water Well	-5.56
	Na	ER-5-3 #2	5.30
	C	Indian Springs	-4.62
	Mg	Indian Springs	4.23
	Mg	ER-5-3 #2	3.98
Gypsum	S	Army #1 Water Well	2.37
	S	ER-5-3 #2	-0.65
	C	Army #1 Water Well	0.37
	S	Indian Springs	-0.36
	S	Cane Spring	-0.25
	C	ER-5-3 #2	-0.20
	C	Indian Springs	-0.19
	Na	Army #1 Water Well	-0.14
NaCl	Cl	Army #1 Water Well	4.02
	Na	Army #1 Water Well	-3.59
	C	Army #1 Water Well	3.33
	Na	ER-5-3 #2	2.43
	C	Indian Springs	-1.82
	Cl	ER-5-3 #2	-1.71
	C	ER-5-3 #2	-1.50
	Cl	Cane Spring	-0.68
Composite Clay	Na	Army #1 Water Well	-3.13
	Na	ER-5-3 #2	2.11
	C	Army #1 Water Well	-1.82
	K	Army #1 Water Well	1.67
	Cl	Army #1 Water Well	1.02
	C	Indian Springs	0.98
	K	ER-5-3 #2	-0.90
	C	ER-5-3 #2	0.49
Composite Glass	Cl	Army #1 Water Well	3.42
	K	Army #1 Water Well	1.98
	C	ER-5-3 #2	-1.37
	K	ER-5-3 #2	-1.14
	Cl	ER-5-3 #2	-1.06
	Ca	Army #1 Water Well	-0.66
	Na	Army #1 Water Well	-0.52
	Mg	Army #1 Water Well	-0.52

Table 8. Sensitivity of each phase to important constraint/well combinations in Rainier Mesa example.

Phase	Constraint	Well	Sensitivity
Calcite	Ca	UE-1c	1.94
	Mg	UE-1c	-1.53
	Ca	ER-12-3	-1.41
	Mg	ER-12-3	1.35
	S	ER-12-3	1.25
	S	UE-1c	-0.73
	K	UE-1c	0.52
	K	ER-12-3	-0.25
CO_2 gas	Na	ER-12-3	3.46
	C	ER-12-3	-3.40
	C	UE-1c	3.32
	Mg	ER-12-3	2.85
	Mg	UE-1c	-2.61
	Na	UE-1c	-1.85
	Na	USGS HTH #1	-1.83
	Cl	ER-12-3	1.60
Ca+Mg/Na exchange	Na	ER-12-3	-3.49
	Na	UE-1c	1.87
	Na	USGS HTH #1	1.84
	Cl	ER-12-3	-1.44
	Na	U12e Tunnel	1.04
	Cl	UE-1c	0.71
	Mg	ER-12-3	-0.67
	Mg	UE-1c	0.64
Gypsum	S	ER-12-3	5.04
	Na	ER-12-3	-3.24
	Mg	ER-12-3	-3.16
	Cl	ER-12-3	-3.14
	Mg	UE-1c	2.99
	S	UE-1c	-2.96
	Na	UE-1c	1.74
	Na	USGS HTH #1	1.71
Composite Clay	K	UE-1c	2.57
	Cl	ER-12-3	2.08
	Na	ER-12-3	1.99
	Mg	ER-12-3	1.94
	Mg	UE-1c	-1.84
	K	ER-12-3	-1.23
	Na	UE-1c	-1.07
	Na	USGS HTH #1	-1.05

Table 8. Sensitivity of each phase to important constraint/well combinations in Rainier Mesa example (continued).

Phase	Constraint	Well	Sensitivity
Composite Zeolite	K	UE-1c	-54.97
	Si	UE-1c	48.19
	Si	ER-12-3	-28.21
	K	ER-12-3	26.40
	Na	ER-12-3	-17.36
	Mg	ER-12-3	-16.91
	Mg	UE-1c	16.00
	Si	U12e Tunnel	13.20
SiO_2	K	UE-1c	-26.37
	Si	UE-1c	23.77
	Si	ER-12-3	-13.87
	K	ER-12-3	12.57
	Na	ER-12-3	-7.68
	Mg	ER-12-3	-7.47
	Mg	UE-1c	7.19
	Si	U12e Tunnel	6.46
Strontianite	Mg	UE-1c	-3.13
	Mg	ER-12-3	3.12
	Na	ER-12-3	3.12
	Sr	UE-1c	2.23
	Na	USGS HTH #1	-1.34
	Na	UE-1c	-1.34
	Cl	ER-12-3	1.34
	Sr	ER-12-3	-1.34

Source-water Fraction

The same analysis can be performed for the source-water fraction, represented in NETPATH output as Init 1, Init 2, and Init 3 (e.g., Appendix A). Using the Frenchman Flat example, the source-water fraction of well 1 (Cane Spring) (Figure 20), well 2 (ER-5-3 #2), and well 3 (Indian Springs) are all most sensitive to C in the downgradient well (Army #1 Water Well), and then sensitive to C in the other source-fractions (Table 9). This is consistent with C having the both the highest concentration in all the groundwater compared with all the other dissolved ions and with C being contained in the carbonate mineral phases calcite and dolomite. In the Frenchman Flat example, more calcite is precipitated in four of the six models than any other phase (see Table 1 and Appendix A).

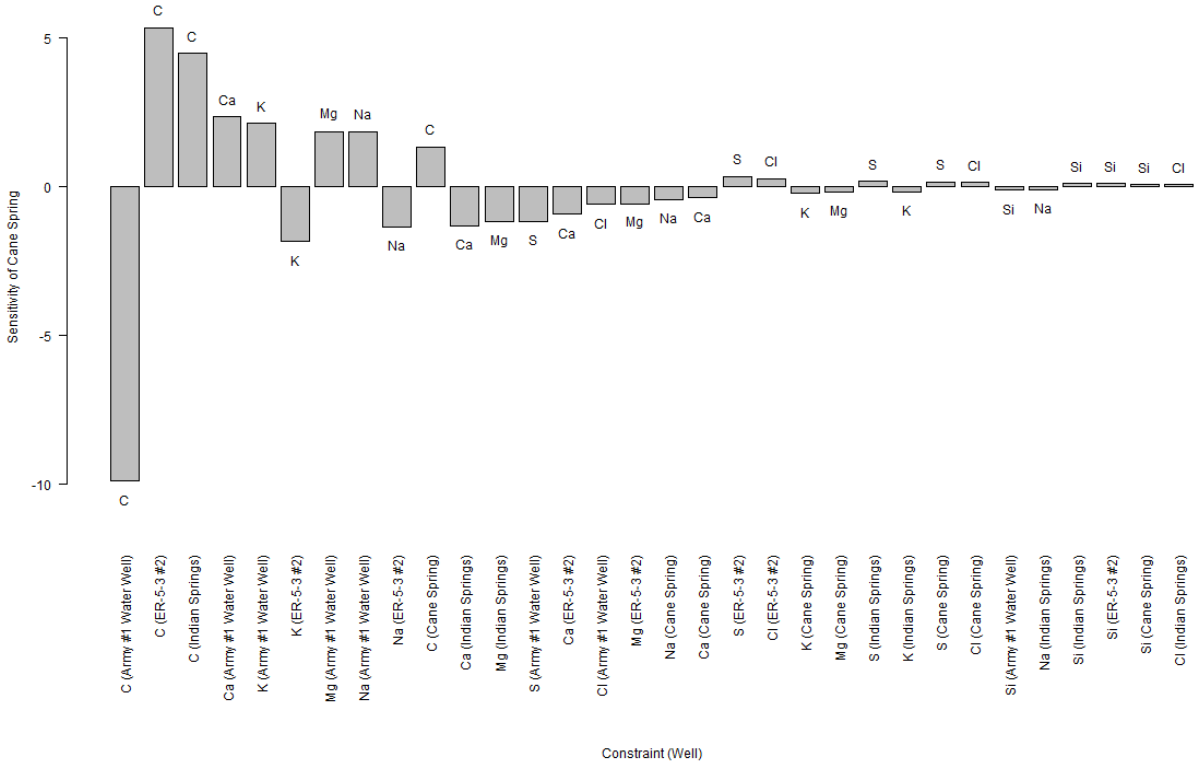

Figure 20. Sensitivity of source-water fraction from Cane Spring to constraint/well combinations in the Frenchman Flat example.

Table 9. Sensitivity of source-water fraction to constraint/well combinations in the Frenchman Flat example.

Source-water Fraction	Constraint	Well	Sensitivity
Init 1 (Cane Spring)	C	Army #1 Water Well	-9.88
	C	ER-5-3 #2	5.34
	C	Indian Springs	4.46
	Ca	Army #1 Water Well	2.34
	K	Army #1 Water Well	2.11
	K	ER-5-3 #2	-1.84
	Mg	Army #1 Water Well	1.84
	Na	Army #1 Water Well	1.83
Init 2 (ER-5-3 #2)	C	Army #1 Water Well	2.96
	C	Indian Springs	-1.55
	C	ER-5-3 #2	-1.28
	Ca	Army #1 Water Well	-0.58
	Mg	Army #1 Water Well	-0.46
	Na	Army #1 Water Well	-0.37
	Na	ER-5-3 #2	0.30
	S	Army #1 Water Well	0.29
Init 3 (Indian Springs)	C	Army #1 Water Well	2.60
	C	Indian Springs	-1.35
	C	ER-5-3 #2	-1.22
	Na	Army #1 Water Well	-0.60
	Na	ER-5-3 #2	0.53
	Ca	Army #1 Water Well	-0.52
	Mg	Army #1 Water Well	-0.41
	Ca	Indian Springs	0.31

In the Rainier Mesa example, the source-water fraction of well 1 (U12e Tunnel) and well 2 (USGS HTH #1) are most sensitive to Cl in the downgradient well (ER-12-3), whereas the source-water fraction of well 3 (UE-1c) is most sensitive to Na and Mg in the downgradient well (ER-12-3) (Table 10). The U12e Tunnel has more Cl (0.25 mmol/Kg water), whereas USGS HTH #1 has less Cl (0.09 mmol/Kg water) than downgradient ER-12-3 (0.17 mmol/Kg water). Because UE-1c has a Cl concentration (0.18 mmol/Kg), there can be very little variation in the mixture between UE-12e Tunnel and USGS HTH #1. The mixtures must either be close to an even percentage of U12e Tunnel and USGS HTH #1 or very little U12e Tunnel and significant USGS HTH #1 with dissolution of NaCl (see model output Appendix B).

Table 10. Sensitivity of source-water fraction in constraint/well combinations in the Rainier Mesa example.

Source-water Fraction	Constraint	Well	Sensitivity
Init 1 (U12e Tunnel)	Cl	ER-12-3	3.75
	Cl	UE-1c	-1.84
	Na	ER-12-3	-1.81
	Mg	ER-12-3	-1.76
	Mg	UE-1c	1.67
	Cl	U12e Tunnel	-1.27
	Na	UE-1c	0.97
	Na	USGS HTH #1	0.95
Init 2 (USGS HTH #1)	Cl	ER-12-3	-3.94
	Cl	UE-1c	1.93
	Cl	U12e Tunnel	1.34
	Na	ER-12-3	-1.14
	Mg	ER-12-3	-1.11
	Mg	UE-1c	1.05
	Cl	USGS HTH #1	0.67
	Na	UE-1c	0.61
Init 3 (UE-1c)	Na	ER-12-3	1.65
	Mg	ER-12-3	1.61
	Mg	UE-1c	-1.53
	Na	UE-1c	-0.88
	Na	USGS HTH #1	-0.87
	Cl	ER-12-3	0.82
	Na	U12e Tunnel	-0.49
	Cl	UE-1c	-0.40

Travel Time

Finally, the sensitivity of ^{14}C travel time is computed in the same manner (Figures 21 and 22). The most important factor in determining the ^{14}C travel time is the mixture of the initial wells (i.e., the source-water fraction of each initial well). In the Frenchman Flat example, the greater the percent of Cane Spring (94 pmc), the greater amount of ^{14}C in the mixture, and therefore the longer the time needed for ^{14}C to decay to the low amount of ^{14}C at the downgradient well (Army #1 Water Well). In the Frenchman Flat example, C in Army #1 Water Well exerts the most influence on travel time, which is exactly the same result for the sensitivity of all three source-water fraction wells. In addition to the mixture of the initial wells in the Frenchman Flat example, the beginning ^{14}C amount (referred to as A_0, see NETPATH output in Appendix A and/or Appendix B) is further modified by the dissolution of dolomite, which adds C at 0 pmc and the precipitation of calcite, which removes ^{14}C from solution (from the mixture) according to the isotopic fractionation factor selected for fractionation from water (in solution) to solid. In the case of Model ad (Model 1 in Appendix A), dissolution of dolomite and precipitation of calcite reduced the amount of ^{14}C in the initial well mixture by 0.14 pmc. In the Rainier Mesa example, ^{14}C travel time is most sensitive to Na and Mg in the downgradient well, ER-12-3 (Figure 22). The same as for the source-water fraction sensitivity for UE-1c (Table 10).

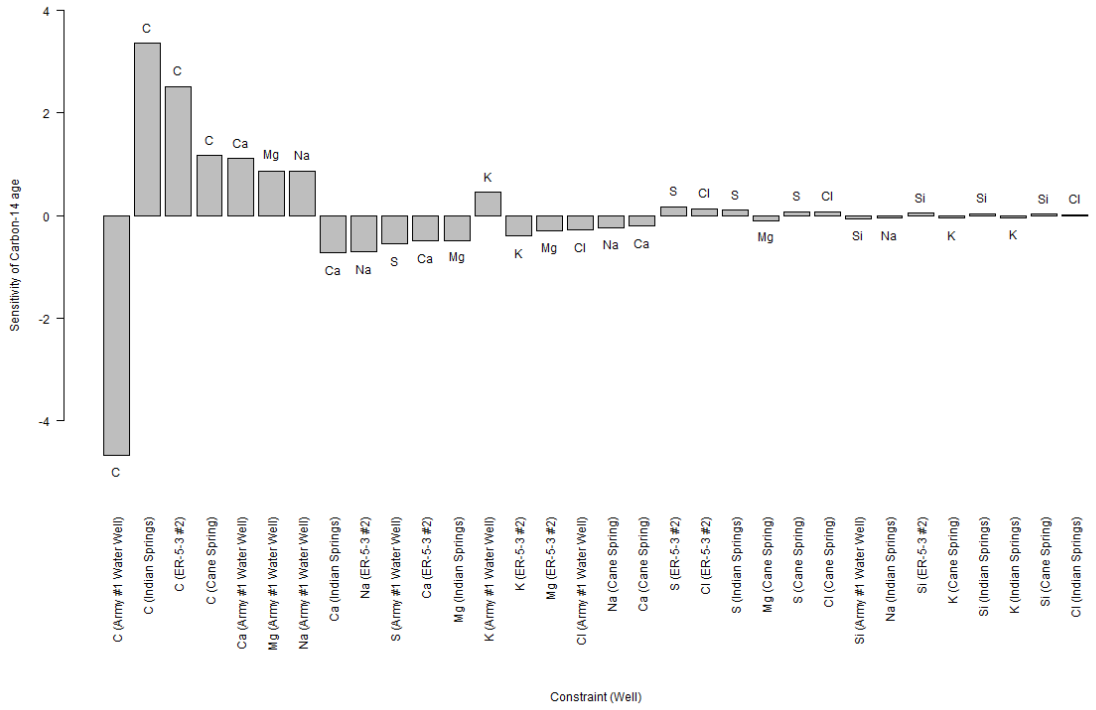

Figure 21. Sensitivity of ^{14}C travel time to constraint/well combinations in the Frenchman Flat example.

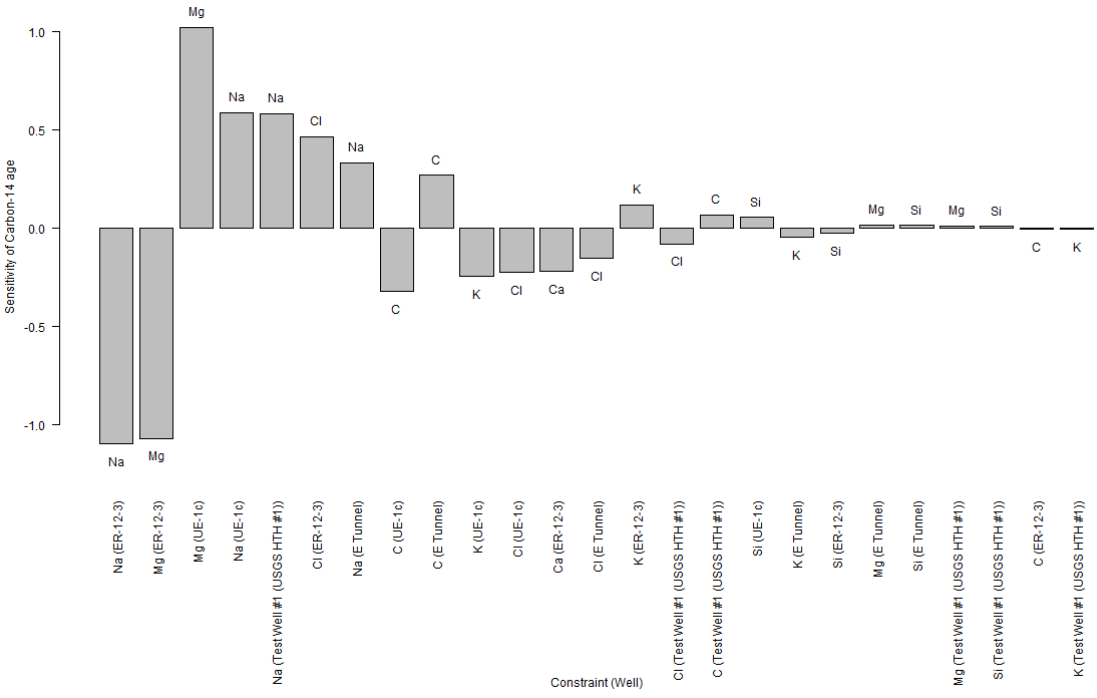

Figure 22. Sensitivity of ^{14}C travel time to constraint/well combinations in the Rainier Mesa example.

As discussed above, there is a strong relationship between source-water fraction and travel time. It is beneficial to water-rock reaction modelers to investigate how source-water fraction affects travel time. However, it is not possible to compute the sensitivity of travel time to source-water fraction in the same manner as for the constraints because the modeler does not have control over the fraction of water from each source. The modeler can adjust constraints that affect phase dissolution or precipitation and source-water fractions, which ultimately affects travel time.

Another way to evaluate the sensitivity of travel time to source-water fraction is by computing a linear model to represent the relationship and compare the slopes of those lines to each other. These linear models are shown below in Figures 23 and 24. For the Frenchman Flat example (Figure 23), there is a strong relationship between travel time and source-water fraction. Travel time is positively correlated with source-water fraction in wells 1 and 2 (Cane Spring and ER-5-3 #2) and inversely correlated with source water in well 3 (Indian Springs). The relative sensitivities (defined here as the slope of the relationship) of travel time to contributions from wells 1, 2, and 3 are 1.5, 3.0, and -1.0. From Figure 23, the ^{14}C travel time is most sensitive to the fraction of well ER-5-3 #2 (steepest slope).

As discussed previously in the Travel Time subsection of the Uncertainty Analysis Results, the proportions of the source-water fraction controls travel times. In the Frenchman Flat example, the variation of travel times is controlled by the fraction of Cane Spring, which is young recharge water with considerable ^{14}C content (94 pmc). The greater the fraction of Cane Spring, the more ^{14}C is in the mixture, the longer time is needed for radioactive decay to reach the low ^{14}C content at the downgradient well, Army #1 Water Well (4 pmc). When the fraction of Cane Spring decreases, the fraction of Indian Springs (representing carbonate groundwater at 8 pmc) increases, which lowers the ^{14}C content in the mixture and reduces travel times. Well ER-5-3 #2 has very low ^{14}C content (1.6 pmc) and its source-water fraction is positively correlated with Cane Springs (Figure 23).

For the Rainier Mesa (Figure 24) example, the relationship is not as well-defined, but there is a positive correlation between travel time and source-water fraction from U12e Tunnel. There possibly is an inverse correlation with USGS HTH #1 and the relationship in UE-1c is not well-defined. Because of the inconclusive results, relative sensitivities were not computed. Similar to the Frenchman Flat example, the fraction of the local recharge well with the large amount of ^{14}C (U12e Tunnel = 85 pmc) controls the ^{14}C content of the mixture, which then determines the travel time for the mixture. The greater the source-water fraction of U12e Tunnel in the mixture, the greater the amount of ^{14}C in the mixture, the more time needed for radioactive decay of the ^{14}C to reach the low ^{14}C content in the downgradient well (ER-12-3 = 3 pmc).

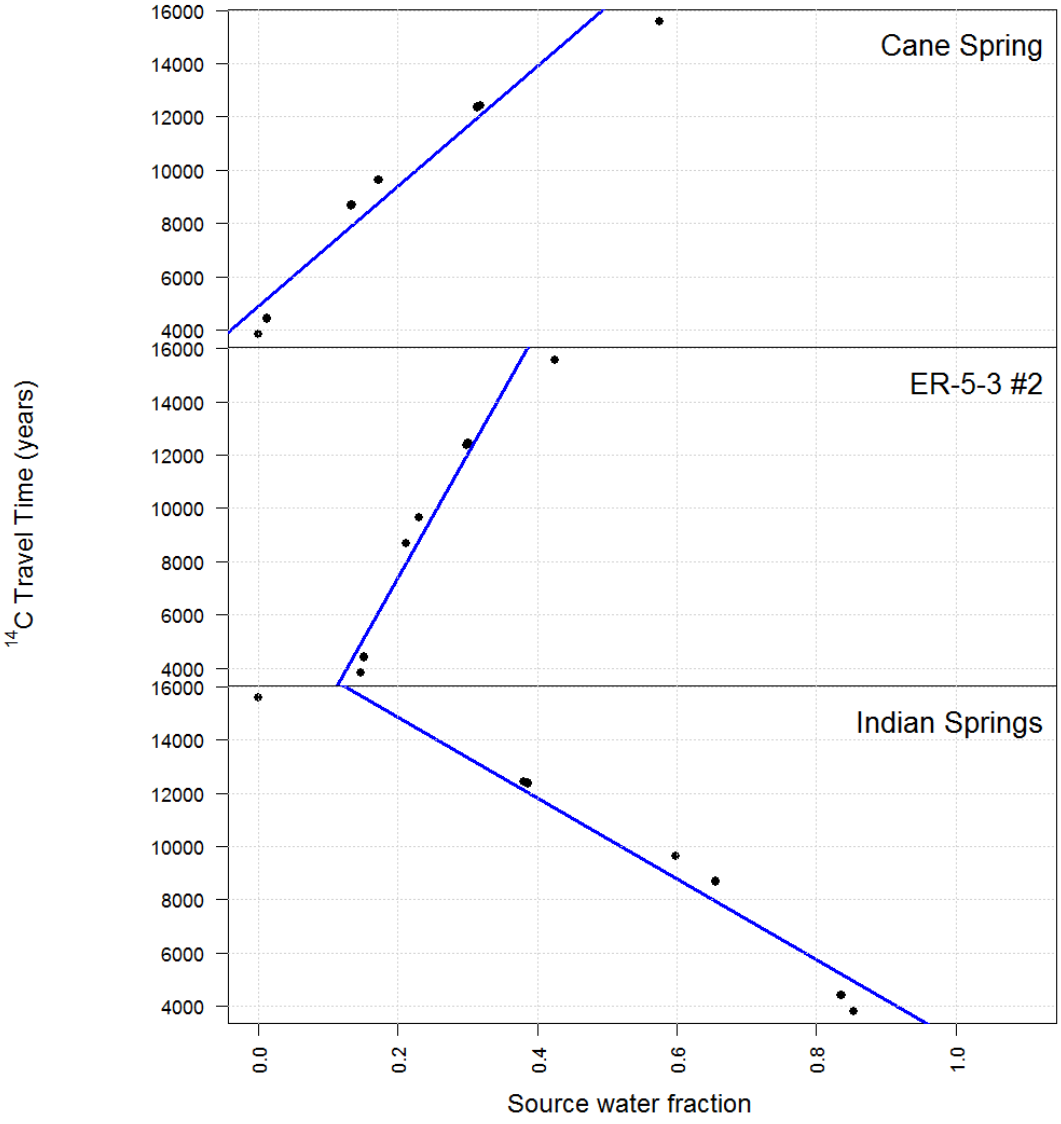

Figure 23. Sensitivity of ^{14}C travel time to source-water fraction in the Frenchman Flat example.

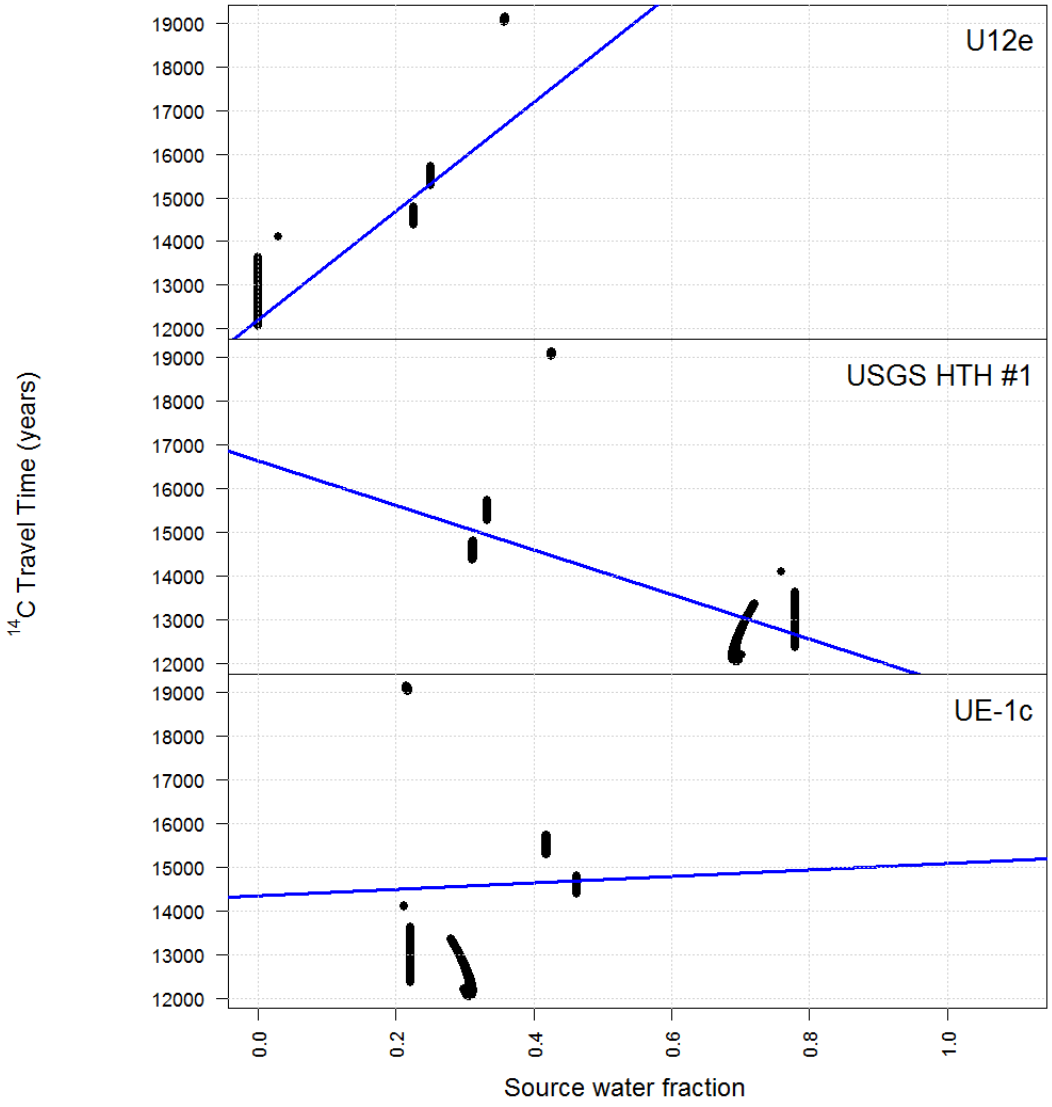

Figure 24. Sensitivity of ^{14}C travel time to source-water fraction in the Rainier Mesa example.

Discussion

In the initial deterministic water-rock reaction simulations used as examples in this study—the Frenchman Flat example (Hershey *et al.*, 2005) and Rainier Mesa example (Hershey *et al.*, 2008)—the input parameters or constraints were limited to actual values from a specific water sample or averages of all available water samples. Mineral phases were selected, and then the ability of those phases to either dissolve or precipitate were limited to actual behavior derived from the mineral saturation indices initially calculated by the DB portion of NETPATH. Finally, NETPATH simulation output was culled to specific criteria of "realistic" geochemical behavior. That is, NETPATH makes calculations based on 1 Kg of water so the amount of phases that could dissolve or precipitate were limited to reasonable amounts ($\leq$ 1 mmol/Kg of water). The other criterion was that modeled $\delta^{13}C$ had to be within

1 ‰ of the downgradient final well $\delta^{13}C$. This approach was selected to limit the potential number of geochemically invalid models that NETPATH might produce and that would then have to be evaluated against other geochemical techniques, including conservative tracer models, Sr and uranium geochemistry, and trace element chemistry. For example, in one of the simulations in Hershey *et al.* (2005), the Frenchman Flat example in this study, resulted in five realistic models for this flow path with the limitations described above.

In this study, the input criteria of the example flow paths for the deterministic simulation were relaxed to allow mineral phases to dissolve or precipitate as necessary regardless of geochemical validity to obtain more NETPATH models. By doing this, six models were produced for the Frenchman Flat example (Appendix A) as opposed to five in Hershey *et al.* (2005). For the Rainier Mesa example, 43 models were produced (Appendix B), but only five met the strict criteria of ≤ 1 mmol/Kg water of mineral phase dissolution or precipitation and $\delta^{13}C \leq 1$ ‰.

Monte Carlo simulations produced many more NETPATH models with a larger range in amounts of mineral phase dissolution and precipitation (e.g., see Figure 6 for calcite precipitation). However, the increased variation in models revolves around the same models as the deterministic simulation models. For example, when the amount of calcite precipitation was broken out by individual models as shown in Figure 7, there were no Monte Carlo models that differed from deterministic models. Monte Carlo simulations produced the same results as the deterministic Frenchman Flat example for source-water fraction, except for one new source-water fraction mixture for Model ae (Figure 9). This one new model also produced a longer ^{14}C travel time (Figure 11). Otherwise, there were no additional NETPATH models produced by the Monte Carlo simulations. The Monte Carlo simulations for the Rainier Mesa example produced similar results (Figures 8, 10, and 13).

The similarity between the deterministic and Monte Carlo approaches in these examples results from both general water-rock reaction geochemistry and the NETPATH program where several, nonunique solutions are the norm. To achieve a more typical Monte Carlo outcome with NETPATH water-rock reaction models, the strict criteria for geochemical viability (feasibility) of ≤ 1 mmol/Kg water mineral phase dissolution or precipitation and $^{13}C \leq 1$ ‰ could be relaxed or even removed completely. The same applies to the program PHREEQC because both NETPATH and PHREEQC solve inverse programs using the same numerical techniques. However, this could produce a source-water fraction mixture in which mineral phases that should only be dissolving are precipitating (for example, plagioclase) while other phases that should only be precipitating are dissolving (for example, clays) and lead to Monte Carlo results for the most frequent NETPATH model that are geochemically unrealistic. Under typical application of the Monte Carlo technique in this situation, ignoring known geochemical behavior would lead to erroneous interpretation about the viability of a groundwater flow path and the travel times associated with it. In future application of the Monte Carlo approach to inverse water-rock reaction modeling, a balance must be struck between realistic geochemical behaviors and applying the Monte Carlo approach as originally intended, regardless of the geochemical program used.

Sensitivity analysis appears to be a very useful technique to apply to water-rock reaction modeling, as can be seen in the Frenchman Flat and Rainier Mesa examples. Sensitivity analysis was able to identify the input constraints (dissolved ion concentrations) that most greatly affected model results. For example, the Cane Spring source-water fraction

in the Frenchman Flat example was most sensitive to variations in C concentration in the downgradient target well (Army #1 Water Well) and most sensitive to C concentrations in the other upgradient initial wells (Figure 20). From this analysis, it is clear that precise measurements of field pH and alkalinity and laboratory analysis of pH and bicarbonate concentrations are critical to understanding the geochemical reactions along a groundwater flow path.

Sensitivity analysis also demonstrated that source-water fraction is the most important parameter in calculating groundwater travel times. In both the Frenchman Flat and Rainier Mesa examples, the fraction of local groundwater recharge with the highest initial ^{14}C content controlled the groundwater travel time. Models in which the local recharge source-water fraction was low resulted in a low amount of ^{14}C in the upgradient mixture of initial wells, travel times were short. Where the contribution of local recharge is greater, travel times became much longer.

SUMMARY

Monte Carlo and sensitivity methods were applied to evaluate uncertainty in water-rock reaction simulations and experimental uncertainty was allowed to propagate through the NETPATH simulations for two example problems. Monte Carlo sampling of assumed distributions provided the variable input for each simulation. A uniform distribution was used for all input constraints for simplicity. A previous study for the Rainier Mesa/Shoshone Mountain CAU concluded that a specific distribution for each constraint (each different dissolved ion) could not be assigned because of a lack of data at sample locations. Different ions had either normal or log-normal distributions, or many ions did not follow either distribution.

Simulations were run, each with a different input, thousands of times to allow for a complete exploration of the parameter space. The uncertainty in input affected the variability of outputs, namely source-water mixing, phase dissolution and precipitation amounts, and ^{14}C travel time.

A sensitivity analysis was also performed. Sensitivity analysis in this study involved changing one constraint concentration at a time by a very small amount and observing the resulting change in output. Results were standardized to allow for comparison of sensitivities across all input constraints. Because simulation results are nonunique and one simulation can result in many outputs, a representative value of sensitivity was computed for each scenario.

The approach taken can yield insight into the uncertainty in flow paths and travel times, but there are several outcomes that should be considered when evaluating flow-path and travel-time results when modeling water-rock reactions with NETPATH. First, the variability in the results is influenced by the assumed distribution for the inputs. It takes many water samples to determine a distribution of dissolved chemical constituents and in the absence of an adequate number of samples, a simple uniform distribution can be used. However, a preliminary sensitivity analysis can reveal which variables have the most influence on source-water fractions and ^{14}C travel times. Once these variables are determined, more focused effort can be applied to determining their proper distribution.

Second, Monte Carlo results for water-rock reaction modeling showed discrete results. For example, an evaluation of the histograms of travel times shows multiple modes. This is a direct result of the nonuniqueness of these simulations. NETPATH provides the solutions that satisfy the constraints of upgradient and downgradient water chemistry. Multiple, discrete solutions can exist for any scenario and these discrete solutions cause grouping of results. As a result, the variability in output may not easily be represented by a single distribution or a mean and variance, and therefore care should be taken in interpreting and reporting results.

RECOMMENDATIONS

This study specifically examined uncertainty in input dissolved-ion concentrations and their effects on model output, but there are other areas of uncertainty in geochemical evaluations and water-rock reaction modeling that need to be examined. For example, uncertainty associated with identifying all the pertinent reactive mineral phases and possible geochemical reactions, understanding the spatial variability of the reactants and their relative abundances, and capturing localized differences in permeable versus nonpermeable pathways in the same HSU. There are also epistemic uncertainties that could be reduced if sufficient samples and/or analytical result were available such that statistical moments and appropriate types of statistical distributions of known reactants could be determined, uncertainty in rates of reactions, analytical error, etc.

This study assumed input distributions for dissolved-ion concentrations based solely on the overall variability present in available analytical datasets. Addressing individual sources of variability within these distributions was not addressed, but could help identify where and what types of data are needed to reduce uncertainty in these geochemical model results. Examples could include analysis of geochemical reactions and phases, the spatial variability of reactants and their relative abundances, reaction rates, and analytical error. Also, a sensitivity analysis of the assumed constraint distribution on the results could be performed by using Normal or log-Normal distributions. The scripts developed to implement these methods are currently able to use these three distributions and are specified by the user in the configuration file (Appendix C). Additional distributions can be added easily with a minor modification to the code.

The difficulties in fitting statistical distributions to water chemistry data were addressed for Rainier Mesa by Hershey *et al.* (2008). A reduction in uncertainty of constraints can be achieved by additional water chemistry data, which will also better define the form of the distribution.

REFERENCES

Al-Issa, T.A., C.T. Haan, 1996. Impact of Parameter Probability Distribution on Model Output Uncertainty Using the AGNPS Model. Environmental Institute, Oklahoma State University, Stillwater, Oklahoma.

Bean, M.A., 2001. Probability: The Science of Uncertainty with Applications to Investments, Insurance, and Engineering. ISBN 0-534-36603-1.

Beven KJ, A.M. Binley, 1992. The future of distributed models: model calibration and uncertainty prediction. Hydrological Processes 1992; 6:279–98.

Blasone, R.S., J.A. Vrugt, H. Madsen, D. Rosbjerg, B.A. Robinson, and G.A. Zyvoloski, 2008. Generalized Likelihood Uncertainty Estimation (GLUE) Using Adaptive Markov Chain Monte Carlo Sampling. Advances in Water Resources, 31, p. 630-648.

Chapman, J.B., R.L. Hershey, and B.F. Lyles, 1995. Groundwater velocities at the Nevada Test Site: ^{14}Carbon-based estimates. Desert Research Institute Publication No. 45135.

Dethlefsen, F., C. Haase, M. Ebert, 2011. Uncertainties in Geochemical Modeling Using Different Software Programs and Thermodynamic Datasets. Geophysical Research Abstracts. v.13, EGU2011-7667-2.

Duan, Q., V.K. Gupta, and S. Sorooshian, 1992. Effective and efficient global optimization for conceptual rainfall-runoff models, Water Resources Research, 28, 1015-1031.

Ekberg, C., 1999. Sensitivity Analysis and Simulation Uncertainties in Predictive Geochemical Modeling: A Case Study. Modified PhD Thesis, Chalmers University of Technology, Department of Nuclear Chemistry, Goteborg, Sweden.

EPA, 1997. Guiding Principles for Monte Carlo Analysis. EPA/630/R-97/001, March 1997.

Farnham, I.M., T.P. Rose, E.M. Kwicklis, R.L. Hershey, J.B. Paces, and W.M. Fryer, 2006. Geochemical and isotopic evaluation of groundwater movement in corrective action unit 97: Yucca Flat/Climax Mine, Nevada Test Site, Nevada. Stoller-Navarro Publication S-N/99205-070, Stoller-Navarro Joint Venture, 7710 W. Cheyenne, Building 3, Las Vegas, NV, 89129.

Haan, C. T., and J. Zhang, 1996. Impact of uncertain knowledge of model parameters on estimated runoff and phosphorus loads in the Lake Okeechobee Basin. Transactions of the ASAE 39(2): 511-516.

Hammonds, J.S., F.O. Hoffman, S.M. Bartell, 1994. An Introductory Guide to Uncertainty Analysis in Environmental and Health Risk Assessment. Prepared by SENES Oak Ridge, Inc., Oak Ridge, Tennessee. ES/ER/TM-35/R1.

Helton, J.C., J.D. Johnson, C.J. Sallaberry, and C.B. Storlie, 2006. Survey of Sampling-Based Methods for Uncertainty and Sensitivity Analysis. Sandia National Laboratories, SAND2006-2901.

Hershey, R.L., J.B. Paces, M.J. Singleton, E.M. Kwicklis, D.L. Decker, W.M. Fryer, and S. Earman, 2008. Geochemical and isotopic evaluation of groundwater movement in Corrective Action Unit 99: Rainier Mesa and Shoshone Mountain, Nevada Test Site. Desert Research Institute, Publication No. 45229.

Hershey, R.L., J.M. Thomas, T.P. Rose, J.B. Paces, I.M. Farnham, and F.C. Benedict, Jr., 2005. Evaluation of groundwater movement in the Frenchman Flat CAU using geochemical and isotopic analysis. Desert Research Institute Publication No. 45207.

Hershey, R.L., and S.Y. Acheampong, 1997. Estimation of groundwater velocities from Yucca Flat to the Amargosa Desert using geochemistry and environmental isotopes. Desert Research Institute Publication No. 45157.

Jackman, S., 2000. Estimation and Inference via Bayesian Simulation: An Introduction to Markov Chain Monte Carlo. American Journal of Political Science, v.44 n.2, April 2000, 375-404.

Kunstmann, H., W. Kinzelbach, T. Siegfried, 2002. Conditional First-order Second-moment Method and its Application to the Quantification of Uncertainty in Groundwater Modeling. Water Resources Research, v. 38, n. 4, 1035, doi:10.1029/2000WR000022.

Ma, L., J.C. Ascough II, L.R. Ahuja, M.J. Shaffer, J.D. Hanson, and K.W. Rojas, 2000. Root Zone Water Quality Model Sensitivity Analysis Using Monte Carlo Simulation. Transactions of the ASAE. v.43(4): 883-895.

Makino, H., S.A. McKenna, K. Wakasugi, 2001. Sensitivity Analysis of Monte Carlo Simulation Results Using the Kolomogorov-Smirnov *d* Statistic. International Association of Mathematical Geology 2001 Annual Meeting, Cancun, Mexico, September 6-12, 2001.

Morse, B.S., 2002. Radiocarbon Dating of Groundwater Using Paleoclimatic Constraints and Dissolved Organic Carbon in the Southern Great Basin, Nevada and California. Master's Thesis, University of Nevada, Reno.

Murphy, J.M., D.M.H. Sexton, D.N. Barnett, G.S. Jones, M.J. Webb, M. Collins, D.A. Stainforth, 2004. Quantification of modeling uncertainties in a large ensemble of climate change simulations. Nature, vol. 430, August 12, 2004.

Parkhurst, D.L., 1995. User's Guide to PHREEQC—A Computer Program for Speciation, Reaction-Path, Advective-Transport, and Inverse Geochemical Calculations. U.S. Geological Survey Water-Resources Investigations Report 95-4227.

Parkhurst, D.L., 1997. Geochemical Mole-balance Modeling with Uncertain Data. Water Resources Research, v.33, n.8, August 1997, p. 1957-1970.

Parkhurst, D.L., and Charlton, S.R., 2008, NetpathXL—An Excel® interface to the program NETPATH: U.S. Geological Survey Techniques and Methods 6–A26, 11 p.

Parkhurst, D.L., C.A.J. Appelo, 2013. Description of Input and Examples for PHREEQC Version 3–A Computer Program for Speciation, Batch-Reaction, One-Dimensional Transport, and Inverse Geochemical Calculations. Chapter 43 of Section A, Groundwater Book 6, Modeling Techniques, USGS Techniques and Methods 6-A43.

Rose, T.P., F.C. Benedict, Jr., J.M. Thomas, W.S. Sicke, R.L. Hershey, J.B. Paces, I.M. Farnham, Z.E. Peterman, 2006. Geochemical data analysis and interpretation of the Pahute Mesa – Oasis Valley groundwater flow system, Nye County, Nevada, August 2002. Lawrence Livermore National Laboratory UCRL-TR-224559.

Srinivasan, G., D.M. Tartakovsky, B.A. Robinson, and A.B. Aceves, 2007. Quantification of Uncertainty in Geochemical Reactions. Water Resources Research, v.43, W12415, doi: 10.1029/2007WR006003.

Thomas, J.M, F.C. Benedict, Jr., T.P. Rose, R.L. Hershey, J.B. Paces, Z.E. Peterman, I.M. Farnham, K.H. Johannesson, A.K. Singh, K.J. Stetzenbach, G.B. Hudson, J.M. Kenneally, G.F. Eaton, D.K. Smith, 2002. Geochemical and isotopic interpretations of groundwater flow in the Oasis Valley Flow System, Southern Nevada. Desert Research Institute, Division of Hydrologic Sciences Publication No. 45190, Reno, Nevada.

Thomas, J.M., A.H. Welch, M.D. Dettinger, 1996. Geochemistry and isotope hydrology of representative aquifers in the Great Basin region of Nevada, Utah, and adjacent states. U.S. Geological Survey Professional Paper 1409-C.

VanBriesen, J.M., M. Small, C. Weber, and J. Wilson, 2010. Modeling Chemical Speciation: Thermodynamics, Kinetics and Uncertainty. Chapter 4, in Modelling of Pollutants in Complex Environmental Systems, Volume II, edited by Grady Hanrahan.

Zhang, D., K. Beven, A. Mermoud, 2006. A Comparison of Non-linear Least Square and GLUE for Model Calibration and Uncertainty Estimation for Pesticide Transport in Soils. Advances in Water Resources, 29 (2006), p.1924-1933.

APPENDIX A: ORIGINAL INPUT AND OUTPUT FOR DETERMINISTIC FRENCHMAN FLAT MODEL FOR THIS STUDY

File: army_model.txt

```
army
 1 2 3 4
 C S CA MG NA CL SI K
CALCITE CA 1.000C 1.000RS 4.000I1 0.000I2 0.000
DOLOMITE CA 1.000MG 1.000C 2.000RS 8.000I1 0.000I2 0.000
GYPSUM CA 1.000S 1.000RS 6.000I3 22.000
NaCl NA 1.000CL 1.000
SiO2 SI 1.000
tmpbglas K 0.369NA 0.403CA 0.025MG 0.004FE 0.030AL 0.803SI 4.148
tmpbclay K 0.017NA 0.161CA 0.141MG 0.138FE 0.050AL 2.438SI 3.462
camgnaex NA 2.000CA -0.560MG -0.440

 3 1 1 0 0 1.0000 0.0000000000 1.000
 0.000 100.000 0.000 0.000 -25.000 100.000 100.000
 0.000 0.000 0. 0. 0.000 0.000
 -40.000 -25.000 0.000 0.000 0.000
 -40.000 -25.000 0.000 0.000 0.000 100.000
 -40.000 -25.000 0.000 0.000 0.000 100.000
 -40.000 -25.000 0.000 0.000 0.000 100.000
```

File: army_run_0000001.lon

```
2010cane
 # 1 of 4




 12.8999996 7.71000004 ********** 147.352951 **********
 ********** 31.5756207 ********** 9.14253902 36.9934196
 4.76545715 18.6236916 29.2053318 ********** 51.6384125
 ********** ********** ********** ********** 0.11000000
 ********** ********** ********** ********** **********
 ********** ********** ********** -12.487122 93.5045242
 ********** ********** -89.800003 -10.900000 **********
 0.70972002 ********** ********** ********** **********
 ********** ********** ********** ********** **********

2010er532
 # 2 of 4




 33.7999992 7.30000019 ********** 497.237823 **********
 ********** 65.1829147 ********** 24.5494099 110.049080
 13.3244686 33.0147247 58.4106636 ********** 58.4106636
 ********** ********** ********** ********** 0.90420002
 ********** ********** ********** ********** **********
 ********** ********** ********** -5.3781176 1.61214697
 ********** ********** -108.00000 -14.050000 **********
 0.71540999 ********** ********** ********** **********
 ********** ********** ********** ********** **********

2010indian
 # 3 of 4




 25.0000000 7.40000010 ********** 221.499695 **********
 ********** 35.5543175 ********** 19.4702206 3.30147243
 0.94055068 2.79355359 11.8514385 ********** 19.4702206
 ********** ********** ********** ********** 0.27000001
 ********** ********** ********** ********** **********
 ********** ********** ********** -9.3962507 8.49399948
 ********** ********** -100.70000 -13.650000 **********
 0.71016002 ********** ********** ********** **********
 ********** ********** ********** ********** **********

2010army
 # 4 of 4




 31.0000000 7.30000019 ********** 247.208084 **********
 ********** 37.2473831 ********** 17.7771587 33.8612556
 4.38923693 16.9306278 44.8661613 ********** 16.0840969
 ********** ********** ********** ********** 0.76999998
 ********** ********** ********** ********** **********
 ********** ********** ********** -7.6653628 4.13112640
 ********** ********** -101.10000 -13.500000 **********
 0.71148002 ********** ********** ********** **********
 ********** ********** ********** ********** **********
```

File: army_results.txt

```
Initial Well 1 : Cane Spring
 Initial Well 2 : ER-5-3 #2
 Initial Well 3 : Indian Springs
 Final well : Army #1 Water Well

 Final Initial 1 Initial 2 Initial 3
 C 5.6414 3.2182 11.2811 4.9900
 S 0.5520 0.3593 0.7190 0.1458
 CA 1.0984 0.9310 1.9232 1.0483
 MG 0.8642 0.4444 1.1941 0.9464
 NA 1.7408 1.9016 5.6607 0.1697
 CL 0.5644 0.6208 1.1012 0.0931
 SI 0.3164 1.0156 1.1496 0.3829
 K 0.1433 0.1555 0.4352 0.0307

 CALCITE CA 1.0000 C 1.0000 RS 4.0000 I1 0.0000 I2 0.0000
 DOLOMITE CA 1.0000 MG 1.0000 C 2.0000 RS 8.0000 I1 0.0000
 I2 0.0000
 GYPSUM CA 1.0000 S 1.0000 RS 6.0000 I3 22.0000
 NaCl NA 1.0000 CL 1.0000
 SiO2 SI 1.0000
 glastmpb CA 0.0250 MG 0.0040 FE 0.0300 AL 0.8030 SI 4.1480
 K 0.3690 NA 0.4030
 claytmpb CA 0.1410 MG 0.1380 FE 0.0500 AL 2.4380 SI 3.4620
 K 0.0170 NA 0.1610
 Ca+Mg/Na CA -0.5597 MG -0.4403 NA 2.0000

 8 models checked
 6 models found
```

```
 MODEL 1 (Model ad)
 Init 1 + F 0.14702
 Init 2 + F 0.20755
 Init 3 + F 0.64543
 CALCITE -0.31066
 DOLOMITE -0.04161
 GYPSUM 0.25585
 NaCl 0.18449
 SiO2 0.00000
 glastmpb 0.03396
 claytmpb -0.13275
 Computed Observed
 Carbon-13 -6.6628 -6.2000
 C-14 (% mod) 12.3914* 4.1000
 ---------------------------------------------------------------------------
 Adjusted C-14 age in years: 9143.* * = based on Original Data

 Model A0 Computed Observed age
 (for initial A0) (initial) (no decay) (final)
 ------------------------------------------------------------
 Original Data 12.39 12.39 4.10 9143.
```

MODEL 2 **(Model ac)**
Init 1 + F 0.31968
Init 2 + F 0.28720
Init 3 + F 0.39312
CALCITE -0.37308
DOLOMITE -0.10799
GYPSUM 0.17333
NaCl 0.01308
SiO2 0.00000
glastmpb -0.11789
Ca+Mg/Na -0.26259
Computed Observed
Carbon-13 -6.5107 -6.2000
C-14 (% mod) 18.8026* 4.1000

Adjusted C-14 age in years: 12590.* * = based on Original Data

Model A0 Computed Observed age
(for initial A0) (initial) (no decay) (final)

Original Data 18.81 18.80 4.10 12590.

MODEL 3 **(Model ab)**
Init 1 + F 0.18564
Init 2 + F 0.22537
Init 3 + F 0.58900
CALCITE -0.32462
DOLOMITE -0.05646
GYPSUM 0.23740
NaCl 0.14615
SiO2 0.00000
claytmpb -0.10306
Ca+Mg/Na -0.05873
Computed Observed
Carbon-13 -6.6278 -6.2000
C-14 (% mod) 13.8612* 4.1000

Adjusted C-14 age in years: 10070.* * = based on Original Data

Model A0 Computed Observed age
(for initial A0) (initial) (no decay) (final)

Original Data 13.87 13.86 4.10 10070.

MODEL 4 **(Model ae)**
Init 1 + F 0.00000
Init 2 + F 0.13973
Init 3 + F 0.86027
CALCITE -0.25751
DOLOMITE 0.01492
GYPSUM 0.32612
NaCl 0.33044
glastmpb 0.16327
claytmpb -0.24579
Ca+Mg/Na 0.22359
Computed Observed
Carbon-13 -6.7768 -6.2000
C-14 (% mod) 6.5604* 4.1000

Adjusted C-14 age in years: 3886.* * = based on Original Data

Model A0 Computed Observed age
(for initial A0) (initial) (no decay) (final)

Original Data 6.60 6.56 4.10 3886.

MODEL 5 **(Model aa)**
Init 1 + F 0.33286
Init 2 + F 0.29328
Init 3 + F 0.37386
CALCITE -0.37785
DOLOMITE -0.11306
GYPSUM 0.16703
SiO2 0.00000
glastmpb -0.12948
claytmpb 0.01013
Ca+Mg/Na -0.28263
Computed Observed
Carbon-13 -6.4995 -6.2000
C-14 (% mod) 19.2755* 4.1000

Adjusted C-14 age in years: 12796.* * = based on Original Data

Model A0 Computed Observed age
(for initial A0) (initial) (no decay) (final)

Original Data 19.28 19.28 4.10 12796.

MODEL 6 **(Model af)**
Init 1 + F 0.03880
Init 2 + F 0.15762
Init 3 + F 0.80358
CALCITE -0.27154
GYPSUM 0.30758
NaCl 0.29193
SiO2 0.00000
glastmpb 0.12915
claytmpb -0.21596
Ca+Mg/Na 0.16459
Computed Observed
Carbon-13 -6.7644 -6.2000
C-14 (% mod) 8.1561* 4.1000

Adjusted C-14 age in years: 5686.* * = based on Original Data

Model A0 Computed Observed age
(for initial A0) (initial) (no decay) (final)

Original Data 8.16 8.16 4.10 5686.

APPENDIX B: ORIGINAL INPUT AND OUTPUT FOR DETERMINISTIC RAINIER MESA MODEL FOR THIS STUDY

File: original_rm_model.txt

```
RM
 38 15 22 6
 C S CA MG NA K CL SI SR
PBR-Glas + K 0.3320000 NA 0.4080000 CA 0.0230000 MG 0.0020000 SR 0.0010000 FE 0.0140000 AL
0.7720000
 SI 4.1870000
PBR-Clay - K 0.6580000 NA 0.0220000 CA 0.0140000 MG 0.2090000 FE 0.5140000 AL 1.3520000 SI
3.4220000
PBR-Feld + K 0.3920000 NA 0.4080000 CA 0.0180000 SR 0.0010000 FE 0.0060000 AL 0.9720000 SI
2.8220000
PBR-Zeol - K 0.2950000 NA 0.2170000 CA 0.0830000 AL 0.7350000 SI 4.2780000
CALCITE CA 1.0000000 C 1.0000000 RS 4.0000000 I1 1.0000000 I2 0.0000000
CO2 GAS C 1.0000000 RS 4.0000000 I1 -18.0000000 I2 100.0000000
DOLOMITE + CA 1.0000000 MG 1.0000000 C 2.0000000 RS 8.0000000 I1 0.1000000 I2 0.0000000
NaCl + NA 1.0000000 CL 1.0000000
STRONITE SR 1.0000000 C 1.0000000 RS 4.0000000 I4 1.0000000 I8 0.0000000 I1 0.0000000 I2
0.0000000
GYPSUM + CA 1.0000000 S 1.0000000 RS 6.0000000 I3 22.0000000
SiO2 SI 1.0000000
EXCHANGE -

 1 1 1 0 0 1.0000 0.0000000000 1.000
 0.000 100.000 0.000 0.000 -25.000 100.000 100.000
 0.000 0.000 0. 0. 0.000 0.000
 -40.000 -25.000 0.000 0.000 0.000
 -40.000 -25.000 0.000 0.000 0.000 100.000
 -40.000 -25.000 0.000 0.000 0.000 100.000
 -40.000 -25.000 0.000 0.000 0.000 100.000
```

File: rm_run_0000001.txt

```
2010ER-12-3
 # 6 of 40



 30.6000004 8.02000046 ********** 120.000000 **********
 ********** 17.3999996 ********** 8.00000000 29.7999992
 2.79999995 6.00000000 26.0000000 ********** 25.2999992
 ********** ********** ********** ********** 0.10040000
 ********** ********** ********** ********** **********
 ********** ********** ********** -5.6999998 3.00000000
 ********** ********** -106.00000 -14.500000 **********
 ********** 0.00110000 ********** ********** **********
 ********** ********** ********** ********** **********

2010Test Well #1 (USGS HTH #1)
 # 15 of 40



 23.1764698 9.00355053 ********** 101.249771 **********
 ********** 2.12695646 ********** 0.17771818 50.4370422
 0.59538096 3.29999995 7.18149996 ********** 18.8329830
 ********** ********** ********** ********** 0.01666667
 ********** ********** ********** ********** **********
 ********** ********** ********** -11.200000 30.0699997
 ********** ********** -110.26666 -14.975000 **********
 ********** 0.00100000 ********** ********** **********
 ********** ********** ********** ********** **********

2010UE-1c
 # 22 of 40



 26.7299995 7.48096752 ********** 240.899994 **********
 ********** 36.4449997 ********** 13.5675001 34.4749985
 12.6099997 6.34999990 33.0499992 ********** 93.3782959
 ********** ********** ********** ********** 0.41499999
 ********** ********** ********** ********** **********
 ********** ********** ********** -4.9499998 2.59999990
 ********** ********** -104.50000 -13.575000 **********
 ********** 0.00100000 ********** ********** **********
 ********** ********** ********** ********** **********

2010E Tunnel
 # 38 of 40



 25.0000000 7.61999989 ********** 90.7500000 **********
 ********** 5.53000021 ********** 0.38999999 39.3800011
 4.94999981 9.00000000 14.6899996 ********** 52.2400017
 ********** ********** ********** ********** 0.01000000
 ********** ********** ********** ********** **********
 ********** ********** ********** -14.300000 85.0000000
 ********** ********** -103.60000 -13.700000 **********
 ********** 0.00100000 ********** ********** **********
 ********** ********** ********** ********** **********
```

File: npxlresults.out

```
Initial Well 1 : E Tunnel
Initial Well 2 : Test Well #1 (USGS HTH #1)
Initial Well 3 : UE-1c
Final well : ER-12-3

 Final Initial 1 Initial 2 Initial 3
 C 1.9821 1.5591 1.5770 4.1941
 S 0.2707 0.1530 0.0748 0.3442
 CA 0.4342 0.1380 0.0531 0.9097
 MG 0.3291 0.0160 0.0073 0.5583
 NA 1.2965 1.7133 2.1943 1.5003
 K 0.0716 0.1266 0.0152 0.3226
 CL 0.1693 0.2539 0.0931 0.1792
 SI 0.4212 0.8696 0.3135 1.5548
 SR 0.0011 0.0001 0.0002 0.0047

 PBR-Glas K 0.3320 NA 0.4080 CA 0.0230 MG 0.0020 SR 0.0010
 FE 0.0140 AL 0.7720 SI 4.1870
 PBR-Clay K 0.6580 NA 0.0220 CA 0.0140 MG 0.2090 FE 0.5140
 AL 1.3520 SI 3.4220
 PBR-Feld K 0.3920 NA 0.4080 CA 0.0180 SR 0.0010 FE 0.0060
 AL 0.9720 SI 2.8220
 PBR-Zeol K 0.2950 NA 0.2170 CA 0.0830 AL 0.7350 SI 4.2780
 CALCITE CA 1.0000 C 1.0000 RS 4.0000 I1 1.0000 I2 0.0000
 CO2 GAS C 1.0000 RS 4.0000 I1 -18.0000 I2 100.0000
 DOLOMITE CA 1.0000 MG 1.0000 C 2.0000 RS 8.0000 I1 0.2000
 I2 0.0000
 NaCl NA 1.0000 CL 1.0000
 STRONITE SR 1.0000 C 1.0000 RS 4.0000 I4 1.0000 I1 0.0000
 I2 0.0000
 GYPSUM CA 1.0000 S 1.0000 RS 6.0000 I3 22.0000
 SiO2 SI 1.0000
 EXCHANGE CA -0.5688 NA 2.0000 MG -0.4312

 495 models checked
 43 models found
```

```
MODEL 1
Init 1 + F 0.09991
Init 2 + F 0.20183
Init 3 + F 0.69825
PBR-Glas + 0.00000
PBR-Clay - -8.24985
PBR-Feld + 17.06392
PBR-Zeol - -4.84760
CALCITE -2.09472
DOLOMITE + 0.34673
STRONITE -0.01927
EXCHANGE - -3.04688
Computed Observed
Carbon-13 -5.4873 -5.7000
C-14 (% mod) 6.8540* 3.0000
--------------------------------------------------------------------------
Adjusted C-14 age in years: 6830.* * = based on Original Data

Model A0 Computed Observed age
(for initial A0) (initial) (no decay) (final)
-----------------------------------------------------------
Original Data 8.94 6.85 3.00 6830.


MODEL 2
Init 1 + F 0.39508
Init 2 + F 0.45802
Init 3 + F 0.14690
PBR-Glas + 0.00000
PBR-Clay - -0.18074
PBR-Feld + 0.32321
PBR-Zeol - -0.13745
CALCITE -0.21926
DOLOMITE + 0.12347
GYPSUM + 0.12548
EXCHANGE - -0.35193
Computed Observed
Carbon-13 -9.1287 -5.7000
C-14 (% mod) 34.1468* 3.0000
--------------------------------------------------------------------------
Adjusted C-14 age in years: 20105.* * = based on Original Data

Model A0 Computed Observed age
(for initial A0) (initial) (no decay) (final)
-----------------------------------------------------------
Original Data 38.72 34.15 3.00 20105.


MODEL 3
Init 1 + F 0.36382
Init 2 + F 0.43088
Init 3 + F 0.20530
PBR-Glas + 3.59961
PBR-Clay - -0.42395
PBR-Feld + 0.00000
PBR-Zeol - -3.26562
CALCITE -0.12217
STRONITE -0.00354
GYPSUM + 0.11219
EXCHANGE - -0.66548
Computed Observed
Carbon-13 -9.5617 -5.7000
C-14 (% mod) 33.6254* 3.0000
--------------------------------------------------------------------------
Adjusted C-14 age in years: 19978.* * = based on Original Data

Model A0 Computed Observed age
(for initial A0) (initial) (no decay) (final)
-----------------------------------------------------------
Original Data 33.63 33.63 3.00 19978.
```

MODEL 4
Init 1 + F 0.09991
Init 2 + F 0.20183
Init 3 + F 0.69825
PBR-Glas + 8.48385
PBR-Clay - -6.80878
PBR-Feld + 12.12319
PBR-Zeol - -11.04453
CALCITE -1.39772
STRONITE -0.02282
SiO2 0.00000
EXCHANGE - -3.11316
Computed Observed
Carbon-13 -6.6736 -5.7000
C-14 (% mod) 8.9292* 3.0000

Adjusted C-14 age in years: 9017.* * = based on Original Data

Model A0 Computed Observed age
(for initial A0) (initial) (no decay) (final)

Original Data 8.94 8.93 3.00 9017.

MODEL 5
Init 1 + F 0.35741
Init 2 + F 0.42532
Init 3 + F 0.21727
PBR-Glas + 0.00000
PBR-Clay - -0.06003
PBR-Zeol - -0.03632
CALCITE -0.19142
CO2 GAS -0.14483
DOLOMITE + 0.08954
GYPSUM + 0.10946
EXCHANGE - -0.28293
Computed Observed
Carbon-13 -8.1965 -5.7000
C-14 (% mod) 29.9785* 3.0000

Adjusted C-14 age in years: 19029.* * = based on Original Data

Model A0 Computed Observed age
(for initial A0) (initial) (no decay) (final)

Original Data 32.68 29.98 3.00 19029.

MODEL 6 **(Model aJ)**
Init 1 + F 0.22629
Init 2 + F 0.31152
Init 3 + F 0.46219
PBR-Glas + 0.00000
PBR-Clay - -0.16606
PBR-Zeol - -0.00553
CALCITE -0.21672
CO2 GAS -0.58264
STRONITE -0.00112
GYPSUM + 0.05372
EXCHANGE - -0.23165
Computed Observed
Carbon-13 -5.6002 -5.7000
C-14 (% mod) 17.9569* 3.0000

Adjusted C-14 age in years: 14792.* * = based on Original Data

Model A0 Computed Observed age
(for initial A0) (initial) (no decay) (final)

Original Data 17.90 17.96 3.00 14792.

```
MODEL 7
Init 1 + F 0.40078
Init 2 + F 0.46296
Init 3 + F 0.13625
PBR-Glas + 0.00000
PBR-Clay - -0.02495
PBR-Zeol - -0.04651
CALCITE -0.18305
DOLOMITE + 0.11916
STRONITE 0.00037
GYPSUM + 0.12790
EXCHANGE - -0.29989
Computed Observed
Carbon-13 -9.2654 -5.7000
C-14 (% mod) 35.1605* 3.0000
--------------------------------------------------------------------------
Adjusted C-14 age in years: 20347.* * = based on Original Data

Model A0 Computed Observed age
(for initial A0) (initial) (no decay) (final)
-----------------------------------------------------------
Original Data 39.74 35.16 3.00 20347.


MODEL 8
Init 1 + F 0.39727
Init 2 + F 0.45992
Init 3 + F 0.14281
PBR-Glas + 0.34198
PBR-Clay - -0.06286
PBR-Zeol - -0.35234
CALCITE -0.17726
DOLOMITE + 0.10784
GYPSUM + 0.12641
SiO2 0.00000
EXCHANGE - -0.33463
Computed Observed
Carbon-13 -9.2957 -5.7000
C-14 (% mod) 35.0311* 3.0000
--------------------------------------------------------------------------
Adjusted C-14 age in years: 20316.* * = based on Original Data

Model A0 Computed Observed age
(for initial A0) (initial) (no decay) (final)
-----------------------------------------------------------
Original Data 39.11 35.03 3.00 20316.


MODEL 9
Init 1 + F 0.36382
Init 2 + F 0.43088
Init 3 + F 0.20530
PBR-Glas + 3.59961
PBR-Clay - -0.42395
PBR-Zeol - -3.26562
CALCITE -0.12217
STRONITE -0.00354
GYPSUM + 0.11219
SiO2 0.00000
EXCHANGE - -0.66548
Computed Observed
Carbon-13 -9.5617 -5.7000
C-14 (% mod) 33.6254* 3.0000
--------------------------------------------------------------------------
Adjusted C-14 age in years: 19978.* * = based on Original Data

Model A0 Computed Observed age
(for initial A0) (initial) (no decay) (final)
-----------------------------------------------------------
Original Data 33.63 33.63 3.00 19978.
```

MODEL 10
Init 1 + F 0.02815
Init 2 + F 0.76037
Init 3 + F 0.21148
PBR-Glas + 0.00000
PBR-Zeol - -0.03986
CALCITE -0.19476
CO2 GAS -0.02598
DOLOMITE + 0.03641
NaCl + 0.05345
GYPSUM + 0.13677
EXCHANGE - -0.39112
Computed Observed
Carbon-13 -8.3901 -5.7000
C-14 (% mod) 19.0733* 3.0000

Adjusted C-14 age in years: 15291.* * = based on Original Data

Model A0 Computed Observed age
(for initial A0) (initial) (no decay) (final)

Original Data 19.76 19.07 3.00 15291.

MODEL 11
Init 1 + F 0.43164
Init 2 + F 0.48974
Init 3 + F 0.07862
PBR-Glas + 0.00000
PBR-Zeol - -0.05376
CALCITE -0.17709
CO2 GAS 0.10303
DOLOMITE + 0.14023
STRONITE 0.00064
GYPSUM + 0.14102
EXCHANGE - -0.31196
Computed Observed
Carbon-13 -10.1305 -5.7000
C-14 (% mod) 42.2714* 3.0000

Adjusted C-14 age in years: 21869.* * = based on Original Data

Model A0 Computed Observed age
(for initial A0) (initial) (no decay) (final)

Original Data 45.79 42.27 3.00 21869.

MODEL 12
Init 1 + F 0.35741
Init 2 + F 0.42532
Init 3 + F 0.21727
PBR-Glas + 0.00000
PBR-Zeol - -0.17022
CALCITE -0.16669
CO2 GAS -0.15642
DOLOMITE + 0.08297
GYPSUM + 0.10946
SiO2 0.36738
EXCHANGE - -0.26906
Computed Observed
Carbon-13 -8.1971 -5.7000
C-14 (% mod) 30.1737* 3.0000

Adjusted C-14 age in years: 19082.* * = based on Original Data

Model A0 Computed Observed age
(for initial A0) (initial) (no decay) (final)

Original Data 32.68 30.17 3.00 19082.

MODEL 13 **(Model aB)**
Init 1 + F 0.24984
Init 2 + F 0.33196
Init 3 + F 0.41820
PBR-Glas + 0.00000
PBR-Zeol - -0.33898
CALCITE -0.15161
CO2 GAS -0.53239
STRONITE -0.00092
GYPSUM + 0.06374
SiO2 0.89974
EXCHANGE - -0.20690
Computed Observed
Carbon-13 -5.9852 -5.7000
C-14 (% mod) 20.0900* 3.0000

Adjusted C-14 age in years: 15720.* * = based on Original Data

Model A0 Computed Observed age
(for initial A0) (initial) (no decay) (final)

Original Data 20.03 20.09 3.00 15720.

MODEL 14
Init 1 + F 0.00000
Init 2 + F 0.79561
Init 3 + F 0.20439
PBR-Glas + 0.08385
PBR-Zeol - -0.11621
CALCITE -0.19283
DOLOMITE + 0.03150
NaCl + 0.05858
STRONITE -0.00005
GYPSUM + 0.14088
EXCHANGE - -0.41174
Computed Observed
Carbon-13 -8.5192 -5.7000
C-14 (% mod) 18.3416* 3.0000

Adjusted C-14 age in years: 14967.* * = based on Original Data

Model A0 Computed Observed age
(for initial A0) (initial) (no decay) (final)

Original Data 18.92 18.34 3.00 14967.

MODEL 15
Init 1 + F 0.00000
Init 2 + F 0.79597
Init 3 + F 0.20403
PBR-Glas + 0.03167
PBR-Zeol - -0.05711
CALCITE -0.19606
DOLOMITE + 0.03357
NaCl + 0.05862
GYPSUM + 0.14098
SiO2 -0.03392
EXCHANGE - -0.40766
Computed Observed
Carbon-13 -8.5072 -5.7000
C-14 (% mod) 18.3188* 3.0000

Adjusted C-14 age in years: 14957.* * = based on Original Data

Model A0 Computed Observed age
(for initial A0) (initial) (no decay) (final)

Original Data 18.93 18.32 3.00 14957.

```
MODEL 16
Init 1 + F 0.40216
Init 2 + F 0.46416
Init 3 + F 0.13368
PBR-Glas + 0.00000
PBR-Zeol - -0.10000
CALCITE -0.17296
DOLOMITE + 0.11749
STRONITE 0.00038
GYPSUM + 0.12849
SiO2 0.14589
EXCHANGE - -0.29493
Computed Observed
Carbon-13 -9.3047 -5.7000
C-14 (% mod) 35.4350* 3.0000
-------------------------------------------------------------------------
Adjusted C-14 age in years: 20411.* * = based on Original Data

Model A0 Computed Observed age
(for initial A0) (initial) (no decay) (final)
-----------------------------------------------------------
Original Data 39.99 35.43 3.00 20411.


MODEL 17
Init 1 + F 0.39055
Init 2 + F 0.45408
Init 3 + F 0.15537
PBR-Glas + 2.80255
PBR-Zeol - -3.27227
CO2 GAS 0.00000
DOLOMITE + 0.00398
STRONITE -0.00252
GYPSUM + 0.12355
SiO2 1.96213
EXCHANGE - -0.51772
Computed Observed
Carbon-13 -10.0553 -5.7000
C-14 (% mod) 37.7831* 3.0000
-------------------------------------------------------------------------
Adjusted C-14 age in years: 20941.* * = based on Original Data

Model A0 Computed Observed age
(for initial A0) (initial) (no decay) (final)
-----------------------------------------------------------
Original Data 37.94 37.78 3.00 20941.


MODEL 18
Init 1 + F 0.35741
Init 2 + F 0.42532
Init 3 + F 0.21727
PBR-Clay - -0.06003
PBR-Feld + 0.00000
PBR-Zeol - -0.03632
CALCITE -0.19142
CO2 GAS -0.14483
DOLOMITE + 0.08954
GYPSUM + 0.10946
EXCHANGE - -0.28293
Computed Observed
Carbon-13 -8.1965 -5.7000
C-14 (% mod) 29.9785* 3.0000
-------------------------------------------------------------------------
Adjusted C-14 age in years: 19029.* * = based on Original Data

Model A0 Computed Observed age
(for initial A0) (initial) (no decay) (final)
-----------------------------------------------------------
Original Data 32.68 29.98 3.00 19029.
```

MODEL 19 **(Model ai)**
Init 1 + F 0.22629
Init 2 + F 0.31152
Init 3 + F 0.46219
PBR-Clay - -0.16606
PBR-Feld + 0.00000
PBR-Zeol - -0.00553
CALCITE -0.21672
CO2 GAS -0.58264
STRONITE -0.00112
GYPSUM + 0.05372
EXCHANGE - -0.23165
Computed Observed
Carbon-13 -5.6002 -5.7000
C-14 (% mod) 17.9569* 3.0000

Adjusted C-14 age in years: 14792.* * = based on Original Data

Model A0 Computed Observed age
(for initial A0) (initial) (no decay) (final)

Original Data 17.90 17.96 3.00 14792.

MODEL 20
Init 1 + F 0.09991
Init 2 + F 0.20183
Init 3 + F 0.69825
PBR-Clay - -1.85894
PBR-Feld + 3.40074
PBR-Zeol - -0.94676
CALCITE -0.61052
CO2 GAS -0.80440
STRONITE -0.00561
SiO2 0.00000
EXCHANGE - -0.75314
Computed Observed
Carbon-13 -4.0869 -5.7000
C-14 (% mod) 8.9758* 3.0000

Adjusted C-14 age in years: 9060.* * = based on Original Data

Model A0 Computed Observed age
(for initial A0) (initial) (no decay) (final)

Original Data 8.94 8.98 3.00 9060.

MODEL 21
Init 1 + F 0.00000
Init 2 + F 0.79610
Init 3 + F 0.20390
PBR-Clay - -0.00623
PBR-Feld + 0.03227
PBR-Zeol - -0.05030
CALCITE -0.19787
DOLOMITE + 0.03465
NaCl + 0.05863
GYPSUM + 0.14101
EXCHANGE - -0.40850
Computed Observed
Carbon-13 -8.5005 -5.7000
C-14 (% mod) 18.3046* 3.0000

Adjusted C-14 age in years: 14951.* * = based on Original Data

Model A0 Computed Observed age
(for initial A0) (initial) (no decay) (final)

Original Data 18.94 18.30 3.00 14951.

MODEL 22
Init 1 + F 0.40078
Init 2 + F 0.46296
Init 3 + F 0.13625
PBR-Clay - -0.02495
PBR-Feld + 0.00000
PBR-Zeol - -0.04651
CALCITE -0.18305
DOLOMITE + 0.11916
STRONITE 0.00037
GYPSUM + 0.12790
EXCHANGE - -0.29989
Computed Observed
Carbon-13 -9.2654 -5.7000
C-14 (% mod) 35.1605* 3.0000

Adjusted C-14 age in years: 20347.* * = based on Original Data

Model A0 Computed Observed age
(for initial A0) (initial) (no decay) (final)

Original Data 39.74 35.16 3.00 20347.

MODEL 23
Init 1 + F 0.09991
Init 2 + F 0.20183
Init 3 + F 0.69825
PBR-Clay - -8.24985
PBR-Feld + 17.06392
PBR-Zeol - -4.84760
CALCITE -2.09472
DOLOMITE + 0.34673
STRONITE -0.01927
SiO2 0.00000
EXCHANGE - -3.04688
Computed Observed
Carbon-13 -5.4873 -5.7000
C-14 (% mod) 6.8540* 3.0000

Adjusted C-14 age in years: 6830.* * = based on Original Data

Model A0 Computed Observed age
(for initial A0) (initial) (no decay) (final)

Original Data 8.94 6.85 3.00 6830.

MODEL 24
Init 1 + F 0.39508
Init 2 + F 0.45802
Init 3 + F 0.14690
PBR-Clay - -0.18074
PBR-Feld + 0.32321
PBR-Zeol - -0.13745
CALCITE -0.21926
DOLOMITE + 0.12347
GYPSUM + 0.12548
SiO2 0.00000
EXCHANGE - -0.35193
Computed Observed
Carbon-13 -9.1287 -5.7000
C-14 (% mod) 34.1468* 3.0000

Adjusted C-14 age in years: 20105.* * = based on Original Data

Model A0 Computed Observed age
(for initial A0) (initial) (no decay) (final)

Original Data 38.72 34.15 3.00 20105.

MODEL 25
Init 1 + F 0.35741
Init 2 + F 0.42532
Init 3 + F 0.21727
PBR-Clay - -0.07631
PBR-Feld + 0.00000
CALCITE -0.19813
CO2 GAS -0.14168
DOLOMITE + 0.09132
GYPSUM + 0.10946
SiO2 -0.09966
EXCHANGE - -0.28669
Computed Observed
Carbon-13 -8.1963 -5.7000
C-14 (% mod) 29.9258* 3.0000

Adjusted C-14 age in years: 19014.* * = based on Original Data

Model A0 (for initial A0)	Computed (initial)	Observed (no decay)	age (final)
Original Data	32.68	29.93	3.00 19014.

MODEL 26 **(Model ad)**
Init 1 + F 0.22590
Init 2 + F 0.31118
Init 3 + F 0.46292
PBR-Clay - -0.16881
PBR-Feld + 0.00000
CALCITE -0.21780
CO2 GAS -0.58347
STRONITE -0.00113
GYPSUM + 0.05356
SiO2 -0.01492
EXCHANGE - -0.23206
Computed Observed
Carbon-13 -5.5941 -5.7000
C-14 (% mod) 17.9230* 3.0000

Adjusted C-14 age in years: 14776.* * = based on Original Data

Model A0 (for initial A0)	Computed (initial)	Observed (no decay)	age (final)
Original Data	17.86	17.92	3.00 14776.

MODEL 27
Init 1 + F 0.00000
Init 2 + F 0.79425
Init 3 + F 0.20575
PBR-Clay - -0.02463
PBR-Feld + 0.02385
CALCITE -0.20593
DOLOMITE + 0.03626
NaCl + 0.05847
GYPSUM + 0.14051
SiO2 -0.13075
EXCHANGE - -0.41131
Computed Observed
Carbon-13 -8.4758 -5.7000
C-14 (% mod) 18.2037* 3.0000

Adjusted C-14 age in years: 14905.* * = based on Original Data

Model A0 (for initial A0)	Computed (initial)	Observed (no decay)	age (final)
Original Data	18.86	18.20	3.00 14905.

```
MODEL 28
Init 1 + F 0.39958
Init 2 + F 0.46192
Init 3 + F 0.13849
PBR-Clay - -0.04665
PBR-Feld + 0.00000
CALCITE -0.19182
DOLOMITE + 0.12060
STRONITE 0.00036
GYPSUM + 0.12739
SiO2 -0.12684
EXCHANGE - -0.30421
Computed Observed
Carbon-13 -9.2315 -5.7000
C-14 (% mod) 34.9238* 3.0000
--------------------------------------------------------------------------------
Adjusted C-14 age in years: 20291.* * = based on Original Data

Model A0 Computed Observed age
(for initial A0) (initial) (no decay) (final)
------------------------------------------------------------
Original Data 39.52 34.92 3.00 20291.


MODEL 29
Init 1 + F 0.40078
Init 2 + F 0.46296
Init 3 + F 0.13625
PBR-Clay - -0.02495
PBR-Zeol - -0.04651
CALCITE -0.18305
CO2 GAS 0.00000
DOLOMITE + 0.11916
STRONITE 0.00037
GYPSUM + 0.12790
EXCHANGE - -0.29989
Computed Observed
Carbon-13 -9.2654 -5.7000
C-14 (% mod) 35.1605* 3.0000
--------------------------------------------------------------------------------
Adjusted C-14 age in years: 20347.* * = based on Original Data

Model A0 Computed Observed age
(for initial A0) (initial) (no decay) (final)
------------------------------------------------------------
Original Data 39.74 35.16 3.00 20347.


MODEL 30
Init 1 + F 0.35741
Init 2 + F 0.42532
Init 3 + F 0.21727
PBR-Clay - -0.06003
PBR-Zeol - -0.03632
CALCITE -0.19142
CO2 GAS -0.14483
DOLOMITE + 0.08954
GYPSUM + 0.10946
SiO2 0.00000
EXCHANGE - -0.28293
Computed Observed
Carbon-13 -8.1965 -5.7000
C-14 (% mod) 29.9785* 3.0000
--------------------------------------------------------------------------------
Adjusted C-14 age in years: 19029.* * = based on Original Data

Model A0 Computed Observed age
(for initial A0) (initial) (no decay) (final)
------------------------------------------------------------
Original Data 32.68 29.98 3.00 19029.
```

MODEL 31 **(Model as)**
Init 1 + F 0.22629
Init 2 + F 0.31152
Init 3 + F 0.46219
PBR-Clay - -0.16606
PBR-Zeol - -0.00553
CALCITE -0.21672
CO2 GAS -0.58264
STRONITE -0.00112
GYPSUM + 0.05372
SiO2 0.00000
EXCHANGE - -0.23165
Computed Observed
Carbon-13 -5.6002 -5.7000
C-14 (% mod) 17.9569* 3.0000

Adjusted C-14 age in years: 14792.* * = based on Original Data

Model A0 Computed Observed age
(for initial A0) (initial) (no decay) (final)

Original Data 17.90 17.96 3.00 14792.

MODEL 32
Init 1 + F 0.40078
Init 2 + F 0.46296
Init 3 + F 0.13625
PBR-Clay - -0.02495
PBR-Zeol - -0.04651
CALCITE -0.18305
DOLOMITE + 0.11916
STRONITE 0.00037
GYPSUM + 0.12790
SiO2 0.00000
EXCHANGE - -0.29989
Computed Observed
Carbon-13 -9.2654 -5.7000
C-14 (% mod) 35.1605* 3.0000

Adjusted C-14 age in years: 20347.* * = based on Original Data

Model A0 Computed Observed age
(for initial A0) (initial) (no decay) (final)

Original Data 39.74 35.16 3.00 20347.

MODEL 33
Init 1 + F 0.00000
Init 2 + F 0.78901
Init 3 + F 0.21099
PBR-Clay - -0.01287
CALCITE -0.20247
CO2 GAS -0.01234
DOLOMITE + 0.03383
NaCl + 0.05802
GYPSUM + 0.13910
SiO2 -0.11019
EXCHANGE - -0.40453
Computed Observed
Carbon-13 -8.4057 -5.7000
C-14 (% mod) 18.0459* 3.0000

Adjusted C-14 age in years: 14833.* * = based on Original Data

Model A0 Computed Observed age
(for initial A0) (initial) (no decay) (final)

Original Data 18.65 18.05 3.00 14833.

MODEL 34
Init 1 + F 0.39958
Init 2 + F 0.46192
Init 3 + F 0.13849
PBR-Clay - -0.04665
CALCITE -0.19182
CO2 GAS 0.00000
DOLOMITE + 0.12060
STRONITE 0.00036
GYPSUM + 0.12739
SiO2 -0.12684
EXCHANGE - -0.30421
Computed Observed
Carbon-13 -9.2315 -5.7000
C-14 (% mod) 34.9238* 3.0000

Adjusted C-14 age in years: 20291.* * = based on Original Data

Model A0 Computed Observed age
(for initial A0) (initial) (no decay) (final)

Original Data 39.52 34.92 3.00 20291.

MODEL 35
Init 1 + F 0.00000
Init 2 + F 0.79526
Init 3 + F 0.20474
PBR-Clay - -0.00995
CALCITE -0.20201
DOLOMITE + 0.03560
NaCl + 0.05855
STRONITE 0.00003
GYPSUM + 0.14079
SiO2 -0.11242
EXCHANGE - -0.40700
Computed Observed
Carbon-13 -8.4876 -5.7000
C-14 (% mod) 18.2544* 3.0000

Adjusted C-14 age in years: 14928.* * = based on Original Data

Model A0 Computed Observed age
(for initial A0) (initial) (no decay) (final)

Original Data 18.91 18.25 3.00 14928.

MODEL 36
Init 1 + F 0.00000
Init 2 + F 0.79221
Init 3 + F 0.20779
PBR-Feld + 0.01457
PBR-Zeol - -0.04474
CALCITE -0.19632
CO2 GAS -0.00868
DOLOMITE + 0.03312
NaCl + 0.05829
GYPSUM + 0.13996
EXCHANGE - -0.40404
Computed Observed
Carbon-13 -8.4483 -5.7000
C-14 (% mod) 18.1816* 3.0000

Adjusted C-14 age in years: 14895.* * = based on Original Data

Model A0 Computed Observed age
(for initial A0) (initial) (no decay) (final)

Original Data 18.78 18.18 3.00 14895.

MODEL 37
Init 1 + F 0.00000
Init 2 + F 0.79649
Init 3 + F 0.20351
PBR-Feld + 0.01938
PBR-Zeol - -0.04666
CALCITE -0.19643
DOLOMITE + 0.03443
NaCl + 0.05866
STRONITE 0.00001
GYPSUM + 0.14112
EXCHANGE - -0.40648
Computed Observed
Carbon-13 -8.5048 -5.7000
C-14 (% mod) 18.3235* 3.0000

Adjusted C-14 age in years: 14959.* * = based on Original Data

Model A0 Computed Observed age
(for initial A0) (initial) (no decay) (final)

Original Data 18.96 18.32 3.00 14959.

MODEL 38
Init 1 + F 0.42097
Init 2 + F 0.48048
Init 3 + F 0.09855
PBR-Feld + 2.08908
PBR-Zeol - -2.84650
CO2 GAS 0.00000
DOLOMITE + 0.07811
STRONITE -0.00154
GYPSUM + 0.13648
SiO2 6.03314
EXCHANGE - -0.43077
Computed Observed
Carbon-13 -10.0342 -5.7000
C-14 (% mod) 40.1516* 3.0000

Adjusted C-14 age in years: 21444.* * = based on Original Data

Model A0 Computed Observed age
(for initial A0) (initial) (no decay) (final)

Original Data 43.59 40.15 3.00 21444.

MODEL 39
Init 1 + F 0.00000
Init 2 + F 0.77925
Init 3 + F 0.22075
PBR-Zeol - -0.03889
CALCITE -0.19600
CO2 GAS -0.03498
DOLOMITE + 0.02916
NaCl + 0.05718
STRONITE -0.00004
GYPSUM + 0.13647
EXCHANGE - -0.39665
Computed Observed
Carbon-13 -8.2789 -5.7000
C-14 (% mod) 17.7583* 3.0000

Adjusted C-14 age in years: 14700.* * = based on Original Data

Model A0 Computed Observed age
(for initial A0) (initial) (no decay) (final)

Original Data 18.27 17.76 3.00 14700.

```
MODEL 40
Init 1 + F 0.02815
Init 2 + F 0.76037
Init 3 + F 0.21148
PBR-Zeol - -0.03986
CALCITE -0.19476
CO2 GAS -0.02598
DOLOMITE + 0.03641
NaCl + 0.05345
GYPSUM + 0.13677
SiO2 0.00000
EXCHANGE - -0.39112
Computed Observed
Carbon-13 -8.3901 -5.7000
C-14 (% mod) 19.0733* 3.0000
--------------------------------------------------------------------------------
Adjusted C-14 age in years: 15291.* * = based on Original Data

Model A0 Computed Observed age
(for initial A0) (initial) (no decay) (final)
---------------------------------------------------------------
Original Data 19.76 19.07 3.00 15291.


MODEL 41
Init 1 + F 0.43164
Init 2 + F 0.48974
Init 3 + F 0.07862
PBR-Zeol - -0.05376
CALCITE -0.17709
CO2 GAS 0.10303
DOLOMITE + 0.14023
STRONITE 0.00064
GYPSUM + 0.14102
SiO2 0.00000
EXCHANGE - -0.31196
Computed Observed
Carbon-13 -10.1305 -5.7000
C-14 (% mod) 42.2714* 3.0000
--------------------------------------------------------------------------------
Adjusted C-14 age in years: 21869.* * = based on Original Data

Model A0 Computed Observed age
(for initial A0) (initial) (no decay) (final)
---------------------------------------------------------------
Original Data 45.79 42.27 3.00 21869.


MODEL 42
Init 1 + F 0.00000
Init 2 + F 0.79619
Init 3 + F 0.20381
PBR-Zeol - -0.02123
CALCITE -0.19802
DOLOMITE + 0.03483
NaCl + 0.05863
STRONITE 0.00003
GYPSUM + 0.14104
SiO2 -0.05452
EXCHANGE - -0.40517
Computed Observed
Carbon-13 -8.4998 -5.7000
C-14 (% mod) 18.3046* 3.0000
--------------------------------------------------------------------------------
Adjusted C-14 age in years: 14951.* * = based on Original Data

Model A0 Computed Observed age
(for initial A0) (initial) (no decay) (final)
---------------------------------------------------------------
Original Data 18.94 18.30 3.00 14951.
```

MODEL 43
Init 1 + F 0.00000
Init 2 + F 0.81656
Init 3 + F 0.18344
CALCITE -0.20046
CO2 GAS 0.04204
DOLOMITE + 0.04163
NaCl + 0.06039
STRONITE 0.00013
GYPSUM + 0.14653
SiO2 -0.12004
EXCHANGE - -0.41542
Computed Observed
Carbon-13 -8.8144 -5.7000
C-14 (% mod) 20.6175* 3.0000

Adjusted C-14 age in years: 15934.* * = based on Original Data

Model A0 Computed Observed age
(for initial A0) (initial) (no decay) (final)

Original Data 19.80 20.62 3.00 15934.

APPENDIX C: EXAMPLE CONFIGURATION FILE FOR MONTE CARLO SCRIPTS

```
#################################################################
#       Current directory
#   xxxxx
#
#################################################################


#   number of Monte Carlo runs
num_mc_runs = 15000

#   sensitivity fraction
#       amount to change for sensitivity
#       e.g., if sensitivity_fraction=0.01, run 0.99, 1.00, 1.01 times mean value
#       e.g., if sensitivity_fraction=0.1, run 0.9, 1.0, 1.1 times mean value
sensitivity_fraction = 0.01

#   new model format
#   if using the model format designed for NetpathXL, the model file must be
#       changed to a more compact format that the original Netpath can read
new_model_format = False

read_from_excel = True
excel_file = 'z:/projects/geochem_uncertainty/rainier_mesa/trial1/rm.xls'
#read_from_excel = False
#excel_file = None

#   maximum dissolution or precipitation (mmol)
#   if a phase precipitates or dissolves more than max_mmol, don't allow that model
#   if max_mmol < 0, ignore this constraint
max_mmol = 1.0
#   maximum value if constraint is ignored
#   if max_constraint_ignored < 0, ignore this constraint
max_constraint_ignored = 0.1
#   maximum difference between computed and observed Carbon-13
#   if max_c13_difference < 0, ignore this constraint
max_c13_difference = 1.0


#   coefficient of variation (sd/mean) of each constituent
conc_cv = {
          #'t':0.1,
               #'ph':0.1,
               'alk':0.1,
               'ca':0.1,
               'mg':0.1,
               'na':0.1,
               'k':0.1,
               'cl':0.1,
               'so4':0.1,
               'sio2':0.1,
               #'sr':0.1,
               'c13':0.1,
               'c14':0.1
               #'h2':0.1,
               #'o18':0.1,
               #'sr8786':0.1
          }

#alk, ca, mg, na, k, cl, so4, sio2, c13, c14

#   model assumed for each constituent's distribution (one of: uniform, normal, log-normal)
conc_model = {
               #'t':'uniform',
               #'ph':'uniform',
```

```
                'alk':'uniform',
                'ca':'uniform',
                'mg':'uniform',
                'na':'uniform',
                'k':'uniform',
                'cl':'uniform',
                'so4':'uniform',
                'sio2':'uniform',
                #'sr':'uniform',
                'c13':'uniform',
                'c14':'uniform'
                #'h2':'uniform',
                #'o18':'uniform',
                #'sr8786':'uniform'
              }


#   lon file order of constituents
#   DO NOT CHANGE
lon_constituents = ['t',
                    'ph',
                    'disso2',
                    'alk',
                    'tritium',
                    'h2s',
                    'ca',
                    'eh',
                    'mg',
                    'na',
                    'k',
                    'cl',
                    'so4',
                    'f',
                    'sio2',
                    'br',
                    'b',
                    'ba',
                    'li',
                    'sr',
                    'fe',
                    'mn',
                    'no3',
                    'nh4',
                    'po4',
                    'doc',
                    'spcond',
                    'density',
                    'c13',
                    'c14',
                    '34sso4',
                    '34sh2s',
                    'h2',
                    'o18',
                    'ch4',
                    'sr8786',
                    'al',
                    'n2',
                    'n15n2',
                    'n15no3',
                    'n15nh4',
                    'depth',
                    'casing',
                    'elevation',
                    'blank'
                    ]
```

APPENDIX D: SOURCE CODE AND DOCUMENTATION FOR MODIFIED NETPATH, DB, AND CUSTOM SCRIPTS

Files are located on the attached CD or zip file.

Directory: Code output comparison/

Contains output from two NETPATH simulations.

- npxlresults.out: Output from original NETPATHXL
- rm_run_0000001.out: Output from NETPATH modified to run in Monte Carlo mode

Directory: Execution scripts/

Custom scripts to perform Monte Carlo analysis and post-processing of output.

- netpath_mc_10.py: Python code to run Monte Carlo NETPATH/DB simulations
- summarize_monte_carlo_3.R: R code to post-process and plot Monte Carlo results

Directory: Modified source code NETPATH DB/

Modified code, executables, and documentation for NETPATH and DB

- db_modifications.txt: Line-by-line comparison of original and modified versions of db.FOR
- db_mod.FOR: Modified FORTRAN source code for DB
- db_mod.exe: Executable for modified DB source code
- netpath_modifications.txt: Line-by-line comparison of original and modified versions of netpath.FOR
- netpath_mod.FOR: Modified FORTRAN source code for NETPATH
- netpath_mod.exe: Executable for modified NETPATH source code

STANDING DISTRIBUTION LIST

Wilhelm Wilborn
UGTA Activity Lead
Nevada Field Office
National Nuclear Security Administration
U.S. Department of Energy
P.O. Box 98518
Las Vegas, NV 89193-8518
Bill.Wilborn@nnsa.doe.gov

Sarah Hammond, Contracting Officer
Office of Acquisition Management
NNSA Service Center
Pennsylvania and H Street, Bldg. 20388
P.O. Box 5400
Albuquerque, NM 87185-5400
Sarah.Hammond@nnsa.doe.gov

Chuck Russell
Division of Hydrologic Sciences
Desert Research Institute
755 E. Flamingo Road
Las Vegas, NV 89119-7363
Chuck.Russell@dri.edu

Jenny Chapman
DOE Program Manager
Division of Hydrologic Sciences
Desert Research Institute
755 E. Flamingo Road
Las Vegas, NV 89119-7363
Jenny.Chapman@dri.edu

*****Nevada State Library and Archives
State Publications
100 North Stewart Street
Carson City, NV 89701-4285

Irene Farnham
Navarro
P.O. Box 98952
M/S NSF167
Las Vegas, NV 89193-8952
Irene.Farnham@nv.doe.gov

Kay Birdsell
Los Alamos National Laboratory
P.O. Box 1663 M/S T003
Los Alamos, NM 87544
khb@lanl.gov

Edward Kwicklis
Los Alamos National Laboratory
EES-16, MS T003
Los Alamos, NM 87545
kwicklis@lanl.gov

P.K. Ortego
National Security Technologies, LLC
P.O. Box 98521
M/S NLV082
Las Vegas, NV 89193-8521
ortegopk@nv.doe.gov

Andy Tompson
Lawrence Livermore National Laboratory
P.O. Box 808, L-231
Livermore, CA 94551-0808
Tompson1@llnl.gov

Jeffrey Sanders
U.S. Geological Survey
Nevada Water Science Center
160 N. Stephanie St.
Henderson, NV 89074-8829
jvsanders@usgs.gov

Ken Rehfeldt
Navarro
P.O. Box 98952
M/S NSF 167
Las Vegas, NV 89193-8952
Ken.Rehfeldt@nv.doe.gov

Archives Getchell Library
University of Nevada, Reno
1664 N. Virginia St.
Reno, NV 89557
dcurtis@unr.edu

DeLaMare Library/262
University of Nevada, Reno
1664 N. Virginia St.
Reno, NV 89557
dcurtis@unr.edu

Document Section, Library
University of Nevada, Las Vegas
4505 Maryland Parkway
Las Vegas, NV 89154
sue.wainscott@unlv.edu

†Library
Southern Nevada Science Center
Desert Research Institute
755 E. Flamingo Road
Las Vegas, NV 89119-7363

‡Nuclear Testing Archive
ATTN: Martha DeMarre
National Security Technologies, LLC
Mail Stop 400
PO Box 98521
Las Vegas, NV 89193-8521
demarrme@nv.doe.gov
(2 CDs)

ʃOffice of Scientific and Technical Information
U.S. Department of Energy
P.O. Box 62
Oak Ridge, TN 37831-9939

All on distribution list receive one electronic PDF copy, unless otherwise noted.

***** 12 paper copies
† 3 paper copies; CD with pdf (from which to print)
‡ compact disc only
ʃ electronic copy (pdf) only